STRESS CORROSION CRACKING

IN MONEL 400

By

LEAH GAIL EVERHART

Bachelor of Science

in Mechanical Engineering

Oklahoma State University

Stillwater, Oklahoma

1987

Submitted to the Faculty of the Graduate College
of the Oklahoma State University
in partial fulfillment of the requirements
for the Degree of
MASTER OF SCIENCE
May, 1989

STRESS CORROSION CRACKING

IN MONEL 400

Thesis Approved:

C E Price

Thesis Adviser

J. K. Good

R L Lowery

Norman N. Durham

Dean of the Graduate College

ACKNOWLEDGMENTS

This work is dedicated to the memory of my father, Winfred F. Henley.

With deep gratitude I thank all who helped me complete this study.

TABLE OF CONTENTS

LIST OF TABLES

LIST OF FIGURES

CHAPTER I

INTRODUCTION TO CORROSION

1.1 Corrosion Costs

It is an essential aspect of nature that everything has a preferred form or state, corresponding to a minimal free energy. Altering a substance will raise the free energy, causing a thermodynamic driving force to develop towards returning the material to its aprioric state. This is the basic trait of corrosion. A few materials are used in their natural state, gold for example. Otherwise, alteration and purification are required to place a metal into a useful form. This higher energy form allows the environment to corrode the metal, returning it to a metal compound such as an oxide or a sulfide.

Due to the understanding that corrosion is a natural process which occurs in all places: at home, at work, and on the road, it is often tolerated as an unavoidable fact of life. Unfortunately, it is also a cause of death. Asphyxiation, explosion, and contamination have been the deplorable, though unforeseen, consequences of uneducated tolerance to corrosion. Society realizes that such a loss of life is not tolerable. This has led to increased safety precautions concurrent with a heightened awareness of the possible effects of corrosion. For the past three decades, this awareness has placed an emphasis on understanding the processes and control of corrosion. The texts of researchers such as Evans, Fontana, Hudson, and

Uhlig have increased what Shrier has termed our "corrosion consciousness" and the need to understand metals.[13]

Even so, it is still a costly business. Tremendous economic loss is suffered by every industrialized nation. In fact, it is estimated that a developed country spends almost four percent of its gross national product on metallic corrosion and its consequences. A congressional directive for a comprehensive cost study by the National Bureau of Standards and Battelle Institute led to the U.S. Department of Commerce statement that "corrosion will cost the U.S. an estimated one hundred and twenty-six billion dollars in 1982."[30] These figures would update to approximately one hundred and seventy billion dollars in 1988.

Furthermore, since there exists a large dependency on foreign sources for critical metals and more nations are pushing toward increased industrialization, there is mounting competition for metal resources. Fontana[30] states that the corrosion "costs will escalate substantially due to worldwide shortages of construction materials and increased energy costs." Additionally, it must be realized that industry is constantly pushing materials to the limit of their capabilities. What is, at one time, considered to be an ultimately harsh environment quickly becomes standard conditions. Therefore, corrosion is expected to continue taking its toll on a nation's economy.

Yet, a nation is not entirely without recourse. Twenty-five to thirty percent of the costs of corrosion are avoidable. Many practical problems can be abated utilizing current corrosion information. Increasing the knowledge and skill of engineers and managers through corrosion education will ensure enlightened material selection and enhanced performance. While education is a vital part of effective corrosion control, it is also neces-

sary that the pool of information should continue to increase. Continued research into the types, causes, and mechanisms of reactions is justified by the beneficial application of such knowledge.

1.2 Environmentally Assisted Cracking

One of the largest problems in the corrosion industry is environmentally assisted cracking, EAC, where an applied stress and a corrosive environment together cause problems that would otherwise not arise if either acted alone. The environments that cause the problems usually produce low general corrosion. Diagnostic efficiency for detection of general corrosion has been improving rapidly, resulting in newer, specialized alloys that resist general corrosion. This allows materials to be used in more severe environments, increasing the operating stresses, temperatures, and concentrations. Consequently, localized corrosion is on the rise, leading to a great increase in the frequency of EAC failures.

A major characteristic of EAC is the embrittlement of the material involved leading to the common term of environmentally induced embrittlement. Such embrittlement introduces a high potential for catastrophic failure. Therefore, the safety, reliability, and cost of a product are affected by a damaging environment. The embrittlement is a very complex phenomenon involving intricate associations between material, geometry, temperature, time, residual and applied stress, and environment. Minute deviations in any part of the system can drastically alter the system's propensity towards embrittlement. For example, only a 4-5^{o}C critical temperature range can occur in some embrittlement systems. It is often difficult to anticipate actual operating conditions of a system, or to determine the total residual stresses present in a system.

With so many variables, prediction of susceptible systems is limited. As a result, tremendous amounts of experimental testing must precede design to ascertain safe operating parameters. The high disaster potential of EAC is often compensated for by the use of overly conservative design. With the increasing costs of materials and the severity of standard environments, overdesigning is less tolerable. Better understanding of the variables and their interactions is necessary.

1.3 Major Categories of EAC

Three major categories of EAC are Hydrogen embrittlement (HE), liquid metal embrittlement (LME), and stress corrosion cracking (SCC). Other, more restricted, examples are solid metal embrittlement and radiation damage. Currently, there is no unified theory to explain the mechanisms of the EAC categories although each has witnessed intense investigation as demonstrated by recent conferences and reviews. A damaging environment is often difficult to avoid and new material-environment combinations for embrittlement are discovered regularly.

While there presently appears to be no obvious system for predicting susceptible cases, many researchers have noted similarities between embrittlement categories. For example, embrittlement typically occurs over a limited temperature range. Cracking, in all cases, propagates in a discontinuous fashion and is proportionally related to the stress intensity factors of a system. Also, the embrittlement can be completely intergranular (IG), transgranular (TG), microvoid coalescence (MVC), or a combination, demonstrating the diverse cracking modes that can be obtained in differing environments. The sensitivity of a particular system can be increased by any, or all, of the following, increased alloy strength, low stacking fault

energy (SFE) or local ordering leading to planar slip, and grain size alteration. Additionally, all can result from a strictly surface phenomenon. In all cases the embrittlement conditions are highly specific to system combinations.

Due to the similarities, individual mechanisms are not completely understood and often the category distinctions are overridden. Actually, numerous researchers have made the suggestion that the same mechanism may be responsible for HE, LME, as well as SCC. For example, Lynch and Trevena[51] have come to the conclusion that the critical factor of adsorption of either adatoms or hydrogen is responsible for embrittlement cracking. This insistence of a single cracking mechanism further complicates the predictions of susceptible systems. The problem may be due in part to the fact that there is currently no means to observe crack initiation or growth, which leads to interpretation of circumstantial evidence that suggests that, since there exist so many similarities, there must be only one active mechanism.

Yet, there exist some obvious practical differences. Liquid metal embrittlement seems to be the simplest case, demonstrating the simplest modes to fracture. It is strictly a surface phenomenon. Neither SCC nor HE need be a surface phenomenon. Specifically, hydrogen can be present initially as an interstitial of the material involved, and it can thereby cause extensive embrittlement damage without being transported across the surface. Hydrogen embrittlement can occur internally in a variety of forms.

Stress corrosion cracking may be transport limited and requires the presence of an anode/cathode combination. A major distinction is that SCC is an anodic occurrence and HE is cathodic. There exist extremes of current

densities that clearly attribute to either the occurrence of SCC or of HE. A pertinent example is demonstrated when an over-potential causes a holiday occurrence which generates hydrogen and induces hydrogen embrittlement. The most intense forms of corrosion act under a combination of stress and corrosive environment. Generally, the main distinction for stress corrosion cracking is a crack propagated under the influence of corrosion. That is, corrosive solution must be pulled toward the crack tip to cause the crack to advance. Also, for SCC crack growth to continue, creep exhaustion must not occur. Neither of these occurrences is necessary for either hydrogen or liquid metal embrittlement.

Therefore, the mechanisms responsible for the stress corrosion cracking failure could be very different from the mechanisms involved in HE and in LME. Indeed, the high specificity of the SCC cases would imply that there is not a single operative mechanism in the categories of EAC failure. It is reasonable that there should be an entire spectrum of embrittlement mechanisms, ranging from being basically corrosive in nature to being strictly mechanically induced. Thus, more study into stress corrosion cracking is warranted.

1.4 Corrosion Resistant Alloys

1.4.1 Stainless Steels

The most important material system utilized in industries for general corrosion resistance is stainless steel. Stainless Steels are simply iron based systems that have been alloyed with Chromium to ensure resistant properties. They have been in use since Faraday first determined the benefit of alloying steels with Chromium in the early 1800s. The chromium addition led to a passivating film that allowed the material to exhibit

resistance in numerous environments previously too corrosive for the use of steel.

Additional alloying elements induce different phase characteristics that have led to five major categories of stainless steels: ferritic, austenitic, martensitic, duplex, and precipitation hardening. An entire spectrum of alloy constituents have led to the development of stainless steels which can be used in almost any environment. During high temperature exposure, the stainless steels develop a protective oxide layer which increases their usefulness. Some stainless steels exhibit temperature resistant characteristics that allow them to be used in the diverse environments of turbine and jet engines, automotive exhaust systems, boiler and feedwater heaters, chemical reaction tubing, and nuclear reactors. They are also typically used in every low temperature application, such as cutlery and surgical devices.

However, stainless steels are not always appropriate since they are often subject to EAC. Problems generally arise due to the occurrence of chrome depletion. It is not uncommon during chrome depletion that the chromium carbides are precipitated to the grain boundaries in a discontinuous fashion. This increases the tendency towards intergranular cracking. Thin sections of stainless steels, or cold worked systems are more prone to depletion and oxidation. Unfortunately, this allows small areas to serve as anodes to the rest of the grain, increasing incidences of localized corrosion. Also, oxygen has a detrimental effect on numerous stainless steel systems. The sensitivity of stainless steels leads to the occurrence of numerous forms of localized corrosion, which can in turn lead to different elements of EAC.

As the more corrosion resistant forms of stainless steels are obtained

by increasing the Molybdenum content, it is distressing that the presence of Mo has been shown to have a detrimental effect on the SCC resistance in some environments.[6,18] Also, in numerous environments, due to the transpassive characteristic of the system, stainless steels are often subject to pitting attack. Indeed, this is the major problem experienced in cooling water systems. The presence of pits can immediately lead to the occurrence of embrittlement cracks.

Actually, there are numerous cases cited where SCC of stainless steels occurs (see Chapter 2). Since chrome depletion and grain boundary segregation play the major roles in the SCC of stainless steels, it is understandable that most cases that occur are intergranular. Yet, transgranular SCC can also occur. It has been long understood that while ferritic stainless steels are generally resistant to TGSCC, austenitic stainless steels commonly suffer from this form of attack, especially in chloride environments. This is basically due to the fact that austenitic stainless steel is a metastable alloy with a low SFE. Also, while duplex materials tend to have the general SCC resistance of ferritic materials, they are often subject to pitting in numerous environments. Additionally, all of the EAC problems in stainless steels are increased in heat affected zones (HAZ). A HAZ can cause otherwise resistant stainless steels to fail. Since welding is a common field fix for corrosion problems, and it can induce a HAZ in most stainless steels, welding operations typically cause major SCC problems for materials already in use. Another form of EAC occurs in stainless steels used in sour gas wells. This environment increases the cathodic reactions of the system, liberating hydrogen which in turn destroys the integrity of the stainless steel. There now exist superalloys exhibiting the phase characteristics of austenitic, or duplexed involving austenite and ferrite.

The Dalamines are examples of Superalloy stainless steels. These alloys are commonly used in sour well environments[5], often considered the severest possible environment.

It is typical that in extremely subversive environments, such as when sour gas, high concentration systems, high temperature and/or pressure combinations are experienced, not only the chromium content, but also the nickel content of a stainless steel is increased to meet the demanding environment. This has led to most of the stainless steel superalloys mentioned previously. Indeed, the Nickel plays a major role in the resistance that is desired. Some superalloys contain over thirty percent, as seen in superaustenitics like Sanicro 28.[5] Even so, the iron based superalloys are not the preferred materials for high temperature use.

1.4.2 Nickel Base Alloys

Nickel base alloys are preferred for high temperature use. Nickel is an inherently face center cubic (FCC) structure that can be strengthened by the formation of precipitates in the matrix. Nickel has become a vitally important engineering material. A wide range of Nickel base alloys is used when applications demand a combination of toughness or high strength and corrosion resistance. The alloys are used extensively in virtually every industry, particularly the chemical, dairy, power, food, textile, marine, and paper industries. The property of passivation, for systems containing as little as thirty percent Nickel,[31] when oxidizing conditions are maintained, ensures the resistance of this family of alloys.

There are several useful categories of Nickel base alloys: Ni, Ni-Cu, Ni-Cr, Ni-Cr-Mo, Ni-Cr-Fe. Obviously, several of the categories form an overlap between stainless steel and Nickel base alloys. Cabots and Hastel-

loys are strictly extensions from the high Mo Stainless Steels. In the extremely subversive environments mentioned previously, the Nickel base superalloys, such as MP35N, Hastelloy C276, the Incoloys, and the Inconels, are completely overriding the use of Stainless Steels.

The solid solution alloys, such as the Monels, are also utilized in numerous environments where stainless steel cannot serve. The Monels exhibit the best general corrosion resistance characteristics in the Ni-Cu series. The Ni-Cu series also offers the benefit of being extremely pure and non-toxic, as well as demonstrating high resistance to fouling. This system is often used in the food industry, witnessing high acidity from lactic, bromic, acetic, and formic environments. It is also commonly used in the chemical industry, where distillation often requires the presence of hydrofluoric, hydrochloric, or sulfuric media.

Since Nickel base alloys are important materials, their tendencies toward environmentally assisted cracking must be understood. A few years ago there existed uncertainty and ambiguity as to the extent of the susceptibility of Nickel base alloys to HE, LME, and SCC. However, certain characteristics had been noted. The presence of halide ions or aeration can adversely affect the resistance of numerous alloys. Also, residual stresses can be severely detrimental to any system. It was generally accepted, though, that the Nickel alloys can operate over extensive temperature ranges, in most environments, without severe problems.

1.5 EAC Investigations in Ni Base Alloys

It is a vital issue to classify which conditions may induce the occurrence of EAC in Nickel base systems. Price and his colleagues have investigated HE and LME by mercury in diverse Nickel base alloys. The

investigations involved slow strain-rate testing and corrosion fatigue methods. They found that all of the alloys investigated were susceptible to some extent, and they noted several similarities. An interesting feature of the EAC demonstrated was that the cracking sequence progressed through IG to TG, to MVC with an increase in the strain or the stress intensity. It was also determined that the most susceptible alloy system was the Ni-Cu system. Within this category, the Monels were most susceptible to cracking at room temperature. Actually, the Monels exhibited their greatest cracking tendencies at room temperature.

While the investigators have not studied the susceptibility of Nickel base alloys to SCC, they have established a firm foundation for contrasting the characteristics of EAC. Generally, Nickel base alloys are considered to be resistant to stress corrosion cracking. However, a few cases have been cited, usually associated with elevated temperatures or the segregation of damaging elements to the grain boundaries. The cited tendencies toward SCC are due to lattice distortions. As an FCC matrix material, the lattice expands readily at elevated temperatures which allows grains to be distorted internally. This automatically induces residual stresses. Also, when continuous precipitates form at grain boundaries, altering the lattice completely in this area, the surface free energy is changed enough to cause preferential attack of atoms near the grain boundary. For example, it has been determined that Inconel 600 tubing used in steam generators experienced SCC due to continuous precipitates at the grain boundaries, and that a discontinuous occurrence yielded better resistance. Of course, for grain boundary segregation to occur, it is likely that extreme temperatures have been experienced, either through manufacturing or operation.

1.6 Investigation Objectives

Since the reports of SCC are extremely limited for Nickel base alloys and several EAC investigations are vague on the details of

what constitutes a problematic environment, extensive research is still required. The work performed by Price, et al., would seem to imply that diverse Nickel alloys could be susceptible to SCC at room temperature, especially the Monels. If a susceptibility does indeed exist, extensive investigation is called for to determine the conditions that will trigger cracking. The slow strain-rate technique can generally pick up SCC tendencies that other methods miss. Several researchers have shown that many environments that can induce IG corrosion can lead to the formation of secondary IG cracks, which are typical in EAC, by the use of slow strain-rate testing. This also concurs with the results of work completed by Price and colleagues. Utilizing these generalities as a basis for procedure, the present investigation is intended as a first step towards classifying the extent and nature of SCC in Nickel base alloys. Combined with the previous work of Price, et al., the mechanisms involved in EAC may be more completely understood.

The purpose of the present work is to investigate the phenomena of stress corrosion cracking in Monel alloys. This study represents the first extension from HE and LME to SCC at room temperature. Monels are the obvious alloys for an initial study because of their high susceptibility to LME and HE. Specific objectives include:

I. Determine whether SCC has been reported in Monel at room temperature.

II. If SCC of Monel at room temperature has been cited, determine the critical characteristics inducing the phenomena.

III. Deduce other environments that could lead to SCC in Monel at room temperature.

IV. Perform immersion corrosion tests and then SSTs on indicated environments.

V. Explore similarities between SCC (if attainable), LME, and HE in Monel at room temperature. For example:

a) cracking sequence dependency with strain

b) effects of surface conditions

c) grain size effects

d) cold work effects

e) yield strength effects

f) the strain rate dependency

g) fractography.

CHAPTER II

LITERATURE REVIEW

As discussed previously, although EAC consequences are devastating, and it has been intensely investigated, a method of reliable prediction does not exist. The procession of EAC is not satisfactorily understood. It is understood that a window exists for any embrittlement mechanism. This window demonstrates extensive dependencies: temperature, strain rate, metallurgical condition, grain size, and cold work. Figure 1 is a schematic illustrating the basic parameters and processes involved in EAC. Numerous mechanisms have been proposed for every category and window variable. None of the generally accepted models account for all of the properties demonstrated by failures. In fact, numerous models have been presented that completely contradict most of the failure problems. Any model proposed strictly on the basis of an isolated environment-material-condition combination does not warrant consideration as a mechanism governing EAC. The models that span several environments and material failures do warrant consideration.

2.1 Mechanisms of LME

Lynch[49] was one of the first researchers to emphasize the similarities in LME and HE. The similarities include fractography, grain size effects, temperature sensitivity, and the inhibition induced by the forma-

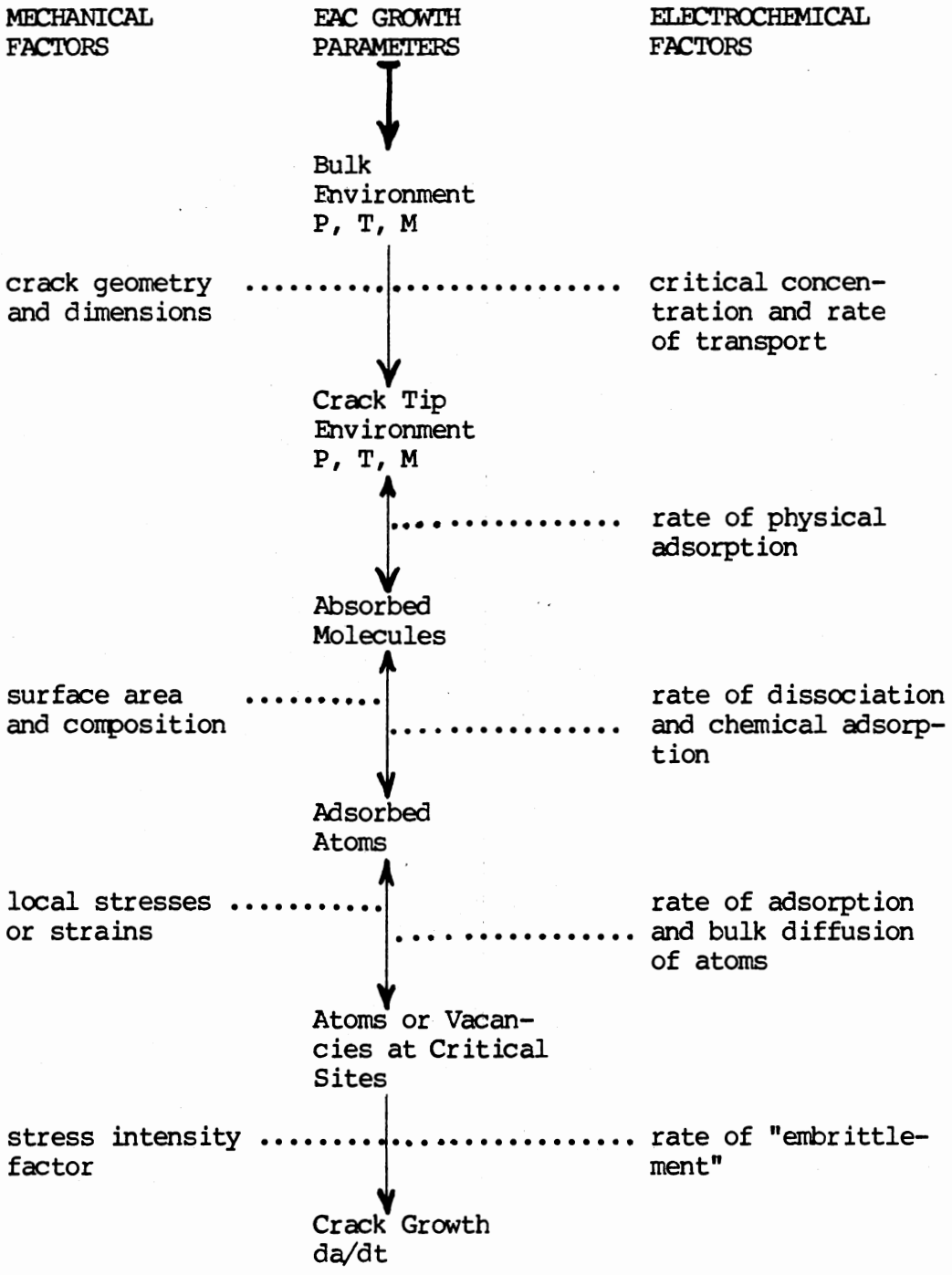

Figure 1. Schematic Illustration of Process and Parameters

tions of stable compounds with the environments. This has led several authors to conclude that more than one mechanism comes into play in LME. It has also led several authors to the conclusion that only one mechanism is effective for LME and HE. However, the conditions[45] necessary for LME occurrence are generally agreed upon.

1. A tensile stress in the material.
2. Pre-existing cracks or obstacles to dislocation motion.
3. Presence of the liquid metal, wetting the solid metal surface, and a transport mechanism to keep the liquid metal in contact with the advancing crack tip.
4. A specific solid metal-liquid metal couple.
5. A specific combination of test conditions (such as temperature and strain rate) and metallurgical conditions (such as grain size, amount of cold work, and the presence or absence of impurities).

Four models for LME mechanisms have come to the forefront. Although these four closely depict major characteristics, each has its problems and cannot be considered conclusive.

2.1.1 Stress Assisted Dissolution

The basis of this model revolves around the removal of highly stressed material atoms by diffusion through the liquid metal, propagating the crack via localized dissolution. However, the propagation rates proposed by this model are often much slower than what is realized through experiments. It must also be considered that such dissolution often leads to crack blunting.

2.1.2 Grain Boundary Diffusion

This model presents a two-step process where the adsorbed liquid metal dissolves into the material and diffuses along preferential paths. An incubation period allows the environment to reach a critical concentration which inhibits planar slip and nucleates a crack. As the name would imply, transgranular fracture is not predicted. Contrary to the following decohesion model, this model indicates that an increased strain rate would decrease embrittlement.

Fredell,[29] based on experimental work involving Hg embrittlement of Ni base alloys, concluded that this model supports the observed embrittlement.

2.1.3 Decohesion

Adsorption of LM at the crack tip reduces the cohesive strength of the material matrix. The model predicts fracture by cleavage. Yet, high magnification fractography of fracture surface often reveals a dominance of shallow voids. Also, the decohesion would have to occur upon contact and therefore does not account for the incubation period that is occasionally reported.

Based on this model, Kamdar[44] concluded that an increased strain rate would increase material embrittlement due to an increase of the ductile-to-brittle transition. However, quite the opposite is usually demonstrated.

King[29] concluded, as several researchers have, that LME characteristics tend to be consistent with the proposed decohesion mechanism for IG fracture, and that TG fractures displayed characteristics of the enhanced dislocation nucleation model. Portions of the results may support these

conclusions. However, these conclusions and the optimum embrittlement conditions present a paradox in several cases.

2.1.4 Enhanced Dislocation Nucleation

With the initial assumption that a common mechanism is shared for the crack propagation of LME and HE, Lynch[50] formulated a model involving the enhancement of slip that can allow a notch to develop. The model speculates that adsorbed atoms interrupt the bonding strength of the metal lattice. Slip systems intersecting at the interruption will be activated. A crack will then propagate on alternating systems, inducing voids ahead of the notch. As the material between the crack tip and the void is weakened, they are connected by mechanical tearing. The sequence indicated by the proposed mechanism is illustrated below.

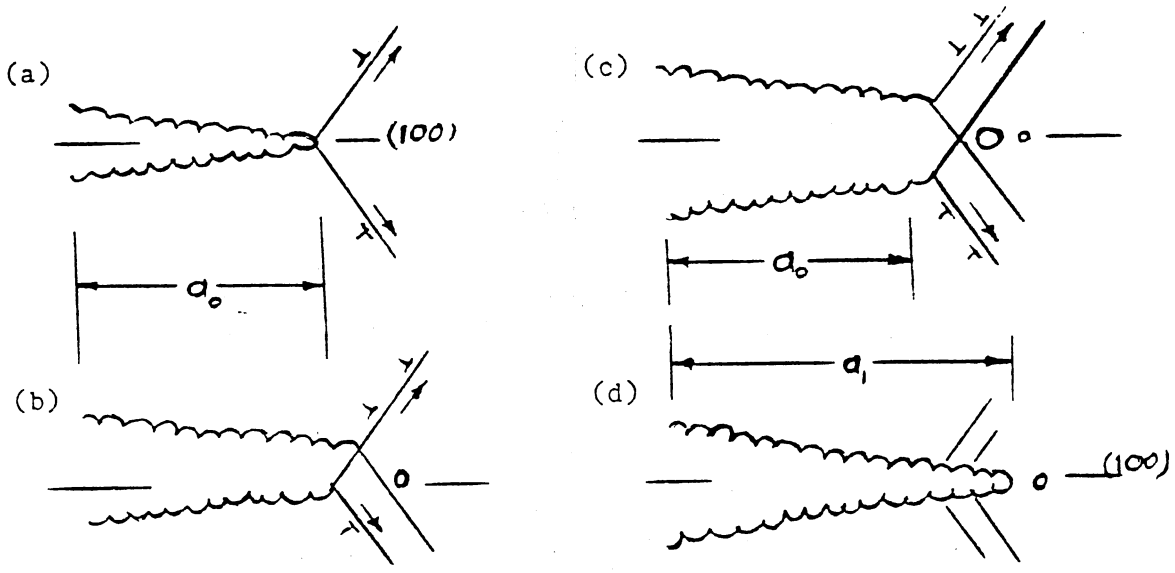

Figure 2. Mechanisms of hydrogen enhanced dislocation nucleation model for transgranular propagation. (From King[45], p.14)

Variations of this model have been proposed by numerous authors. Although there are reservations, this mechanism can generally describe a majority of witnessed fracture characteristics.

2.2 Mechanisms of HE

A significant proportion of the hydrogen embrittlement research has been conducted with respect to high strength steels. At room temperature, hydrogen can rapidly diffuse into the metal lattice of steel, demonstrating a rate of approximately $10^{-9} m^2 s^{-1}$. Therefore, most of the resulting models rely on large amounts of hydrogen movement through the metal lattice. Such models must be discounted for HE of single phase nickel alloys as the rate of diffusion is decreased by as much as four orders of magnitude. Speculation of active mechanisms must consider the slower diffusion rate.

2.2.1 Internal Pressure

Hydrogen atoms can diffuse along dislocation systems until trapped in voids or defects within the metal matrix. When numerous atoms are trapped, they recombine, forming hydrogen gas which increases the internal pressure. The pressure can cause numerous problems, especially where the pressurized voids are located near the front of a crack tip. Yet, in nickel, the internal pressure is unlikely to reach significant levels. Therefore, it should be concluded that internal pressure mechanisms may enhance but not induce embrittlement.

2.2.2 Brittle Decohesion

This model is a counterpart of the decohesion described for LME with the understanding that the hydrogen is not confined to adsorption at the crack tip. It is proposed that the presence of hydrogen will reduce the cohesive strength of the metal matrix. The internal hydrogen can also present a dislocation barrier which can promote brittle behavior by increasing the shearing properties. This allows brittle cracks to advance by plastic tearing or shear.

The decohesion theory is presently accepted by most researchers. However, no evidence has been found that hydrogen decreases atomic bonding when it is present as an interstitial. There also exist fractographic discrepancies.

2.2.3 Hydrogen Enhanced Plasticity

This model states that, on a localized basis, the hydrogen that diffuses into a metal lattice, just ahead of the crack tip, will enhance the process of mechanical deformation thereby increasing the plasticity. There is experimental support that nickel plasticity is facilitated by hydrogen.[68] The model also accounts for a transgression of fracture through IG, TG, and MVC.

2.2.4 Enhanced Dislocation Nucleation

Lynch's proposal[50] of this model was discussed in the previous section. It is supported in HE by evidence indicating the phenomena occurs due to surface effects. The induction of voids by hydrogen is illustrated in Figure 3. This mechanism also predicts that cracks will propagate in highly specific directions. Extensive research has indicated that

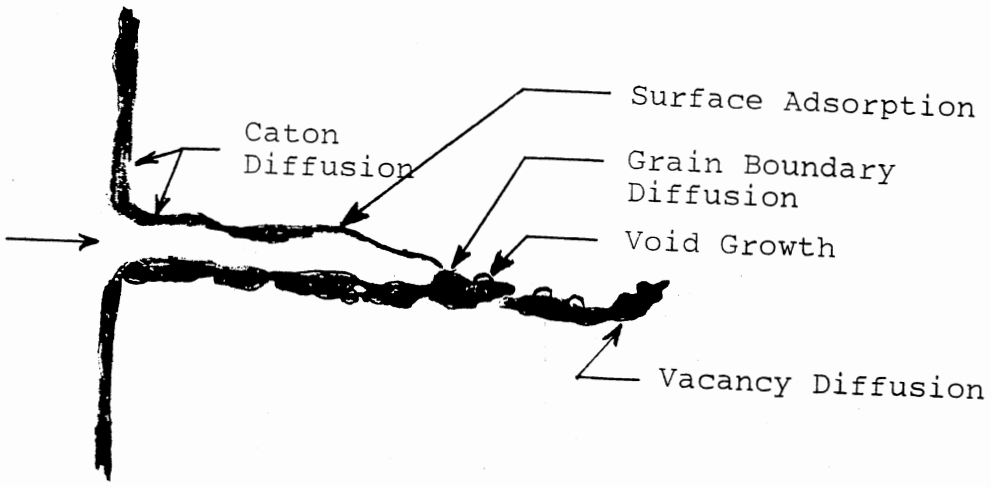

Figure 3. Schematic representation of enhanced void growth by grain boundary diffusion of gas species. (From Fatigue and Microstructure[27], p.321)

preferential slip planes are a vital parameter for brittle cracking.

2.2.5 Plastically Blunted Decohesion

Due to research indicating that cracks do not exactly proceed along slip planes, this mechanism extends the decohesion model. Basically, a brittle crack initially proceeds by decohesion. Subsequently, the crack suffers blunting through dislocation emission. Microscopic observations have revealed micro cracks formed around a crack tip causing enclaves of uncracked material to experience necking. Meanwhile, the crack front progresses. The observations led to the conclusion that the procession and blunting occurs in steps less than Ø.1 μm. The model correctly correlates many of the parameters of HE.

2.3 LME and HE in Nickel Base Alloys

The experimental work conducted by Price, et al., demonstrated that all of the alloys they analyzed experienced LME and HE. The work of Price and Good[69-71] indicated that the major discrepancy found in the fractography of HE and LME was the greater plastic deformation exhibited by the hydrogen-induced fracture. It was assumed that this resulted from the ability of hydrogen to affect areas other than the crack tip material. Following research confirmed that, overall, the hydrogen significantly affected the initiation of cracks, while mercury embrittlement increased the crack propagation rate. In each case, side and secondary cracks resulted in all alloys. Their experiments included a diverse range of nickel base alloys:

Nickel 200

Monels 400, 405, K500

Inconel 600, 625, 718, X750

Incoloy 800, 825

Hastelloy C.

Tests revealed that alloys belonging to similar categories of composition generally exhibited similar fracture characteristics. The alloy exhibiting the greatest tendency towards embrittlement was the 400, followed by 200, 600, and then 800.

It was also noted that as the embrittlement was decreased, through various means, the fractography revealed a transition from intergranular to transgranular, to microvoid coalescence. An example of this is the resulting fracture characteristics at indicative strains. When test conditions obtained greater than fifty percent strain, microvoid coalescence cracking resulted. Below forty percent strain, intergranular cracking

resulted. Transgranular cracking was exhibited at the interim.

As a result of LME trials, it was speculated that environment-material combinations leading to an intermediate wetting characteristic were most likely to exhibit embrittlement. If wetting does not occur, or complete wetting does occur, the surface will not be adversely affected. However, intermediate wetting leads to localized wetting which enhances the localized adsorption that causes embrittlement. Numerous researchers have noted this relationship, and the tests with the mercury embrittlement of nickel alloys also suggest the possibility. Yet, further tests by Price and associates with differing liquid metals have been inconclusive.

Another generality exhibited by the work of Price, et al., deals with the grain size dependency of embrittlement. The greatest tendencies for brittle cracking occurred at intermediate grain sizes. For large grains, a significant amount of deformation allowed the stresses to be reduced, thereby relieving or blunting cracks. Conversely, small grains are capable of obtaining very high energy states due to the large amount of grain boundary area. This would tend to allow high stresses to exist without causing alteration in dislocation densities, thereby inhibiting embrittlement. The intermediate grain size of the test series was in the range of 250 μm.

Several studies have been conducted on the hydrogen embrittlement in nickel and its alloys. These studies have determined several characteristics of embrittlement. Generally, the tensile strength is not adversely affected although HE is often accompanied by a loss of ductility and in most cases an alteration in the reduction of area.

Also, embrittlement is inhibited with an increase of the strain rate and/or a decreased grain size. The embrittlement can be enhanced by the

presence of any impurities. Grain boundary impurities have long been recognized as the cause of sensitization of numerous materials. In addition, it should be noted that a vast amount of experiments have been performed demonstrating transgranular cracking of diverse metals under LME, HE, and SCC. However, a major portion of these tests has been conducted on single crystals which would preclude TG fracture. On polycrystalline material, HE is usually intergranular.

One of the generalized characteristics determined by previous studies should be noted as a peculiarity. It has been noted that the hydrogen embrittlement of nickel is decreased by copper or iron additions.[46] However, as mentioned earlier, the Monels are the nickel alloys most susceptible to embrittlement. Side and secondary cracks are also most extensive in the HE suffered by the Monels. Therefore, the protection offered by the copper or iron constituents must be limited.

2.4 LME and HE of Monel

Monel 400 is a solid solution alloy of nickel and copper, with a nominal ratio of 2:1. It was generally accepted that nickel is embrittled by hydrogen, but not mercury. It was also assumed that copper is embrittled by mercury, but basically resistant to HE. It would be a logical assumption, then, that Monel would be adversely affected by both LME and HE, but perhaps more susceptible to HE.

Although the environmental cracking of Monel has occasionally been noted (see sections 2.5 and 2.7), it is generally not recognized by industry. Indeed, technical literature seemed to imply that, while Cu-Ni alloys are EAC suspect, Ni-Cu are only adversely affected by general corrosion environments. As a result only limited information is available.

The accumulative work of Price, in association with Fredell[29,68], Good[69-71], King[45,72], Morris[73], Norman[74], Peevy[75], Traylor[76,77,91], and Willoughby[75], forms the basis of any understandings available and is therefore the foundation of current work.

The initial work established the benefit of the slow strain rate testing technique as Monel embrittlement is highly sensitive to a strain rate parameter. Normal ductile (cup and cone) fracture results from rapid tensile straining. However, at lower strain rates, LME of Monel 400 demonstrated complete, flat IG fracture, occurring well above the yield stress. LME of alloy K500 behaved similarly. However, greater ductility is demonstrated by Monel 405 in that fracture occurred after necking had begun. This could result due to the reduced flow stress characteristics of 405 which can enhance shearing over embrittlement.

It has been determined that mercury causes a greater degree of embrittlement than hydrogen, but this is also strain rate dependent. Otherwise, the fractures due to HE and LME have the same specific features, as mentioned previously. In HE, as in LME, cracking tends to transform towards MVC as the strain intensity is increased. However, in the Monels, HE occurred most readily in small grain samples, where LME severity relied on an intermediate grain size. This should imply that any mechanism for LME specifying dissolution or grain boundary diffusion cannot be operative here, since it would be conditional that LME reaches its highest potential in samples with small grains. Additionally, side and secondary cracks were seen in HE more than LME, but in both cases the extent was similarly grain size dependent. The side cracks were predominantly IG and occurred transverse to the tensile axis.

Embrittlement of Monel is also sensitive to prestresses. Increasing

prestress inhibits embrittlement. A gradient corresponding to a transition from plane stress to plane strain conditions arose as the ductility was increased. Therefore, the degree of embrittlement extremes can occur depending upon specimen condition.

It was mentioned in the previous section that impurities will enhance embrittlement. Monel is an exception. Several studies have verified that an increased concentration of phosphorous at the grain boundaries enhances resistance to LME and HE. As phosphorous improves the packing efficiency at grain boundaries, the high energy state normally associated with grain boundaries is reduced. This allows a greater deviation in energy to be obtained before the integrity suffers, and it reduces the capabilities of hydrogen or mercury for adsorption.

One other important observation must be made. Due to the fact that plasticity increases are demonstrated by the strain development leading from IG to TG to MVC, the sample thickness is a vital parameter for embrittlement. Naturally, decreasing the specimen thickness would increase any embrittling tendencies. This has been verified for Monel tested under LME and HE conditions. Therefore, it will be an important aspect in SCC.

2.5 Stress Corrosion Cracking

In-service failures and experimental pursuits have developed a vast amount of details regarding SCC. The results have been so diverse that it is difficult to determine what constitutes common features. The following list marks the most consistent points.

- Stress and corrosion react symbiotically.
- Conditions are highly specific.

- Rate of corrosion attack is low ensuring the formation of fine cracks.
- Progression between IG, TG, and MVC dominance can be induced.
- Cracks follow direction of maximum potential energy density usually determined by orientation of grain and stress.
- Secondary cracking decreases as major SCC crack propagates.
- Crack closure does not occur.
- Creep or crack yawning stops crack progression.
- Detrimental strain is rate dependent, usually within 10^{-5} to $10^{-8} s^{-1}$.
- Prevention occurs with cathodic current potential.

Stress can cause the deformation and fracture of a material in several ways, as demonstrated in Figure 4. Each way can be enhanced by localized corrosion. Also, the occurrence of localized corrosion can be enhanced by the deformation of a gain by stress.

The extent of the interaction between stress and corrosion controls the rate at which a crack will grow. The interaction is governed by numerous parameters:

- material elements
- material condition
- stress concentration
- electrochemical potential
- solution concentration
- loading mode
- pH
- time
- strain
- temperature
- pressure
- aeration

The stress concentration governs the stage of growth rate for a system. As Figure 5 demonstrates, stage III will result in catastrophic failure. The stress is dependent upon the strain. The strain rate can

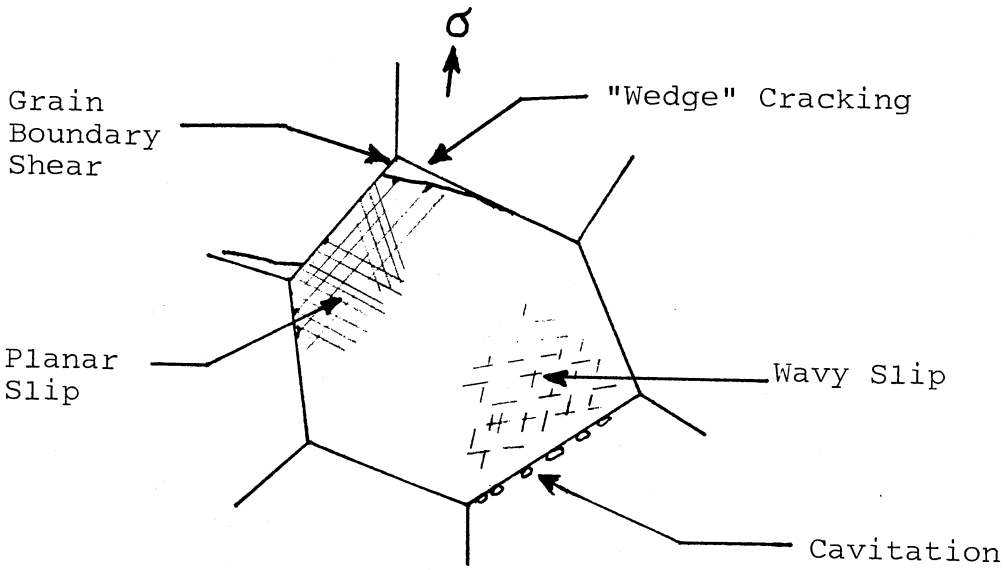

Figure 4. Possible mechanical deformation and fracture modes of a metallic sample subjected to a tensile load. (Modified from Fatigue and Microstructure[27], p. 3120

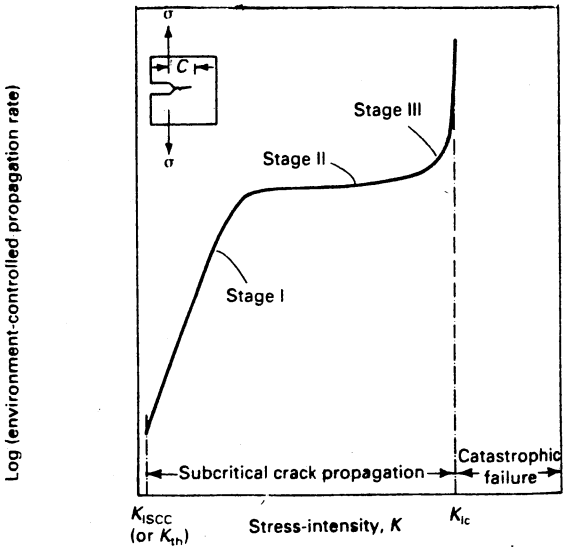

Figure 5. Typical, subcritical crack propagation rate versus stress intensity relationship. Stress intensity, K, is defined as $L = A\sigma\sqrt{\pi C/B}$, where σ is the total tensile stress, C is the crack length, and A and B geometrical constants. (From Craig[18])

directly affect stress-corrosion interaction. Thresholds exist that do not allow any interaction (see Figure 6). The strain effect can be affected by temperature (see Figure 7). also, the loading mode often determines the type of embrittlement experienced.

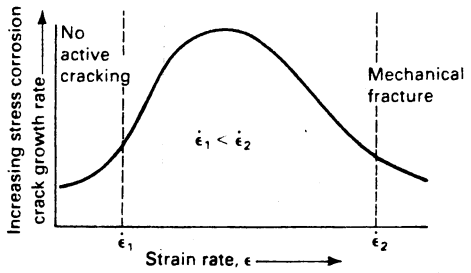

Figure 6. Stress-corrosion crack growth as a function of the two strain rate threshholds, $\dot{\epsilon}_1$ and $\dot{\epsilon}_2$. (From Craig[18])

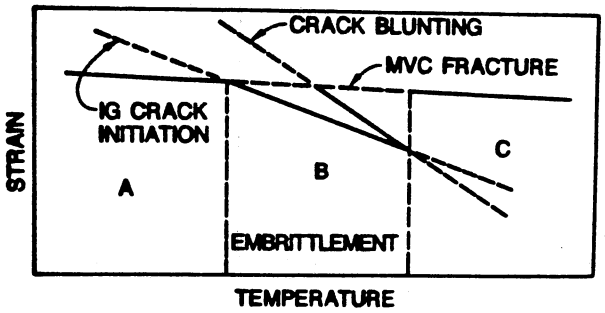

Figure 7. The HE window. In Region A, a microvoid coalescence (MVC) fracture occurs before intergranular (IG) cracks can be initiated. In Region C, plastic deformation occurs easily. (From Price and King[72])

Figure 8 demonstrates the hydrostatic stress gradient occurring around the crack front. The loading mode can determine the type and degree of stress in the area, thereby determining the propensity to failure.

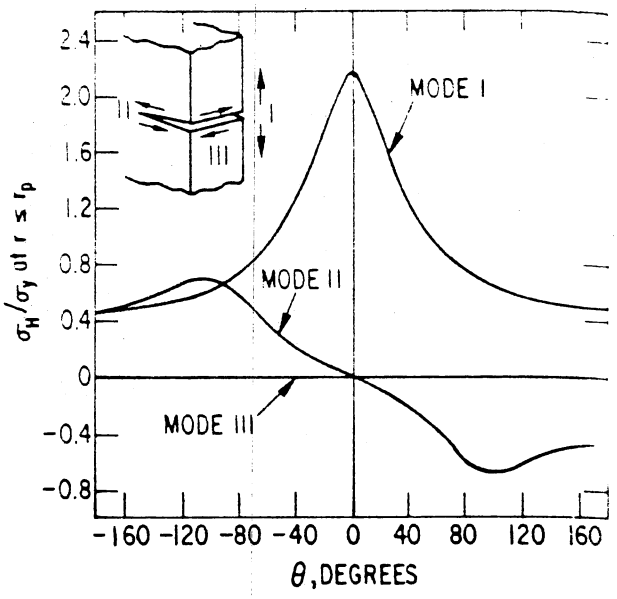

Figure 8. Hydrostatic stress gradients for crack loaded in Modes I and II. (From Nichols[61])

The window for SCC activity can be shifted by altering any combination of the parameters. The location of conditions within the window can determine the mode of fracture, and perhaps even the controlling mechanism. It is not surprising, then, that a vast amount of material-environment combinations demonstrate stress corrosion cracking. An extensive list of the combinations has been compiled in Appendix A. The list covers the major engineering metals, but not the entire spectrum of SCC.

The system, series, and alloys are included with the damaging environment, and occasionally the pertinent temperature. References are provided to allow further consideration of the parameters.

Plastic deformation is a necessary characteristic of an embrittled failure. In stress corrosion cracking, anodic corrosion paths can induce the plastic deformation. It is important to note that such deformation is a result, not a cause, of crack propagation. It is an observed fact that the corrosion path is anodic to the grain(s) involved, not an explanation of the preferential path. These points should be kept in mind when reviewing mechanisms proposed as SCC explanations.

Significant progress has been made toward understanding SCC. Over the last sixty years, numerous speculations have been put forth and either accepted or rejected consequently. Appendix B presents the major aspects of developed theories. As can be noted, successive modifications have enabled the theories to incorporate more of the fracture characteristics. SCC proceeds in two steps. The first step is an induction period which is generally believed to constitute the major portion of life in a component. During this step a crack of discontinuity is developed in the metal surface. The second step involves crack propagation. Although this is usually the shortest stage, proposed mechanisms appear to only consider this stage. However, since all materials contain pre-existing flaws, a mechanism for initiating the flaw would be redundant.

Three classifications of models are under current consideration:

1) Dissolution Models
    a) film rupture
    b) selective dissolution
2) Ductile Mechanical Fracture

a) corrosion tunnel

b) adsorption-enhanced plasticity

3) Brittle Mechanical Fracture

a) film-induced cleavage

b) adsorption-induced brittle fracture

c) hydrogen embrittlement

2.5.1 Selective Dissolution

The preferential dissolution of alloy elements, first described by Robertson[81] and Bakish in 1954 (see Appendix B), can inject vacancies in the region of the crack tip. Dislocation gliding becomes more difficult, causing a localized brittle fracture. Alternatively, when the dissolution removes an area of vacancy, the matrix can be hardened by increased slip functions. As the material hardens it becomes more brittle. This model cannot account for intergranular cracking, cleavage, or the cracking of pure metals.

2.5.2 Film Rupture

The integrity of a protected film can be reduced by stress concentrations. The stress allows slip dislocations to rupture the film, as illustrated in Figure 9. Once ruptured, the crack is propagated by rapid corrosion of the unprotected base metal. The rate of crack growth, or blunting, depends upon the capabilities of the material to reform the protective film. It should be realized that, if this mechanism is actually in play, the fracture should demonstrate extensive material loss and numerous changes in direction.

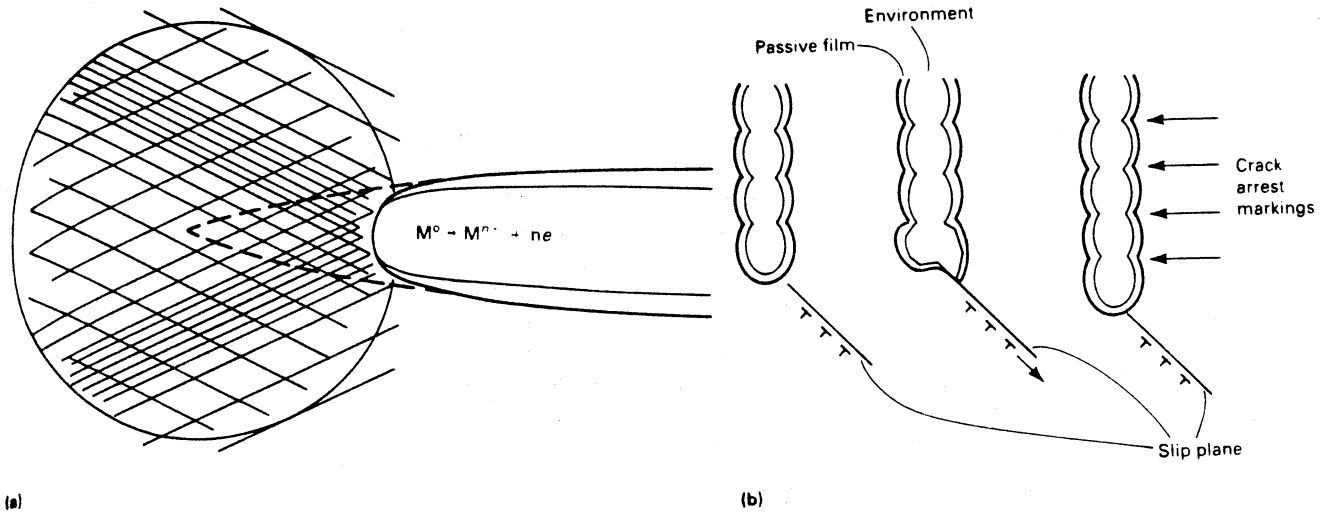

Figure 9. Schematic representations of crack propagation by the film rupture model. (From Craig[18])

2.5.3 Corrosion Tunneling

An array of tunnels is formed in materials by corrosive action along any emerging slip steps. The material between the tunnels will suffer from increased stress and deform to fracture in a ductile mode. The fracture surface would then demonstrate an alteration of grooves and microvoid coalescence. If the corrosion procession results in slots instead of tunnels, the fracture surface would be flat. This model is represented in Figure 10.

2.5.4 Adsorption-Enhanced Plasticity

This model, based on the common process of chemisorption, explains many of the similarities between LME, HE, and SCC. Voids formed ahead of the crack tip induces alternate slipping. The chemisorption promotes the brittle cleavage-like fracture that is characteristic of EAC. This model

was discussed in more detail in a previous section.

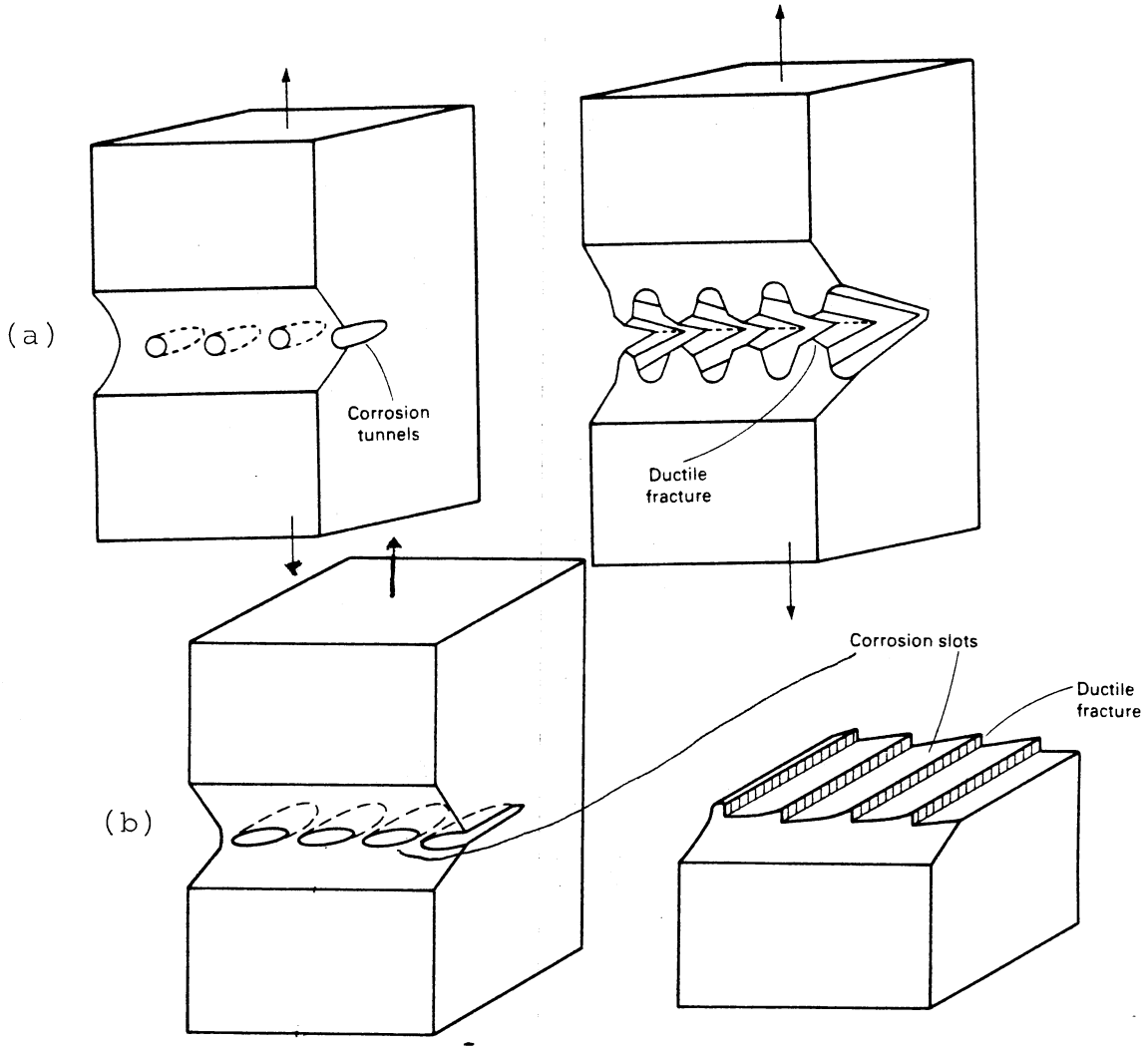

Figure 10. Corrosion tunnel models. (a) Schematic of tunnel model showing the initiation of a crack by the formation of corrosion tunnels at slip steps and ductile deformation and fracture of the remaining ligaments. (b) Schematic diagram of the tunnel mechanism of SCC and flat slot formation. (From Craig[18])

2.5.5 Film-Induced Cleavage

This model extends from the film rupture model. Brittle cracks formed in the film proceed into the metal matrix. Eventually it is blunted and the process must be repeated to ensure propagation. This model has been discussed previously. The proposed mechanism can explain the crack arrest markings, illustrated in Figure 11, that are often seen on the fracture surface. It also suggests the presence of cleavage-like facets.

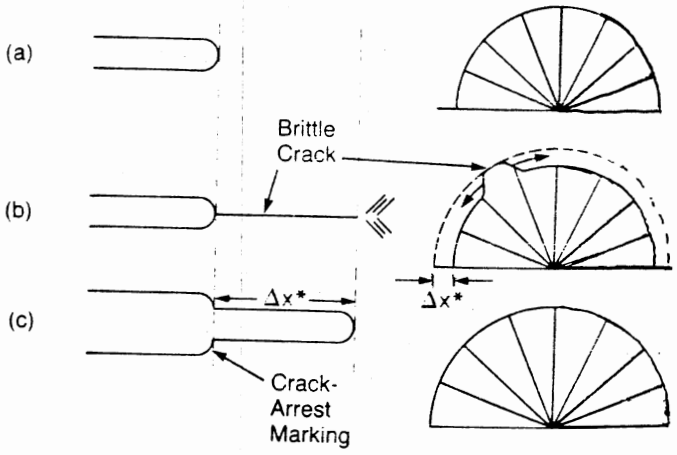

Figure 11. Schematic illustration of successful events during the propagation of transgranular stress corrosion cracks: (a) through (c) represent a section at crack tip; (d) through (f) represent plan view of semicircular crack, showing cleavage steps radiating from initiation site; (c) and (e) indicate the crack advance distance per event, ΔX^*. (From Pugh[79])

2.5.6 Adsorption-Induced Brittle Fracture

This model is similar to models proposed for LME and HE. The stress leading to cleavage fracture is reduced by the adsorption of environmental atoms onto the surface of the crack tip.

2.5.7 Hydrogen Embrittlement

Often, hydrogen presence can cause a material to be subjected to stress corrosion cracking. There are several proposed roles of action for a hydrogen atom. Numerous researchers rely on one role or another to explain the SCC results they obtain. However, as mentioned previously, SCC is quite separate from HE in that it is an anodic reaction. Also, since the exact mechanism describing hydrogen embrittlement has not been determined, it should not be used to explain stress corrosion cracking.

2.6 SCC in Monel

The corrosion rate of a material in a particular environment is an important consideration in EAC. As discussed in the introduction, incidences of EAC are increasing as general corrosion rates are reduced. Most EAC failures occur due to localized corrosion. Within a material system, then, the alloy exhibiting the lowest corrosion rate in a particular environment would be assumed most susceptible to EAC. In the Ni-Cu system, 20 to 40% Cu allows the greatest reduction in the corrosion rate, as illustrated in figure 12. The composition ratio of 2:1 corresponding to Monel has approximately 30% Cu.

The work of Robertson and Bakish (see 2.5) would confirm the assumed susceptibility of approximately 30% copper alloyed in Nickel. Monels can also exhibit transgranular and microvoid fractography. Additional support

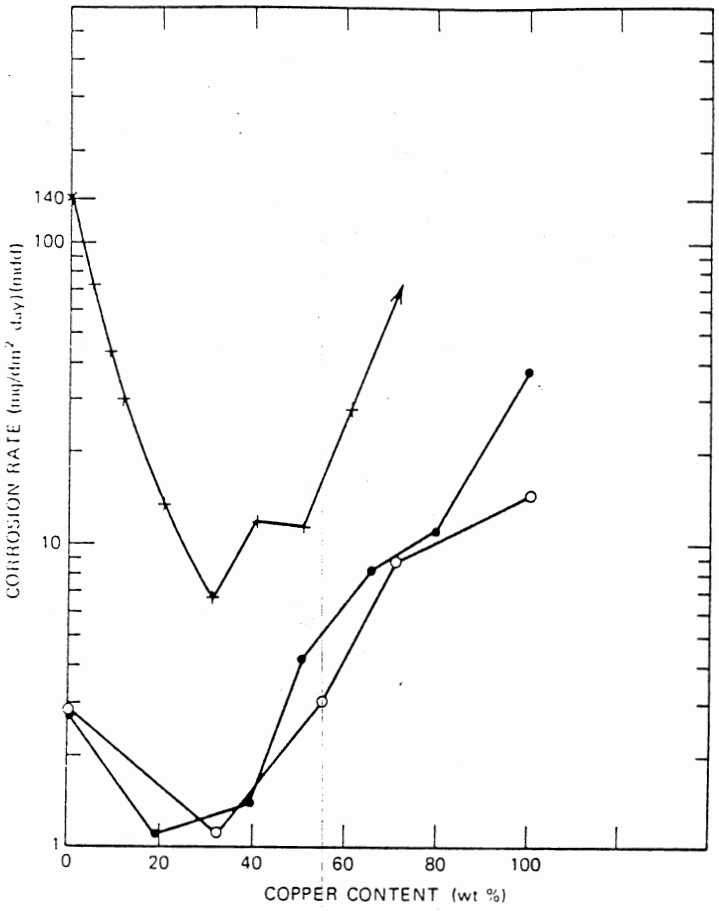

Figure 12. Effect of copper content on corrosion of nickel-copper alloys (From Comley and Evans[13])
(●) 4% NaCl, aerated, 25 C, three days
(o) Flowing seawater, velocity 1.5 to 3.0 ft/sec, 427 days
(+) 80% HF, 0.5 to 1.0% H_2O, 4.0% tars, remainder intermediate organic polymers, unaerated, 130 to 145 C (270 to 290 F), pressure 110 to 145 lb/in.^{2}, 102 days.
In-plant test. Ni-Cu specimens containing 70, 80, 90, and 100% copper corroded away during test.

for the assumption comes from LME and HE susceptible. As demonstrated by the work of Price and his colleagues, this Nickel base alloy exhibited the greatest embrittlement. Therefore, it would be most beneficial to examine the available literature involving SCC of Monel.

As illustrated by the table listing of Appendix A, several cases of SCC of Monel involve a hydrogen fluoride environment. Figure 13 demonstrates the corrosion rate of Monel 400 exposed to HF acid. The diagram indicates a dependency upon the acid concentration. The diagram in Figure 14 is the isocorrosion chart of Monel 400 in HF. The lowest corrosion rate, independent of acid concentration, occurs near room temperature. This could imply that, contrary to common assumption, Monel 400 will demonstrate its greatest tendency towards SCC at room temperature, as it does for LME and HE.

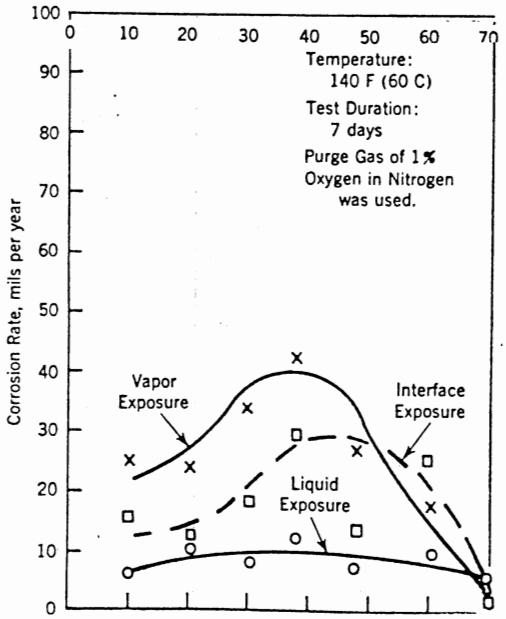

Figure 13. Effect of hydrofluoric acid concentration on corrosion of Monel alloy 400. (From Comley and Evans[13])

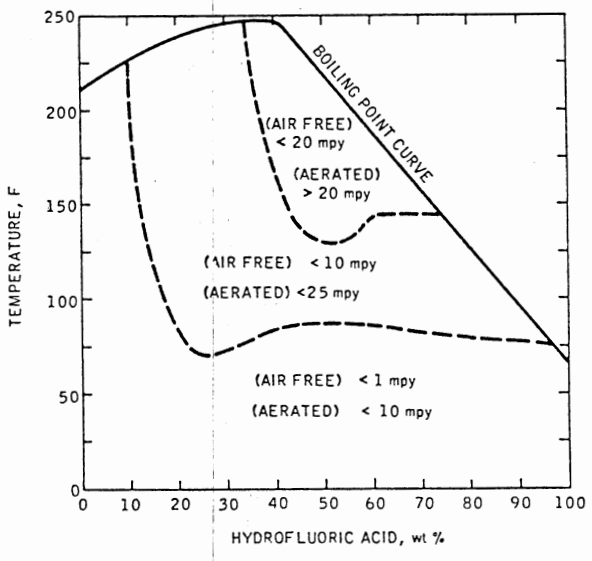

Figure 14. Isocorrosion chart indicating corrosion of Monel alloy 400 in hydrofluoric acid solutions. (From Comley & Evans[13])

However, since the common assumption is that SCC of Ni alloys is an elevated temperature phenomenon, only limited information is available. Table I supplies corrosion rate data for the effect of oxygen presence in boiling HF acid. Table II supplies limited room temperature data for the effect of HF on Monel 400 corrosion by H_2SiF_6. In each concentration, HF reduces the corrosion rate of H_2SiF_6. If SCC is dependent upon localized corrosion, then Monel will be more likely to fail in hydrogen fluoride than in hydrofluosilicic acid.

TABLE I

EFFECT OF OXYGEN ON CORROSION OF MONEL ALLOY 400 AND COPPER-NICKEL ALLOYD IN HYDROFLUORIC ACID (FROM COMLEY AND EVANS[13])

Purge gas nitrogen plus oxygen (ppm O_2)	Corrosion rate (mils/year)[a]					
	Monel alloy 400		70/30 copper-nickel		90/10 copper-nickel	
	Liquid	Vapor	Liquid	Vapor	Liquid	Vapor
BOILING 38% HYDROFLUORIC ACID 112 C (234 F)						
<5	9.5	6.8	3.5	3.2	2.4	2
<500	17	12	2.6	2.9	2.9	3
1500	31	49	12	43	11	53
2500	29	18	13	48	13	42
3500	34	54	18	54	17	61
4700	53	107	30	144	53	170
10,000	46	25	20	80	18	83
BOILING 48% HYDROFLUORIC ACID 108 C (226 F)						
<5	11	3	3	1	2	1
<500	22	4	7	12	—	—
1500	28	24	7	30	7	40
2500	27	9	13	42	11	54
3500	34	29	19	60	17	65
4700	43	83	22	91	29	118
10,000	48	75	29	132	36	156

[a] 4 day tests.

TABLE II

LABORATORY TESTS OF MONEL ALLOY 400 IN FLUOSILICIC ACID SOLUTIONS (FROM COMLEY AND EVANS[13])

Acid concentration (wt %)		Temperature		Corrosion rate (mils/year)
H_2SiF_6	HF	C	F	
10	0	24	75	3.7
10	30	24	75	2.4
20	0	24	75	2.4
20	30	24	75	2.2
30	0	24	75	1.1
35.2	0	24	75	1.5
22	0	80	175	15
22	2	80	175	9

• Test duration, 96 hr. No aeration.

Regardless of the preceding implications, only limited references of SCC occurrence in Monel are available. The conditions cited are highly variable. Each case will be discussed.

Case 1.[15]

The earliest case of stress corrosion cracking of Monel occurred years later. A 10x8x5 inch tank of 0.06 inch thick Monel, annealed to R_B = 71, containing 60% HF, was placed in a sink which intermittingly contained water. The corners eventually failed under TG cracking from the outside. No corrosion was evident.

Case 2.[15]

By 1944, it was accepted that Monel was susceptible to SCC by hydrofluosilicic acid. Results had led to the conclusion that SCC in high nickel alloys and Monel only occurred intergranularly. The cracking was typical of that cited by Copson and Cheng. Monel tubing, 0.84 inch OD,

Ø.11 inch thickness, R_B = 96, with a hoop stress near 31ksi, was used as a depth gauge for a 12Ø°F H_2SiF_6 (2Ø-25%) storage tank. The tube split over its entire length with the main crack being Ø.Ø2 inches wide. The same type of tubing fractured in just a few months when used to conduct the acid to a chamber containing the acid, its vapors, air, water, and carbon dioxide at 225°F. In each example, failure was IG.

Case 3.[62]

The publication of International Nickel Company in 1947 specified that only a few specific solutions would demonstrate SCC in its alloys. For Monel, fused caustic soda in concentrations greater than 75% can cause embrittlement. Stress relief annealing prior to exposure would prohibit cracking. It was also stated that there was substantially no difference between age hardened Monel K5ØØ and Monel 4ØØ.

Case 4.[15]

In 1948, Monel K5ØØ bolts failed due to SCC in a transgranular fashion in hydrofluoric acid vapor. This initiated intense investigation into the SCC of Monel. The bolts that caused the problems were 6 inches long, Ø.75 inch diameter, and completely threaded. They were used to fasten the external flanged joints of pipelines. Leaks in the pipe, which conducted atmospheric temperature anhydrous hydrogen fluoride, caused the bolts to fail in less than fifteen hours. Every thread root displayed cracks and a copper deposit was generally present. Bolts with the highest hardness (Rc = 36) failed under TG conditions while others (Rc = 31) failed while exhibiting both TG and IG.

Case 5.[15]

The investigation following the failures noted in case 4 revealed many characteristics. Test for 48% HF vapor were conducted at 14Ø°F.

Results showed that Monel 400 and K500 reacted similarly and that as the hardness was decreased, fracture proceeded from TG to IG. When numerous cracks occurred in an IG manner, the cracks would stop growing. Also, alloy additions of Si, Ni and Al had no significant influence.

Hydrofluosilicic acid vapor tests were also conducted. At 140°F, the environment from 30% H_2SiF_6 contained moisture, hydrogen fluoride and silicon tetrafluoride. Cracking results were identical to those exposed to HF vapors. Conversely, for immersion tests for both fluids, cracking only occurred after two weeks and then only for aerated conditions.

Case 6[15]

Copson and Cheng cite three more examples of the cracking of Monel exposed to HF. The basic fracture characteristics are the same as already noted. Additionally, cuprous oxide and metallic copper presence was noted. One of the examples failed by SCC although a high corrosion rate was experienced.

Case 7.[13]

In 1963, Comley and Evans noted that the resistance to corrosion for the Ni-Cu series was best demonstrated by the Monels. The use of Monel in HF media instead of steel had reduced shut-down periods significantly, even though SCC could be induced.

An interesting investigation demonstrated that Monel could suffer SCC in other environments at elevated temperature. Table III illustrates the cracking observed in 570°F hydroxides, and the relationship between condition, applied stress, and the type of cracking.

Case 8[35]

In 1966, Graf published results from extensive research conducted on Nickel base alloys by himself and his colleagues. This work is the first

TABLE III

STRESS-CORROSION TESTS ON MONEL ALLOY 400 AND MONEL ALLOY K-500 IN ALKALI HYDROXIDES AT 300 C (570 F) (FROM COMLEY & EVANS[13])

Alloy	Heat treatment[a]	Yield strength (ton/in^2)	Applied stress (ton/in^2)	Type and Degree of Cracking[b] NaOH	KOH
Monel 400	None, as cold drawn	43.8	33.1	1 IG	4 NI
	850C(1562F)/¼hr/WQ	12.8	10.3	5	5
Monel 400	Stress relieved, 540C (1004F)/½ hr	24.0	20.7	0 IG	0 IG
Monel 400	Works anneal, 950C (1742F)/½ hr	11.4	8.3	5	5
Monel K-500	None, as cold drawn	52.5	33.1	3 IG+ TG	5
	870C(1598F)/5min/WQ	21.2	10.3	5	5
	580C(1076F)/8hr/FC[c]	65.5	37.2	4 TG	5
	870C(1598F)/5min/WQ + 580C(1076F)/ 16hr/FC[c]	44.9	37.2	0 TG	0 IG
Monel K-500	None, as cold drawn	53.2	33.1	4 NI	
	870C(1598F)/5min/WQ	ND[d]	10.3	5	
	580C(1076F)/8hr/FC[c]	ND	37.2	0 IG	
	870C(1598F)/5min/WQ + 580C(1076F)/ 16hr/FC[c]	ND	37.2	0 IG	

[a] WQ = Water quenched; FC = furnace cooled.
[b] 0 = Specimen fractured; 1 = coarse cracks visible to naked eye; 2 = fine cracks visible to naked eye; 3 = deep cracks visible under microscope; 4 = shallow cracks visible under microscope; 5 = no cracks; TG = transgranular cracks; IG = intergranular cracks; NI = type of cracking not identified, cracks very short.
[c] Furnace cooled at about 10C(18F)/hr to 480C(896F), then air cooled to room temperature.
[d] ND = Not determined.

example of experiments conducted on other than U-bend samples of Monel.

The tests were conducted on thin, flat waisted specimens, 0.3 mm thick, 8

mm wide. The environments contained various concentrations of HF acid contaminated with CuO. The work confirmed that Monel is the alloy most susceptible to SCC in HF as the diagram in figure 15 illustrates. Also, the time to failure in 0.75MCuF_2+18MHF is almost constant for alloys containing 90 to 65% Ni. This may explain why earlier investigations (Case 5) found no deviation in SCC for Monel when the nickel content was increased by as much as 15%.

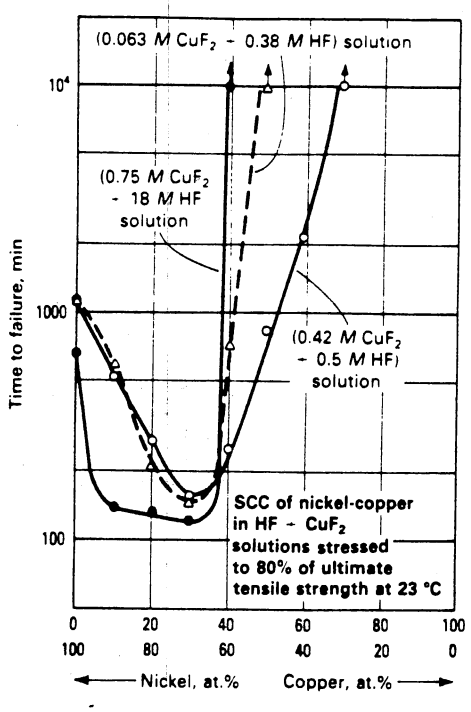

Figure 15. Time to failure of stressed nickel-copper alloys in HF + CuF_2 solutions (From Degnan[20], as modified from Graf and Wittich[35])

The tests also confirmed that severe cracking can occur at room temperature (Figure 16). The most embrittling environment occurred at Ø.Ø63MCuF_2+Ø.38MHF, with the pH being an important consideration. Fractographic tendencies were as noted previously.

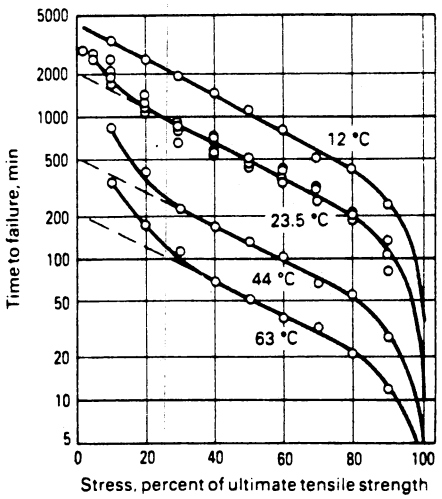

Figure 16. Effect of stress and temperature on SCC resistance of Monel 4ØØ in HF + CuF_2 solution. (From Degnan[2Ø] as modified from Graf and Wittich[35])

Case 9.

The remaining examples of SCC in Monel 4ØØ by HF do not extend any more information. A case is cited by McGuire[52] in 1986 that is typical of those cited by Copson and Cheng[15]. Degnan's work in the 1987 edition of

the ASM Metals Handbook[20] mentions that the presence of cupric chloride increases the cracking rate of Monel 400 in HF solutions. However, the reference noted is that of Graf and Wittich[35] discussed in Case 8. Graf's work involved cupric fluoride. Although it is possible that Degnan did not intend the mention of chloride, the compound is an oxidizer, as is cupric fluoride. Therefore, the possibility that the noted effect was intended should not be ruled out.

CHAPTER III

PROPOSED INVESTIGATIONS

3.1 Susceptibility at Room Temperature

From the preceding chapter, it becomes obvious that Monel can suffer stress corrosion cracking in room temperature environments. The environments cited for this temperature range involve the presence of hydrogen fluoride. Hydrofluosilicic acid vapors were noted as a problematic environment, but a natural component of such vapors is hydrogen fluoride. It is also recognized that the presence of cupric fluoride can enhance the embrittlement process. Therefore it is assumed that the damage induced by HF may require the presence of an oxidizer, perhaps in combination with an element nobler than Monel, such as copper. The first two objectives of this investigation have been achieved with these conclusions and the referenced cases of Chapter 2.

3.2 Immersion Tests

The preliminary experimental stage involves performing immersion tests. Prepared Monel coupons should be placed in selective corrosive solutions. The solutions will be selected based upon an anticipated corrosion behavior. The desired behavior will demonstrate only light or localized attack leading to slight pitting. If severe general attack occurs in a solution, stress corrosion cracks would not be anticipated.

Conversely, stress corrosion cracks would not be anticipated if the Monel demonstrates complete resistance in a solution. The following solutions were selected and illustrate the broad spectrum of environments to which Monel is commonly subjected.

It is assumed that no embrittlement of Monel occurs in normal atmospheric conditions. For such applications, the general corrosive attack on Monel is less than 0.001 inches per year (ipy). This rate, and subsequent noted rates, are quoted by Hoyt.[42] The atmospheric rate will be used as a minimal corrosive limit since some attack must occur. Yet, the attack must remain low, as stated earlier, for stress corrosion cracking to occur. Therefore, an arbitrary upper limit of attack will be set at 0.050 ipy.

It is desired that twelve solutions be chosen for the immersion tests. With the attack limits set, the spectrum limits should now be set. The major point of consideration is that Monel should be in standard use for the solutions considered. Also, a full range of pH values should be considered. Therefore, acids and bases will be selected.

Initially, a solution that is known to cause stress corrosion cracking on Monel, as determined by the literature review, will have to be considered. Additionally, it is stated in previous chapters that Monel is the Nickel alloy that is most susceptible to LME and HE. It has been assumed and theoretically supported in previous chapters that Monel will demonstrate the same behavior in SCC. Therefore, any solution inducing SCC in other Nickel alloys will be considered. Such environments are listed in Appendix A. Furthermore, environment solutions that drastically deviate in behavior as minor alterations in temperature and concentration occur should be investigated. It is anticipated that such solutions could

be devastating under proper conditions if the corrosion rate remains within the set limits. The solutions to be used are selected based on the following reasons. The rates of corrosion are supplied by Hoyt.[42]

1. Ammonium hydroxide; 27% at room temperature yields a Ø.Ø36 ipy rate. Nickel alloys are resistant to aqueous ammonia only in concentrations lower than 1%. All copper alloys are subject to SCC in this environment.
2. Ammonium Persulfate; 1Ø% at room temperature yields a rate noted as >2.9 ipy. This rate is over the set limit. However, the objective is to obtain an oxidizing acid salt environment. Copper sulfate (2-5%) results in a rate of Ø.Ø18. Since copper would be liberated by ammonia solutions, the persulfate seems a reasonable environment if the concentration is kept low. Additionally, numerous sulfur environments are noted for SCC in Inconel 6ØØ.
3. Hydrogen Peroxide; no rate is available, but it is presumed to be within limits, due to extensive use. The solution is considered to be a mineral acid with oxidizing agents. Therefore, it is in the same category as ferric or cupric contaminated acids. It is assumed, then, that this solution will be capable of inducing pits without general corrosive behavior. Furthermore, the effects due to the presence of oxidizing compounds have been noted previously.
4. Hydrofluoric acid; 6Ø% at room temperature yields a Ø.ØØ3 ipy. This solution is cited most often for causing SCC in Monel. It is also the most investigated solution.
5. Hydrobromic acid; no rate is available. Solutions contaminated

with 7A elements are often noted for inducing stress corrosion cracking. These elements include fluorine, chlorine, bromine, iodine, and astatine. Astatine is not commonly encountered. Iodine could conceivably cause discolorations that would inhibit extensive examination. It is assumed that hydrobromic acid would exhibit characteristics similar to hydrofluoric, but not so severe due to its larger molecular size.

6. Ferric chloride; 10% at room temperature yields a rate of 3.2 ipy. This rate is out of range. For application, the concentration should be kept low to reduce the general corrosive behavior. However, ferric chloride is a standard for tests determining pitting susceptibility.
7. Nitric acid; 5% at room temperature yields a 0.065 ipy. This acid demonstrates a highly variable nature. At elevated temperatures it is extremely corrosive, regardless of concentration. At room temperature, with a concentra tion below 0.5%, it is not corrosive. Also, it plays a major role in etchants for Monels. Therefore, selective attack is characteristic.
8. Hydrochloric acid; 20% at room temperature yields a 0.022 ipy. SCC of various Nickel base alloys subjected to salt contaminated hydrochloric acid has been noted. Additionally, 7A elements, noted previously, should be considered.
9. Acetic acid; glacial yields a rate of 0.0014 ipy. Organic acids typically show deviating behavior on Monel when the temperature is altered. Acetic acid also demonstrates selective etching capabilities.
10. Potassium chromate; A rate not available. The chromate offers

an oxidizing agent. The influence of potassium contamination is uninvestigated.

11. Lead chromate; rate not available. The chromate ensures an oxidizing environment. Lead salt contaminants are noted for SCC inducement in Ni-Cr-Fe alloys.
12. Lactic acid; 45% at room temperature yields a Ø.Ø2 ipy rate. This is a typical organic acid environment for Monel. Organic acids can drastically alter its corrosion rates on Monel as the temperature is increased.

Finally, although hydrofluosilicic acid vapors have been noted to cause SCC in Monel, it will not be considered. Since hydrogen fluoride is a typical constituent of the vapor, the HF solution and vapors should demonstrate any characteristic that H_2SiF_6 would demonstrate.

3.3 Slow Strain Rate Tests

Combining the conclusions of Section 3.1 with the experimental results for Section 3.2, appropriate environments will be prepared for further examination. The environments will be used for exploratory slow strain rate testing. Preliminary tests will be conducted to allow the variation of numerous parameters. The solution, strain rate, grain size, alloy and alloy condition will be altered. The effects of each alteration will be noted. Conclusions can then be drawn on anticipated damage to Monel subjected to various conditions. In addition, it can be determined which paraeter might offer the greatest conditional effect.

3.4 Confirmation SSRT

The testing procedure of 3.3 will determine a particular environment that proves to be most detrimental to Monel. That environment will be used for further investigation. This investigation will also utilize slow strain rate techniques. Within the chosen environment, parameters will again be altered. The variables will involve grain size, strain rate, cold work, and yield strength. The provisional conclusions drawn in Section 3.3 can then be verified.

CHAPTER IV

EXPERIMENTAL PROCEDURES

4.1 Immersion Tests

4.1.1 Material and Heat Treatment

Manufacturer's data, as noted in previous chapters, indicates essentially no difference in the corrosion behaviors of Monel 400 and Monel K500. Therefore, the immersion tests will be conducted on available Monel K500 sheet. Nominal composition of Monel K500 is listed below.

TABLE IV

CHEMICAL COMPOSITION OF MONEL K500

Element	Weight Percentage
Ni	63.7
Cu	30.2
Al	2.6
Fe	1.5
Mn	1.0
Si	0.3
C	0.2

Solution heat treated Monel K500 demonstrates properties relevant to those of Monel 400. The solution heat treated properties are tensile

strength = 96ksi; yield strength = 51ksi; Rockwell hardness (B scale) = 79; and strain hardening exponent, n = 0.35. The material will be a cold rolled, solution heat treated sheet with a sample grain size of approximately 25 μm. Sample coupons of approximately 25 mm x 12 mm dimensions are to be cut from a 1.5 mm thick sheet.

4.1.2 Surface Preparation and Condition

The coupons will be sanded through a 600 grit finish. Further mechanical polishing, through 0.05 μm alumina using flooded wheels at low speed, will remove any detectable abrasion damage. The samples are then chemically polished in an 85^{o}C solution containing

30 ml nitric acid,

10 ml sulphric acid,

10 ml orthophosphoric acid,

50 ml glacial acetic acid.

The samples are to remain immersed in the polish solution for a minimum of thirty seconds and a maximum of sixty seconds. Sample dimensions and weights are to be noted subsequent to final polish.

4.1.3 Test Procedure

Individual sample coupons are to be placed in 50 ml containers with 30 ml of prepared solution. The solutions are to remain stagnant at all times. Coupons will be removed periodically for observation.

4.1.4 Observation and Measurement

Each coupon will be examined in solution every ten minutes for the first hour of testing, but removed on the half hour for closer scrutiny. After the first hour, each coupon will be examined on the half hour, removed from solution each hour, for the next five hours. Subsequent examination will occur each hour, removing the sample from solution only as necessary. Tests demonstrating extensive attack will be terminated. Otherwise, testing may continue for thirty hours.

Each sample removed from solution for examination will be thoroughly rinsed with water, then sprayed with Methanol and dried with forced warm air. As each test is terminated, the samples will be vigorously rinsed in water, followed by ultrasonic cleaning while immersed in Methanol. Coupons will then be dried with forced warm air. Final examination will include determining final weight.

4.2 Slow Strain Rate Tests

4.2.1 Material

The slow strain rate tests will be conducted primarily on Monel 400 with subsequent tests on K500. The 400 alloy offers a readily variable grain size. It also has the ability to be strengthened by cold work. The K500 alloy permits a high yield strength without cold work. Nominal composition of Monel 400 is listed in Table V.

TABLE V

CHEMICAL COMPOSITION OF MONEL 400

Element	Weight Percentage
Ni	65.47
Cu	31.97
Fe	1.16
Mn	1.01
Si	0.19
C	0.15
Al	0.05
S	0.002

The material is cold drawn, stress relieved, 12.7 mm diameter bar from Huntington Alloy. The heat number is M1604B, lot 1A. The Monel 400 bar properties are tensile strength = 113ksi; yield strength = 95ksi; Rockwell hardness (B scale) = 97; and strain hardening exponent, n, = 0.36.

As illustrated in Figure 17, the tests are to be conducted on waisted tensile specimens which have a minimum diameter of 6.35 mm. This corresponds to a minimal cross sectional area of 30.68 mm^2. The waisted specimen will allow the presence of a strain gradient along the gage length. Therefore, a damage gradient is anticipated. The extreme of the damage gradient should illustrate a MVC fracture, adjacent TG cracking, and IG cracking near the shoulders. The strain at different locations can be measured directly on a specimen subsequently. The proposed geometry will ensure a localized fracture zone. Additionally, the geometry is identical to the geometry used by King[45] and Fredell[29], facilitating comparison.

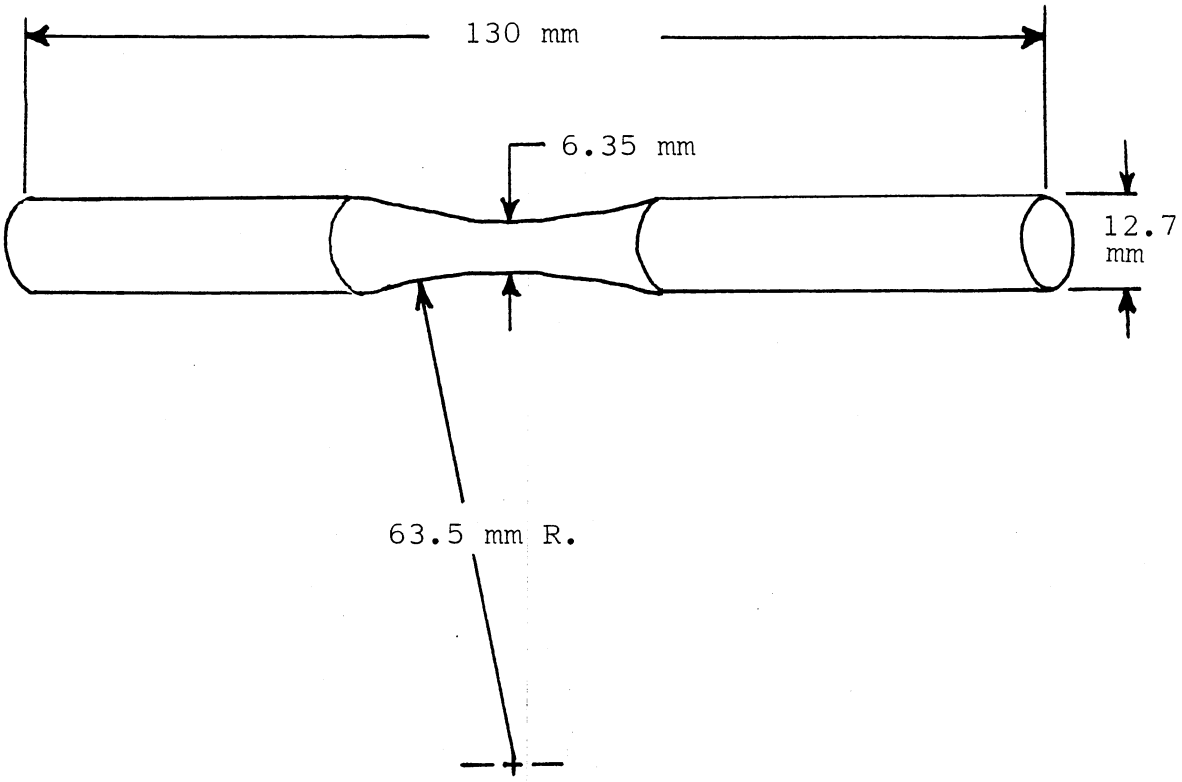

Figure 17. Slow Strain Rate Sample Geometry
(From King[45], p. 44)

4.2.2 Heat Treatment

Heat treatment will be varied to obtain several conditions. The treatment ensures different hardness and grain sizes. Test samples are to be treated in a vacuum oven, under 13 to 15 Pa pressure. Oven temperatures, treatment duration, and approximate resulting grain sizes are listed in Table VI.

The duration is noted for length of time at full temperature. Oven heat-up time was forty-five minutes. The grain sizes correspond to the conditions set up by King[45] and Fredell.[29] All samples were furnace cooled to room temperature.

TABLE VI

VACUUM ANNEALING SCHEDULE FOR MONEL 400
(AFTER KING[45])

Time (hr)	Temperature (C)	Grain Size (μm)
as received	---	25
1.25	750	35
2.25	750	50
3	750	100
3	1050	250
4	1050	350
12	1050	500

4.2.3 Surface Preparation and Condition

Disagreement occurs regarding the role of surface condition in corrosion attack. It is generally, but not universally, agreed that machining marks leave the surface with built-in stress risers. Such a condition will enhance localized corrosion attack and, subsequently, induce SCC. However, if a material is considered resistant to an environment, as Monel often is, and the material is annealed to relieve the machining stresses, the surface condition may not play a significant role. The point is debatable. Therefore, preliminary tests may be conducted without altering the surface condition.

Generally, though, a standard preparational procedure will be followed.

1) Machine finished sample will be washed with water and then swabbed with trichlorethylene.
2) The sample will be heat treated under vacuum conditions for 1.25 hours at 750°C, and furnace cooled (differing schedule for varied grain size, as discussed previously).

3) The sample will be mechanically polished through a 600 grit finish, over the entire waisted section.

4) The sample will be further polished and lightly etched by submersion in a 50/50 solution of nitric acid and acetic acid, duration of forty-five seconds.

5) The sample will then be rinsed in water, flooded with methanol, and then dried with forced warm air.

4.2.4 Test Procedure

All slow strain rate tests will be conducted on an MTS machine at room temperature. The testing shall be conducted under displacement control conditions. Stroke control will be set at 100% to allow a full tensile stroke of three inches. The strain rate will be determined from ram displacement rate specifications. To remain well within the previously noted strain rate limits, the ram speed will be allowed to deviate between $3.6(10^{4})$ and $1.8(10^{6})$ seconds for a three inch ram displacement. The corresponding strain rate will vary between $3(10^{-5})$ and $6(10^{-7})s^{-1}$. The orders of magnitude of these rates are comparable to those cited in tests of Monel for LME and HE.

Preliminary tests will be conducted in air. This test will permit direct measurement of strain experienced at different gage length locations. Also, the standard cup and cone fracture surface will serve as a comparison basis for subsequent test fractures.

Subsequent tests will be conducted in active environments. The environments will be confined to the waisted portion of the sample. A diagram[45] of the environment chamber is supplied in Figure 18. The chamber is constructed with a resistant plexiglass body. A neoprene O-ring

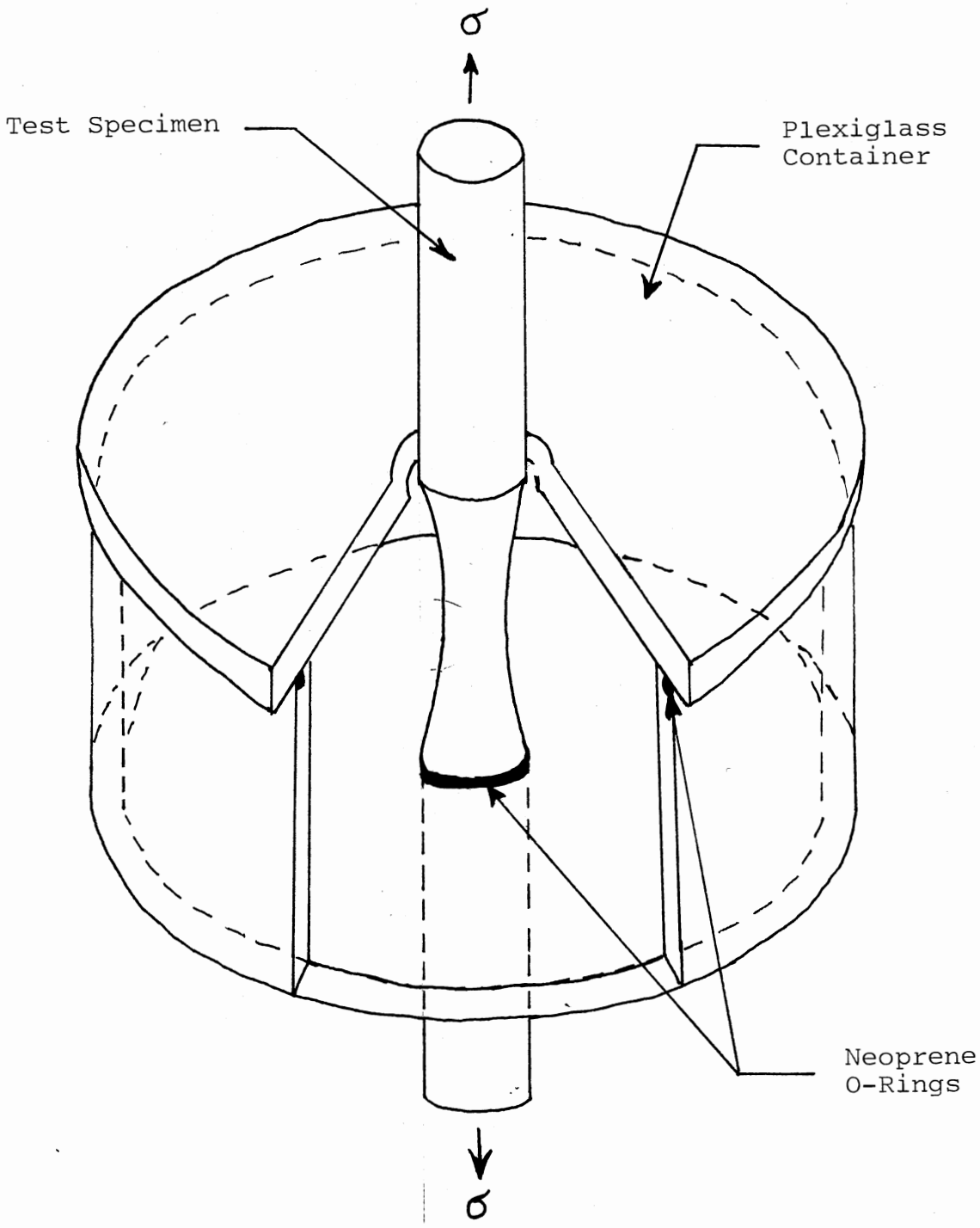

Figure 18. Environmental Chamber Used in Stress Corrosion Cracking Tests (After Fredell[29])

embedded in the bottom layer of plexiglass ensures the maintenance of a tight seal. The lid contains a half inch diameter opening. When placed on the sample body, the top of the test chamber falls below the upper shoulder. This leaves a gap between the sample and the container's lid. The gap supplies sufficient room for the addition of the environment fluid.

Three other variable effects will be examined. First, some tests will be conducted with the test chamber only partially filled. This will allow the examination of a liquid phase effect, a vapor phase effect, and the interface effect. Secondly, some tests will be conducted under conditions of aeration. Oxygen will be forced into the test solution at a constant rate. This will allow the examination of the effects of aeration and agitation. Lastly, some tests will be conducted under a zero ram displacement rate. A prestrain will be placed on the sample and the ends held at the resulting position. This will determine the effect of a zero strain rate.

Once a test is complete, the sample will be removed from the test chamber. The sample will then be washed with water and flooded with methanol. Further cleaning will be accomplished with the sample placed in an ultrasonic cleaner while immersed in trichlorethylene. The sample will be subsequently dried in still air and placed in a desiccator.

4.2.5 Observations and Measurements

All specimens will be observed under a Bausch & Lomb stereoscopic zoom microscope (SZM) at magnifications up to 70X. Pertinent samples will be sectioned and mounted. The mounted samples will be viewed under a Reichert optical microscope. Other selected specimens will be sectioned for examination in a Jeol Model 35 Scanning Electron Microscope (SEM).

All pertinent observations will be recorded. Characteristic cracking features will be photographed.

CHAPTER V

EXPERIMENTAL RESULTS

5.1 Immersion Tests

The results of the immersion tests are summarized in Table VII. It should be noted that the corrosion rates illustrate an extreme deviation from those suggested by Hoyt[42] in Chapter 4. However, the concentrations are similar. It appears that, when determining proper solutions for the slow strain rate tests, the limiting corrosion rates must be modified. Numerous examples of stress corrosion cracking in Monel, when subjected to Hydrogenfluoride, were noted in Chapter 2. Thus the corrosion rate limits will be reset to the order of magnitude demonstrated by the immersion test for Hydrofluoic Acid. Proper solutions for continued testing also rely on a preference of localized or pitting attack. A summary of conclusions regarding appropriate behavior is contained in Table VIII. Three environments were deemed appropriate for the slow strain rate tests:

1) Ammonium Hydroxide (NH_4OH),

2) Ammonium Persulfate ($(NH_4)_2S_2O_8$),

3) Hydrofluoric Acid (HF).

As Sodium Hydroxide (NaOH) is often detrimental at elevated temperatures, it will also be tested.

TABLE VII

IMMERSION TEST RESULTS

TEST NO.	SOLUTION CONCENTRATION	CORROSION RATE mpy (ipy)	OBSERVATIONS
1	Ammonium Hydroxide 29%	23.74 (Ø.93)	selective attack shows darkened patches
2	Ammonium Persulfate Ø.175 M	1Ø9.34 (4.3Ø)	severe general corrosion after 1 hr of no reaction
3	Hydrogen Peroxide 1Ø%	3.Ø2 (Ø.12)	immediate gas release subsequent polishing with emphasized scratches
4	Hydrofluoric Acid 26%	51.79 (2.Ø4)	fuzzy sediment precedes localized attack with subsequent general corrosion
5	Hydrobromic Acid 12%	29.96 (1.18)	no visual reaction, sample brightened under presumed general attack
6	Ferric Chloride Ø.125 M	32.Ø2 (1.26)	general corrosion attack forming dark scale
7	Nitric Acid 28%	2952.5Ø (116.24)	immediate reaction forming green film, subsequent darkening
8	Hydrochloric Acid 19%	14.67 (Ø.58)	scratches darkened initially, subsequent scale loosens and precipitates
9	Acetic Acid 2Ø%	2.7Ø (Ø.11)	slight discoloration with darkened scratches
1Ø	Potassium Chromate Ø.15 M	6.47 (Ø.26)	immediately forms pale yellow powder, subsequently precipitates, leaving material mottled
11	Lead Chromate Ø.1 M	26.98 (1.Ø6)	bright polishing with subsequent pits
12	Lactic Acid 1Ø%	-3.63 (-Ø.14)	No color change, scratches pronounced, shallow pits

TABLE VIII

CONCLUSIONS REGARDING THE CORROSION ATTACK OF IMMERSION SAMPLES

TEST NO.	SOLUTION	DECISION	REASON
1	NH_4OH	use	corrosion rate within range, selective attack
2	$(NH_4)_2S_2O_8$	use	initial reaction shows very low corrosion; reduce concentration to reduce subsequent reaction
3	H_2O_2	don't use	corrosion rate too low
4	HF	use	"control" solution, intermediate reaction is localized attack
5	HBr	possible	corrosion rate within range, but attack was general
6	$FeCl_3$	don't use	corrosion rate within range, but no pits observed, only general attack
7	HNO_3	don't use	corrosion rate too harsh, concentration was too high
8	HCl	don't use	corrosion rate is a bit low, also anticipate problems with the sediment
9	CH_3COOH	don't use	corrosion rate too low
10	$K_2CrØ_4$	don't use	corrosion rate too low; also, solute precipitates, concentration unstable
11	$PbCrO_4$	possible	corrosion rate within range, also formation of pits, but sediment could be a problem
12	$CH_3CH(OH)CO_2H$	don't use	pits noticed may be strictly associated voids in the obvious scale formation, scale analysis would be necessary

5.2 Initial Slow Strain Rate Tests

All test specimens exhibited a cup and cone fracture surface. Each sample was subsequently examined under the stereoscopic zoom microscope (SZM). Most of the test samples exhibited limited stress corrosion cracking. The slowest strain rate used, $\dot{\epsilon} = 1.2(10^{-6})s^{-1}$, induced the greatest amount of cracking in all environments. This strain rate was often sufficient to cause limited propagation. Yet, it was insufficient to cause total propagation before the tensile strength in air was exceeded. Observations from the SZM for each environment are as follows.

5.2.1 Sodium Hydroxide (0.25M)

Fused sodium hydroxide can cause stress corrosion cracking in Monel at elevated temperatures. It has not been determined to cause SCC at room temperature. One sample was tested in an environment of 0.25M NaOH for elimination purposes. The test was conducted at a strain rate of $\dot{\epsilon} = 1.2$ (10^{-6}) s^{-1} on a fine, 35μm, grain size specimen. There was no indication of cracking or corrosion.

5.2.2 Ammonium Persulfate (0.175M)

Four tests were conducted in this environment. The grain size was varied through heat treatment to determine possible affects. A strain rate of $\dot{\epsilon} = 6.7$ (10^{-7}) s^{-1} was used for all four tests.

An as received sample, with a grain size of 25μm, HRB = 95, was tested first. The test sample suffered numerous pits. However, no discernable cracking could be noted under the SZM.

A test sample with a grain size of 250 μm, HRB = 53, was tested subsequently at the specified strain rate. The sample developed a large

amount of black deposit. Under the deposit, and in its vicinity, the sample surface suffered numerous, but very shallow, transgranular cracks.

Two slow strain rate tensile tests were conducted on coarse grains. The samples were approximately 350 μm and had HRBs of 39 and 40. Stress corrosion cracking was induced in each of the samples. Near the shoulders of both samples, the cracking was conspicuously intergranular. The cracking gradually changed to transgranular as the fracture location was approached. The cracks blunted in the zone of plastic deformation. The fracture surfaces showed cup and cone failures. General corrosion over the sample surface was also noted. The sample with the HRB = 40 was later viewed under the scanning electron microscope (SEM).

Several of the SEM photographs are supplied to illustrate the damage to the test sample. Figure 19 is a view of the sample surface near the fracture. It can be seen that minor grain rumpling only occurred near the fracture. The extent of general corrosion can be seen in Figures 20 through 22. The photographs are details of the sample surface, proceeding from the fracture to the outer right hand end as depicted in Figure 19. Near the fracture, extensive corrosion, severe grain etching, and slight cracking parallel to loading direction occurs, associated with grain boundaries.

Figure 20 details the surface farther away from the fracture. Intergranular cracking has begun to occur with the general corrosion. The cracks are fine, with only occasional grains being separated. Figures 21 and 22 were taken at the right hand end. Many of the grains have been separated.

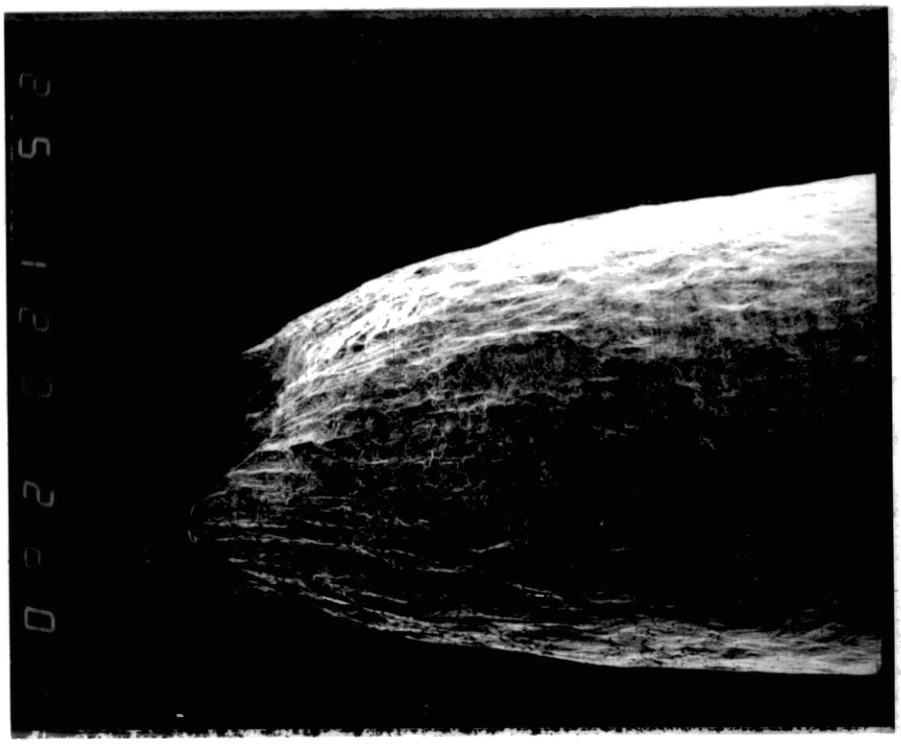

Figure 19. Ammonium Persulfate fracture zone. The ductile failure illustrates extensive plastic deformation with no discernable cracking at this magnification; X 12

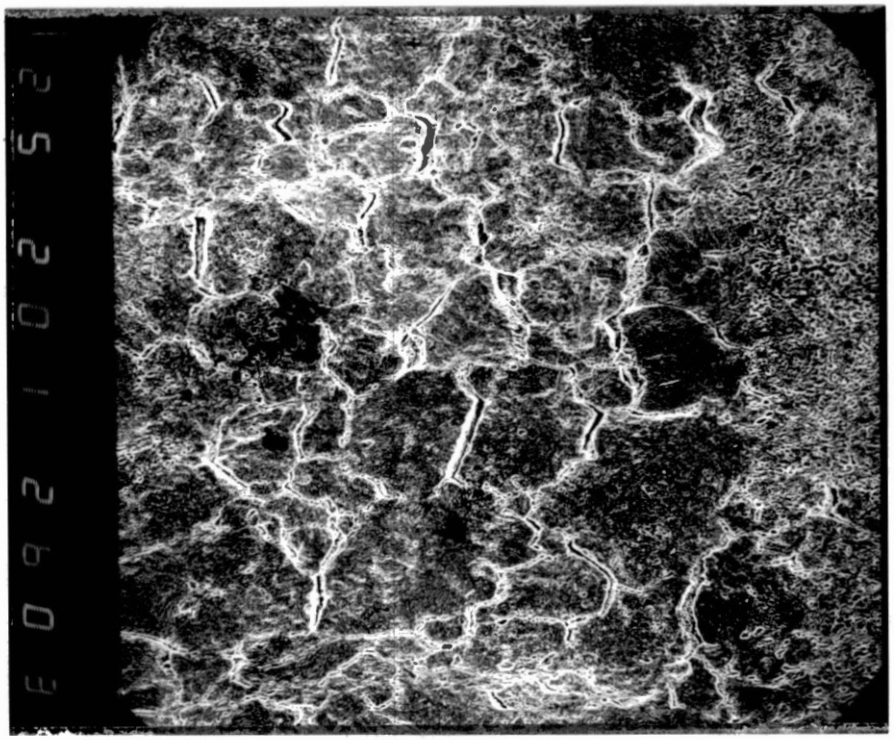

Figure 20. Ammonium Persulfate sample details of Figure 19. The details of the surface, away from fracture vicinity, show pitting but only minor deformation. IG cracking is obvious; x 200.

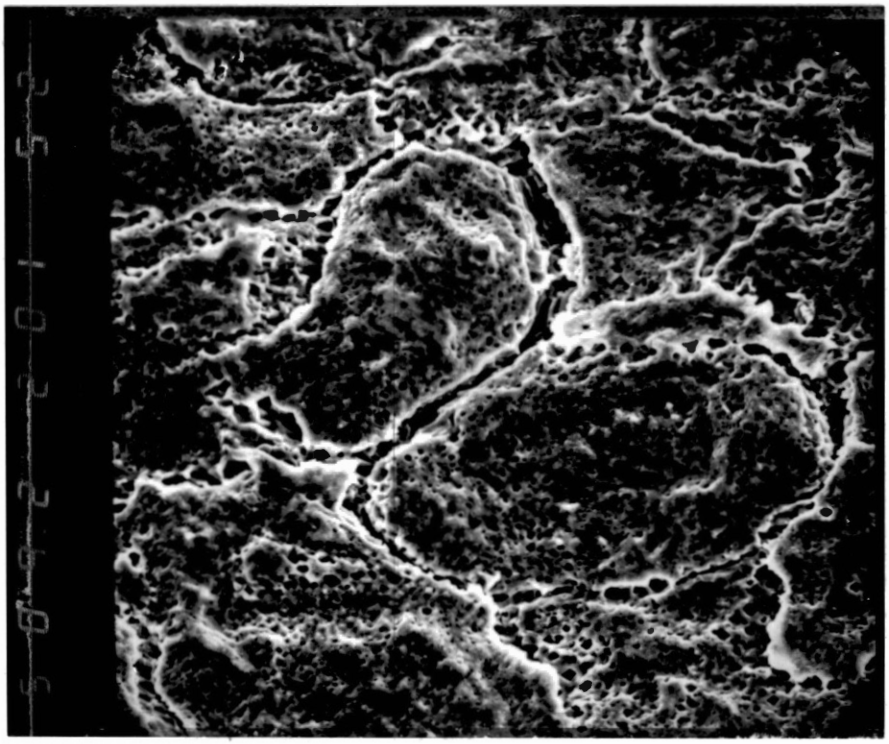

Figure 21. Ammonium Persulfate sample details bordering the shoulder area. IG cracking and pitting are obvious; X 1000.

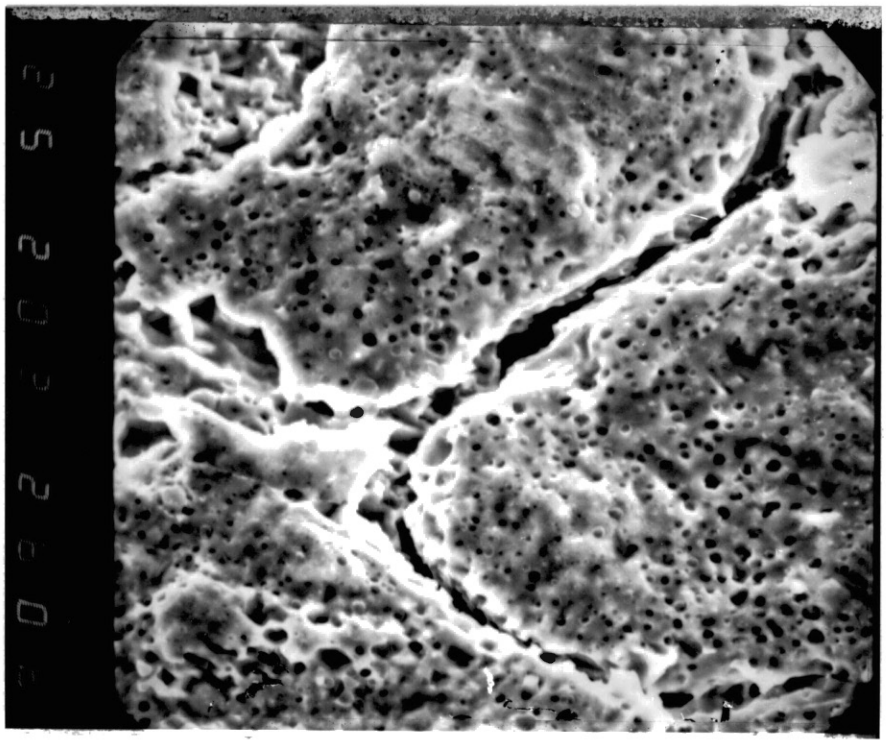

Figure 22. Ammonium Persulfate sample details of Figure 21. The photograph emphasizes the pitting attack of the grains, the pitting nature of the IG cracking, and the complete absence of TG cracking; X 2000.

5.2.3 Ammonium Hydroxide (29% and 15%)

A total of seven specimens were tested in Ammonium Hydroxide. The series allowed numerous variables to be tested. Three grain sizes and four strain rates were examined. The first four tests were conducted in 29% NH_4OH.

The first test was conducted on an as received sample. The sample hardness was HRB = 1Ø3, and the grain size was approximately 25 μm. The test strain rate was set at $\dot{\epsilon} = 6.7\ (1Ø^{-7})\ s^{-1}$. The sample showed general corrosion occurring with a black discoloration. Subsequent examination under the SZM revealed no stress corrosion cracks. The fracture was cup and cone.

The next three tests were conducted on coarse grain specimens, 25Øμm, HRBs = 5Ø. The three tests were run with 29% NH_4OH. All three specimens demonstrated cracking characteristics similar to the results obtained with a coarse grain test in Ammonium persulfate, but to a slightly lesser degree. Stress corrosion cracking occurred with shallow IG cracks near the shoulders. The cracks progressed to TG in the higher strained regions near the center of the gage length. The upper halves illustrated the characteristics noted. However, the lower halves suffered more extensive general corrosion, leading to black deposits. Pitting also occurred in the lower halves. The lower halves were constantly submersed in the test solution while the upper halves were subjected to solution vapors. One test was concluded without fracture, prior to necking, for examination.

Three further tests were conducted on fine grain size, 35 μm, specimens in a solution concentration of 15%. The strain rate was varied from $3.Ø\ (1Ø^{-5})\ s^{-1}$, to $6.Ø\ (1Ø^{-6})\ s^{-1}$, to a minimum rate of $1.2\ (1Ø^{-6})\ s^{-1}$. Compared to the 29% tests, the SZM showed a marked decrease in the

extent of cracking. By reducing the concentration to only 15%, no cracking was evident on the two faster strain rates. Only the sample tested at the slowest rate, 1.2 (10^{-6}) s^{-1}, showed mild intergranular cracking.

5.2.4 Hydrofluoric Acid

Although Monel is used extensively in Hydrofluoric acid environments, it has been known to fail, particularly when exposed to air contaminated with Hydrofluoric vapors. The situation was investigated for a sample with a coarse grain size of 500 μm, placed in a 26% solution of HF. The test was conducted at the medium strain rate of 6.0 (10^{-6}) s^{-1}. The fracture surface was completely immersed in the fluid and resulted in a cup and cone failure. The test exhibited no cracks in the necked region except for a few slip band cracks, which is usual for tests conducted in air. Some minor pitting occurred on the immersed section. Interestingly, slight localized IG cracking was noted at the top shoulder zone. This zone was above the liquid interface.

5.2.5 Hydrofluoric Acid and Copper Chloride

A series of four tests was conducted in the acid solution contaminated with Copper Chloride. Due to the difference between the immersion zone and the vapor zone, as noted above, the test specimens were subjected to a liquid zone to just above the waist. Each of the tests will be considered individually.

1) The test was conducted on a 350 μm grain size sample, with a hardness of HRB = 47, at a strain rate of 4.08 (10^{-6}) s^{-1}. A solution of 18M HF with 0.5M $CuCl_2$ was used. A cup and cone fracture occurred. The interface zone was covered with a green caked salt that demonstrated no

cracking. The lower fracture surface contained extensive crystal deposits, and the grain boundaries showed an IG outline. The grain boundaries on the upper half were attacked and outlined from the shoulder towards the neck.

2) The test was conducted on a 100 μm grain size sample, with a hardness of HRB = 49, at a strain rate of 9.74 (10^{-6}) s^{-1}. A solution of 1M HF containing 0.5M $CuCl_2$ was used. A cup and cone fracture occurred. The interface zone was covered with bright green salt and dark solution marks. Tight single grain TG cracks occurred in the interface zone. At the shoulders, IG cracking was illustrated in several grains.

3) The test was conducted on a 100 μm grain size sample, with a hardness of HRB = 52, at a strain rate of 3.26 (10^{-6}) s^{-1}. A solution of 0.5M HF containing 0.125M $CuCl_2$ was used. A cup and cone fracture occurred. The sample was covered with a dark green and black scale that was incompletely salt encrusted. Extensive cracking occurred at the shoulders.

4) The test was conducted on a 100 μm grain size sample of Monel K500, with a hardness of HRB = 66, with a strain rate condition of 3.26 (10^{-6}) s^{-1}. A solution of 0.5M HF containing 0.25M $CuCl_2$ was used. A cup and cone fracture occurred. The solution area was darkened, and salt was encrusted on approximately 6.5mm of the sample below the necked region of the lower half. The scale is pitted, going to cracks and severe corrosion. The elongated grains on the upper necked region have shallow pits, with shallow 45^{o} grooves near the fracture. The shoulders showed extensive cracking.

5.2.6 Hydrofluoric Acid and Copper Fluoride

A series of four tests was conducted in the acid solution contaminated with Copper Fluoride. Some the test specimens were subjected to a vapor zone above the waist. Each of the tests will be considered individually.

1) The test was conducted on a 350 μm grain size sample, with a hardness of HRB = 43, at a strain rate of 3.62 (10^{-7}) s^{-1}. A solution of 0.38M HF with 0.063M CuF_2 was used. A cup and cone fracture occurred. The immersed area was covered with a slightly darkened scale. The upper half contained a powdery blue salt. The sample was entirely covered with small gaping cracks. The surface cracking looked like fish scales under the SZM. The cracks blunted as the zone of plastic deformation took over, leading to fracture.

2) The test was conducted on a 500μm grain size sample, with a hardness of HRB = 48. The sample was loaded to approximately 30 ksi (about 0.3TS), and held for ninety hours in a solution containing 0.38M HF and 0.125M CuF_2. Failure did not occur. Copper was plated out near the upper edge of the liquid interface. Salt was present in conjunction with the copper flash. A copper oxide scale bordered the salt. The upper half had pronounced grains, but no cracking occurred. All evidence of the machining marks wa eradicated from the upper half of the test section.

3) The test was conducted on a 250μm grain size sample, with a hardness of HRB = 48, at a strain rate of 6.0 (10^{-6}) s^{-1}. A solution of 26% HF was used. The test continued until the load reached about 75% of the tensile strength, 70.7 ksi. At this point the sample was removed from the test environment. Only slight grain rumpling had occurred. The sample showed slight discoloration at the upper shoulder where the solu-

tion had been applied. Dusty patches of salt had collected on the upper half and were easily wiped away.

4) The test was conducted on the sample of Monel 400 noted in test 3, above. The sample was subjected to a solution containing a mixture of 26% HF and 0.05 M CuF_2, at a strain rate of 6.0 (10^{-6}) s^{-1}. The environment chamber was filled. A brown powdery scale formed near the shoulder of the upper half. The powder was easily wiped away, revealing a deep red, coppery sheen. The fracture was completely ductile, illustrating extensive grain rumpling. Slight side cracking occurs occasionally near the lower plastic deformation zone. The cracking appears to be IG.

5.2.7 Aerated Hydrofluoric Acid

In view of the preceding tests, a series of four tests were conducted under the condition of aeration. A strain rate of $3.62(10^{-6})S^{-1}$ was used for each test. The specimens were subjected to 26% hydrofluoric acid solution up to the waist. Air was bubbled through the solution at a constant rate.

1) The test was conducted on the 500 μm grain size specimen listed as number 2 in the previous section. The surface finish was sanded and polished to remove any prior damage. Once the stress reached 60 ksi, the displacement was stopped. The sample was then subjected to a twelve hour hold period at the constant load. Subsequently, the displacement was resumed and the strain rate was observed till fracture occurred.

Examination revealed extensive gaping cracks that advanced to a depth of approximately three grains. IG cracking occurred at the shoulders. Several of the cracks contained a white grainy deposit.

The sample was also examined under the SEM. Two photographs of the

fracture surface are supplied, Figures 23 and 24. Figure 24 is a magnification of the detail of the lower outer edge seen in Figure 23.

2) The test was conducted on a 250 μm grain size sample, with an HRB = 47. The environment chamber was filled with the acid, up to the waist, with air bubbled through the solution. The test sample was loaded to a stress of 60 ksi and held at that point for seven hours before loaded to fracture. The fracture sections resulted in very shallow IG cracking at the shoulders, proceeding to shallow, blunted TG cracks in the plastic deformation zone. The section that had been immersed in the fluid suffered corrosion at slip bands, and it was covered with a green scale.

3) The test was conducted on a sample identical to the one used for test 2. However, the strain rate control was continued without any delayed hold time. The immersed section blackened while the upper section was rainbowed with reds and greens. Only the early stages of TG cracking could be noted, near the zone of deformation.

4) The test was conducted on an as received sample which had a hardness of HRB = 95. Patches of dark scale formed on the lower section, with brown areas on the necked region. The failure was cup and cone. No cracking or pits were detected, and the machining grooves did not show preferential attack.

5.3 Standard Solutions Tests

Although cracking has been demonstrated in most of the tests examined thus far, the HF contaminated with CuF_2 combination has caused the most conspicuous cracking. In static loading tests, Graf and Wittich[35] found the composition of 0.38M HF + 0.063M CuF_2 caused the most rapid failure in Monel. This solution was used for exploring the trends with selected

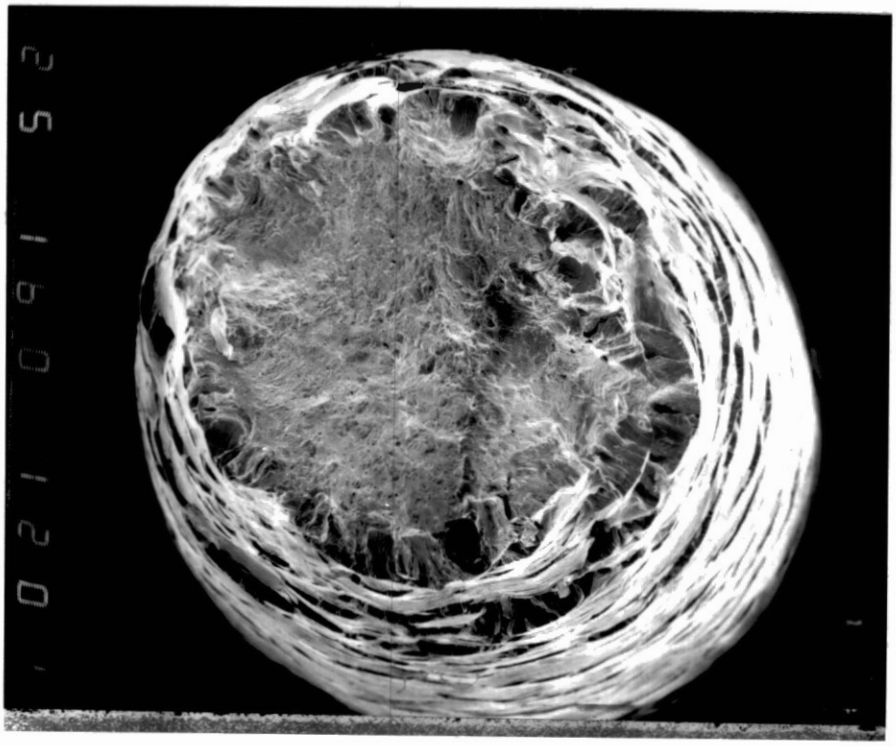

Figure 23. Aerated HF solution sample with TG cracking rim about one grain deep; X 16

Figure 24. Aerated HF solution sample fracture, details of bottom of Figure 23. Transition region from TG to MVC illustrates extensive degree of plastic deformation associated with TG cracking, occasional secondary cracking; x 330.

materials and variables. The grain size of 35 μm was used routinely with a strain rate of 1.2 (10^{-6}) S^{-1} unless stated otherwise.

All subsequent test failures occurred with a cup and cone fracture. The tensile strength corresponded to that of tests completed in air. Both halves of the fractured samples were examined under the SZM. Occasionally, the characteristics of the two halves of a sample differed. The major differences occurred near the shoulders of the upper half, corresponding to the vapor zone above the liquid interface. To permit comparisons, the observations for each test emphasize the nature and extent of the side cracking. When appropriate, the examinations were completed under the SEM.

5.3.1 Variable Strain Rate

A series of three strain rates was examined, ranging from 1.2 (10^{-6}) to 6.0 (10^{-6}) to 3.0 (10^{-5}) S^{-1}. SZM observations revealed extensive TG side cracking for the two slower strain rates. The cracks extended about 18 mm from the fracture location. The upper halves showed a pale blue crystalline deposit rim at a distance of 16 mm above the fracture. The deposit corresponds to the location of the liquid vapor interface. At this location, there was no distinct variation in the crack appearance.

Comparison between the tests of the slower strain rates revealed a similar extent of cracking. The cracks, however, were smaller in the 6.0 (10^{-6}) S^{-1} test. Indeed , with a further increase of the strain rate, to 3.0 (10^{-5}) S^{-1}, there was more general corrosion, with broad, shallow depressions, leading towards pits. Only a few shallow transverse cracks, within 6 mm of the fracture, were noted.

The three specimens were examined under the SEM. It was confirmed

that the extent of cracking decreased with an increase in the strain rate. The lowest strain rate induced shallow IG cracking 12 to 16 mm from the fracture. In the same zone, on the intermediate strain rate sample, only the occasional beginnings of IG cracking was noted. The sample subjected to the fast strain rate showed preferential pitting associated with the grain boundaries, but no evidence of IG cracking.

The transgranular cracks noted previously were more pronounced under the SEM using magnifications greater than X 50. The following series of SEM photographs illustrate the major points of interest. It is also noted that, contrary to the characteristics of the ammonium persulfate tests, the IG cracks are not associated with pitting.

5.3.2 Prior Cold Work

Two tests were conducted to determine the effects of cold work. The tests were run under the most damaging strain rate, determined in the previous section to be 1.2 (10^{-6}) S^{-1}. The first utilized an as received sample of Monel 400. With a hardness of HRB = 97 and a grain size of 25 μm, the sample obviously contained cold work. When the fractured specimen was viewed under the SZM, cracks were shown to be present within 10 mm of the fracture location. An examination of the fracture surface revealed a distinct border of TG cracking. The border was 0.2 - 0.5 mm deep. The sample was subsequently examined under the SEM and compared to an annealed, 35 μm grain size, sample run previously under the same test conditions. Both samples displayed similar side cracking but to a lesser extent in the cold worked sample. Also, the cold worked sample did not show any IG cracking. The test sample is also presented in the next section for comparison with a Monel K500 test.

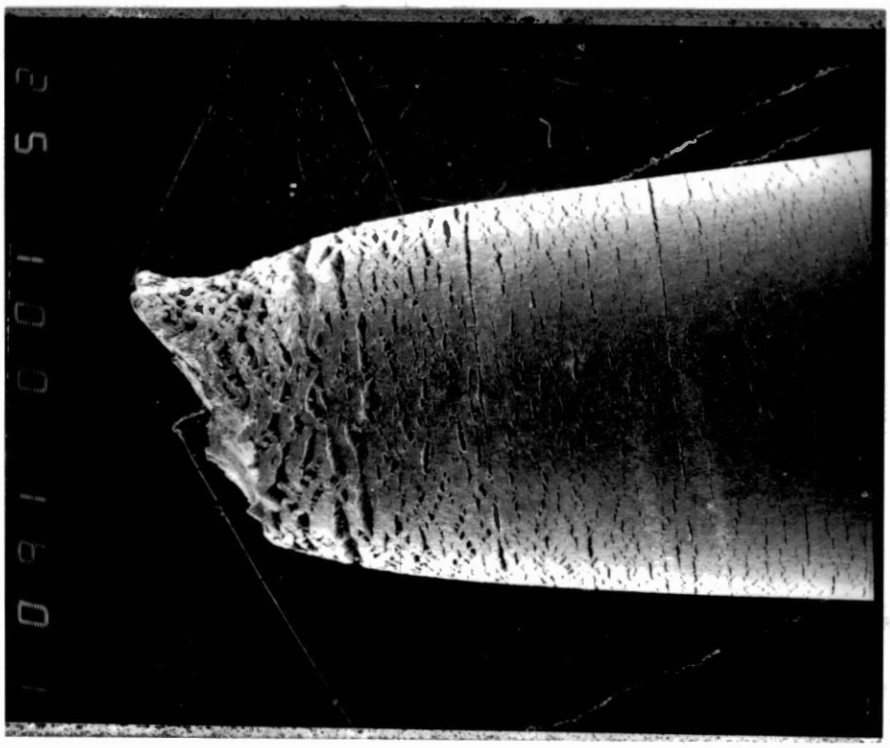

Figure 25. Slow rate test sample side view of fracture zone. Extensive transverse cracking with gaping is seen in the fracture vicinity. Except where associated with machine grooves, cracks are short and wavy; X 10.

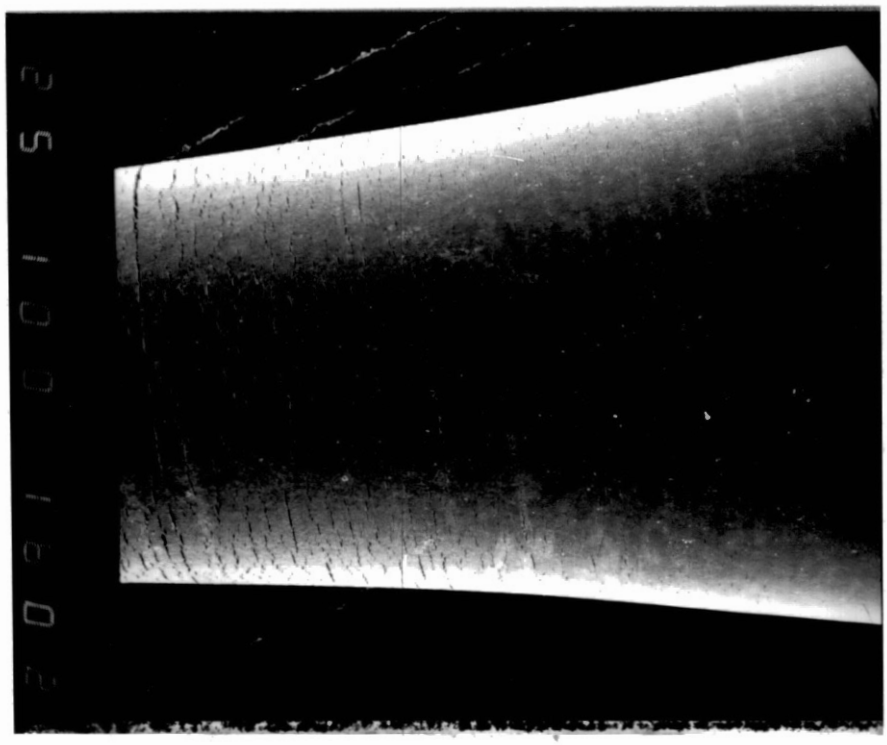

Figure 26. Slow rate test sample side view near shoulder. The matching groove on the left is seen in Figure 25. The cracking continues; X 10.

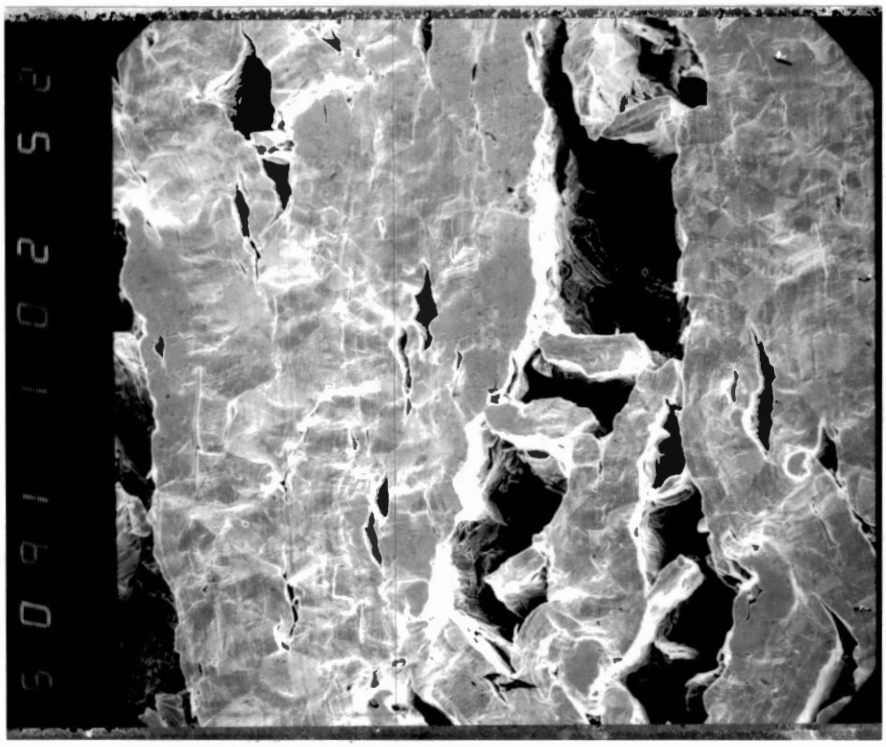

Figure 27. Slow rate test details of Figure 25 showing the blunting of the gaping cracks and numerous smaller cracks; x 200.

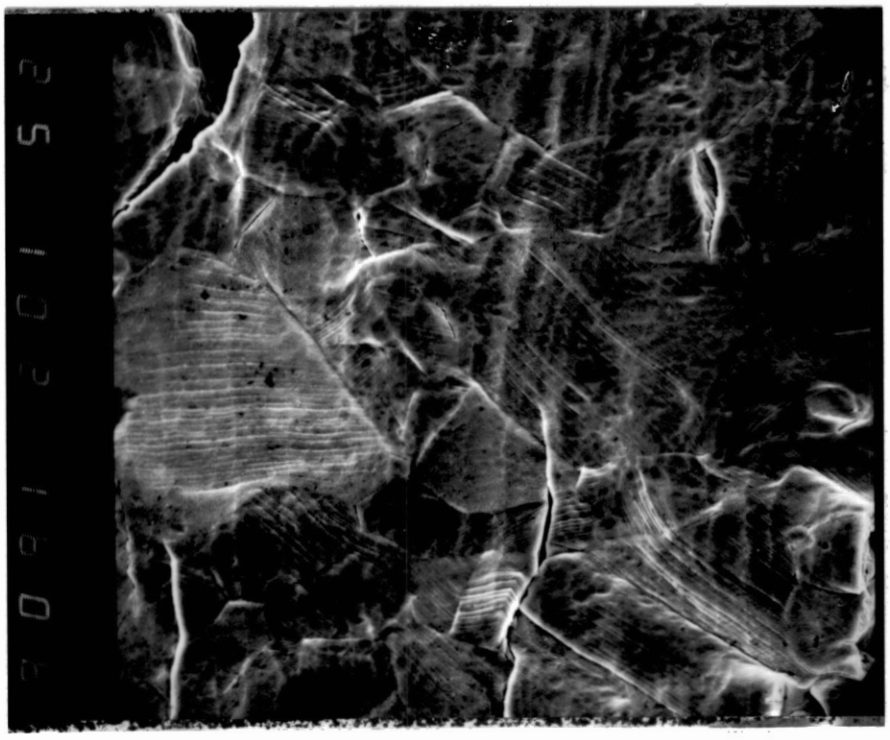

Figure 28. Slow rate test details of Figure 27 showing slip bands and slight, local IG cracking; X 1000.

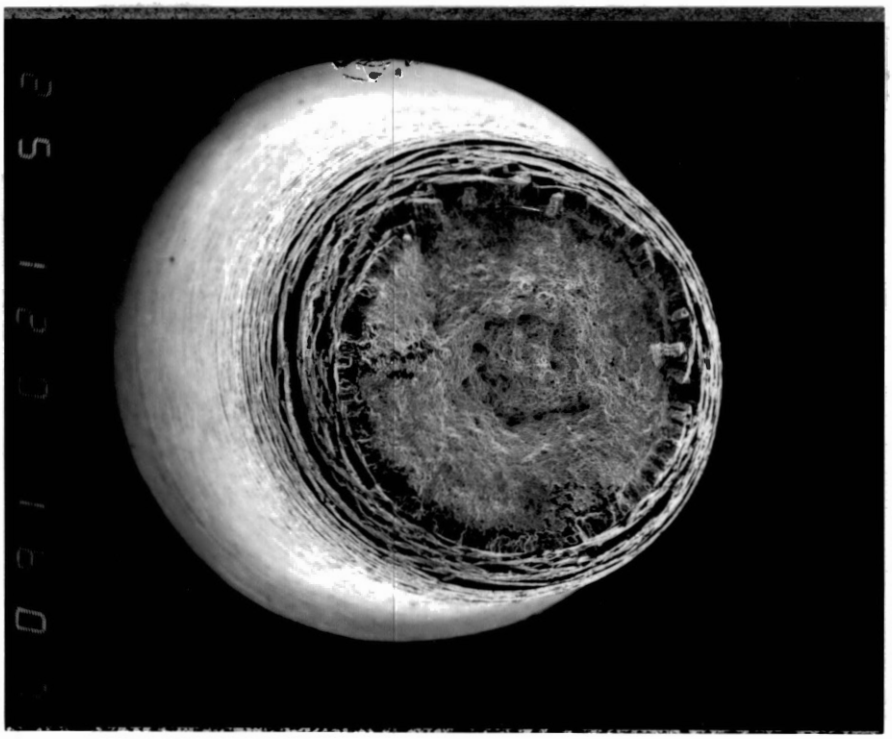

Figure 29. Slow rate test fracture surface showing rim of TG cracking; X 12.

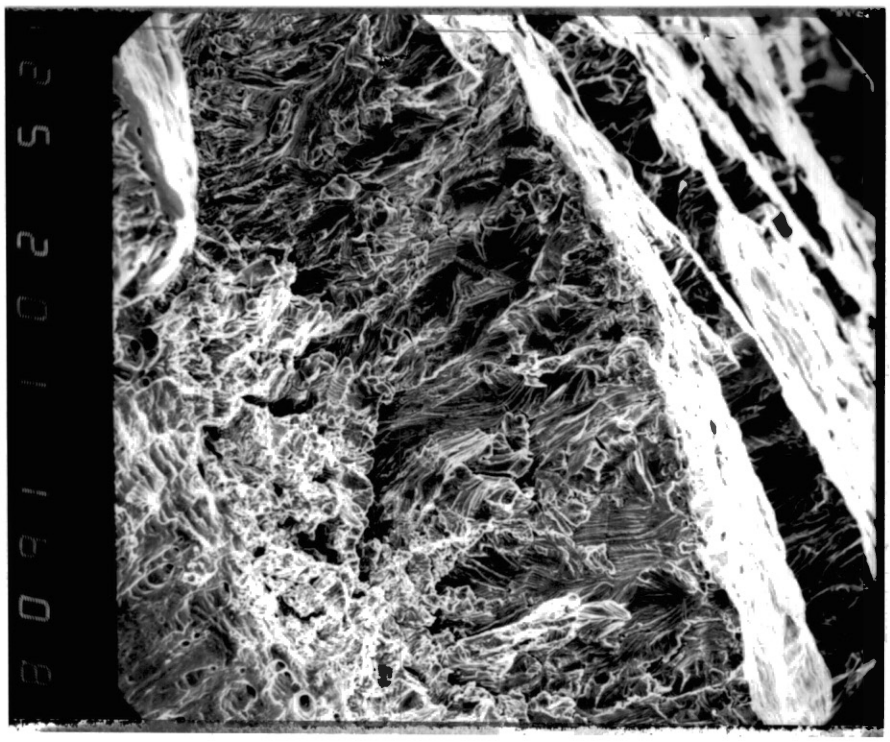

Figure 30. Slow rate test details of Figure 29. The TG zone is rather discontinuous and secondary cracks are evident; X 200.

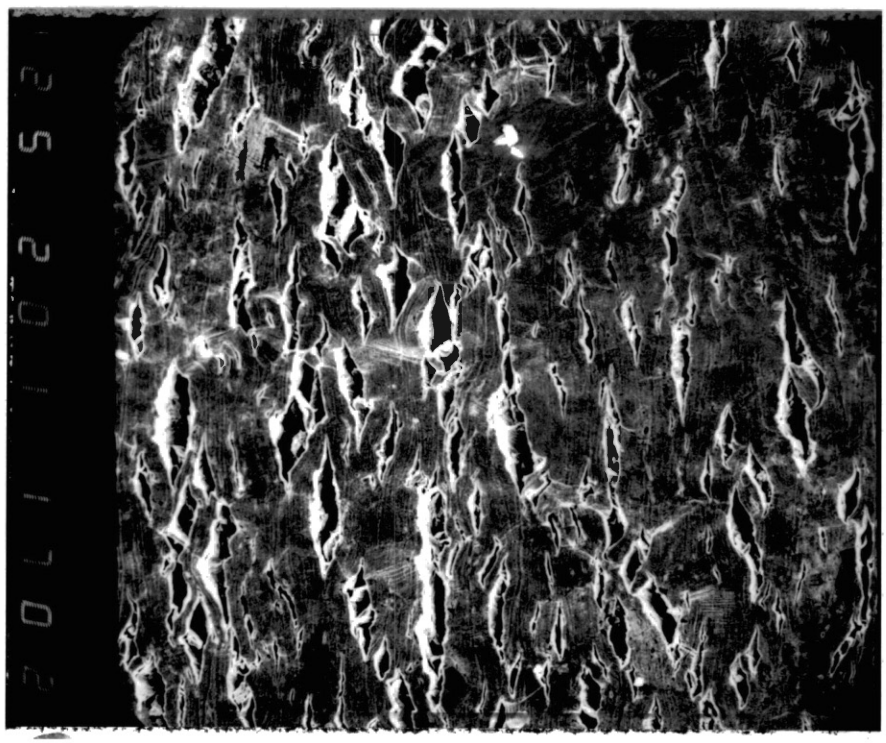

Figure 31. Intermediate rate test details illustrating the size and gaping of the cracks near the fracture. Compared to Figure 27, this sample has more cracks, but the cracks are smaller and not gaping as much; X 200.

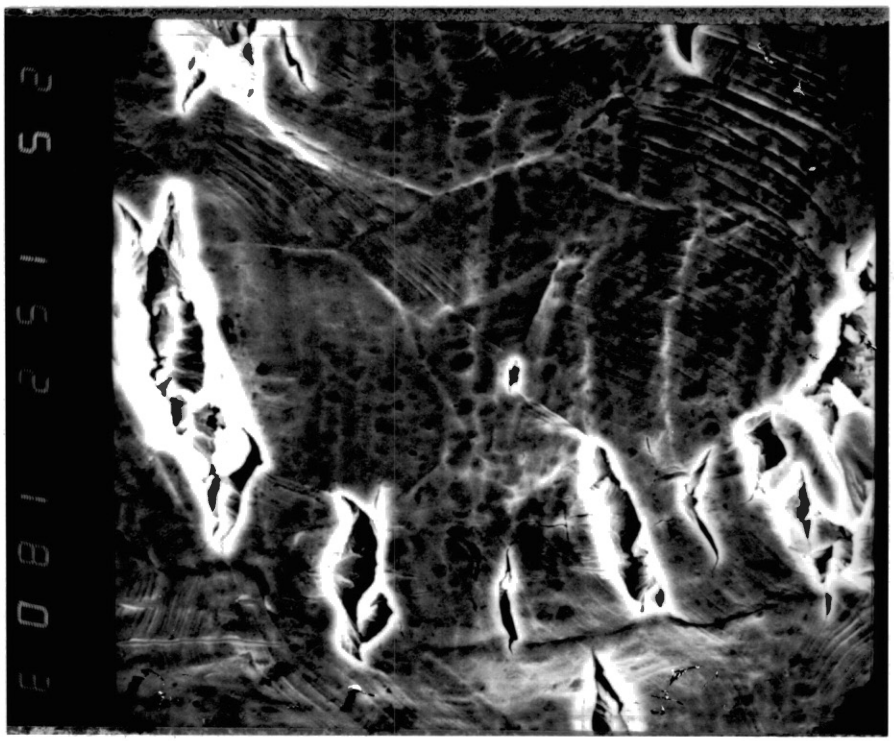

Figure 32. Fast rate test details near the fracture. Smaller cracks, slip bands, and pronounced grain boundaries are revealed; X 1500.

The second test for cold work utilized a 35 m grain size annealed sample. The sample was placed in the MTS machine and rapidly loaded to a pre-stress of 67.2 ksi. The load was then removed and the slow strain rate test was started under a control of 1.2 (10^{-6}) S^{-1}. The resulting fracture and surface cracks were similar to the as received test.

5.3.3 Monel K500

Monel K500 samples were tested in both the as received and annealed condition. The as received sample was supposed to be in the age hardened state. However, handbooks quote a hardness of HRC = 32 for the age hardened state. The obtained sample had a hardness of only HRB = 103, or HRC = 23, therefore was not fully aged. The sample hardness was only a little higher than the cold worked, as received sample of Monel 400.

SZM viewing of the fractured, as received, sample showed a 10 mm side cracking zone near the fracture. The cracking was similar to that noted for the as received Monel 400, discussed in the previous subsection. The similarity was also noted when the SEM was used. Figure 33 is an SEM photograph of the Monel 400 as received sample. Figures 34 and 35 contain the SEM photographs of the Monel K500 as received sample. It should be noted that the finish on the sample is parallel to the loading direction. Pitting attack and minor tight cracks occurred preferentially along the finish marks, perpendicular to the TG cracking.

The annealed Monel K500 had a hardness of HRB = 72. The fractured specimen displayed side cracking like the fine grain sized, annealed Monel 400. SZM observations confirmed a 16mm cracking zone near the fracture. Close to the fracture, the side cracks were widely gaping.

Figure 33. As received Monel 400 specimen, side view of the fracture. Compared to Figure 25, the cracking is less extensive; X 12.

Figure 34. As received Monel K500 specimen, side view of the fracture. The sample is similar to Figure 33 and illustrates less extensive cracking than Figure 25; X 12.

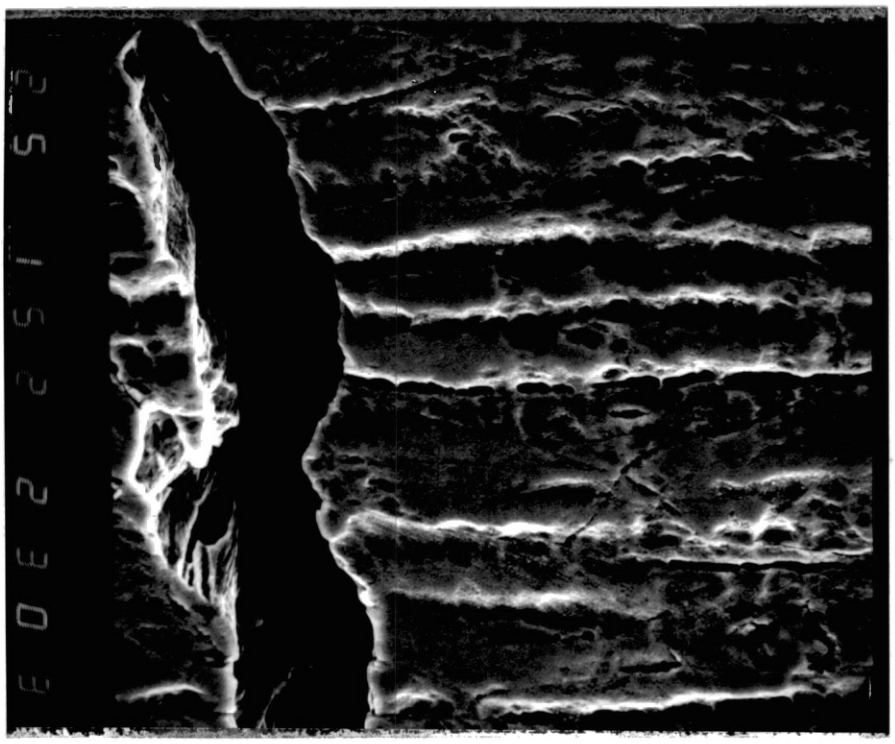

Figure 35. As received Monel K500 details of Figure 34. The pitting associated with the finish grooves is pronounced; X 1500.

5.3.4 Coarse Grain Size

A coarse grained, 250 μm, specimen demonstrated extensive cracking. The grain boundaries of the upper test half, as viewed under the SZM, were attacked with shallow IG cracks over a 5 mm zone, beginning approximately 3 mm from the shoulder. At 6 mm from the shoulder, the cracks became intermixed with TG cracking preferentially associated with machining grooves. Light IG cracking persisted to the vicinity of the light blue deposit zone marking the interface of the solution liquid and vapor. Within the liquid zone, only TG cracking was noted.

Over the entire lower half of the test specimen, the grains were lightly etched. However, the SZM revealed no distinct IG cracking. The TG cracking on the sample surface was more severe than the TG cracking of the 35 μm grain size. The fracture surface contained a rim of TG cracking.

The coarse grain size facilitated extensive SEM observations. The photographs contained in Figures 36 through 46 display the details of the damage that occurred. The features are reminiscent of those observed with the finer grain size samples, but are much more exaggerated. The cracking was more extensive. Also, the plastic deformation was more severe, causing the cracks to gap more. The slip bands are distinct in this grain size. The sample details will allow extensive comparisons with the previous investigations of LME and HE.

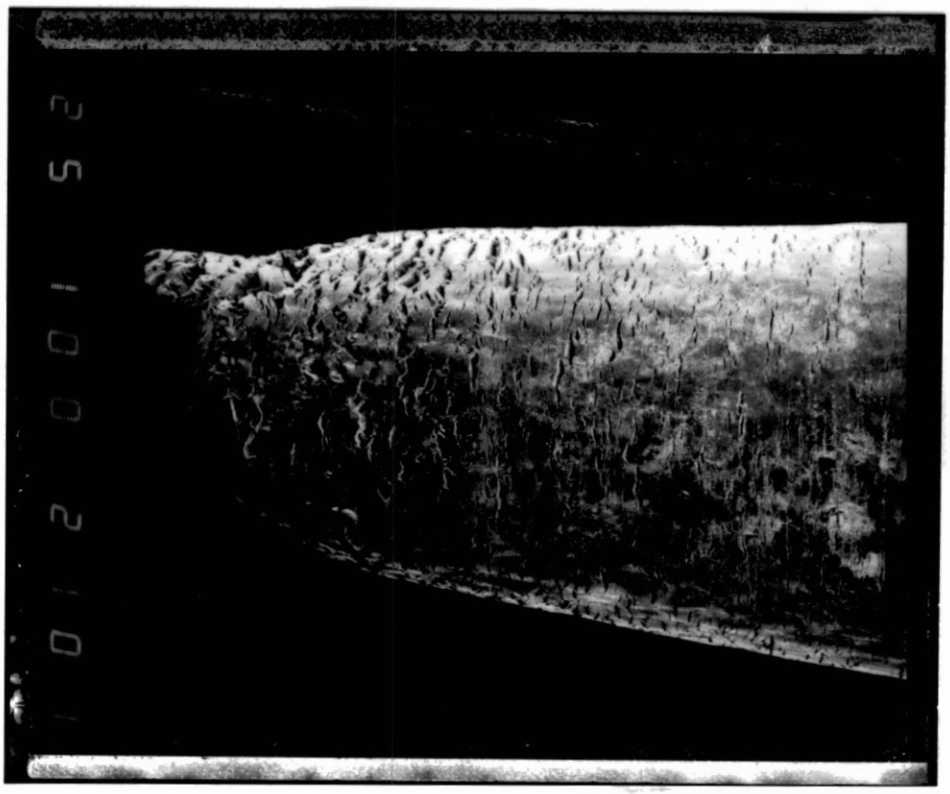

Figure 36. Coarse grain test side view in the vicinity of fracture. Multiple cracking and gaping occurs, and is more extensive than illustrated in Figure 25; X 10.

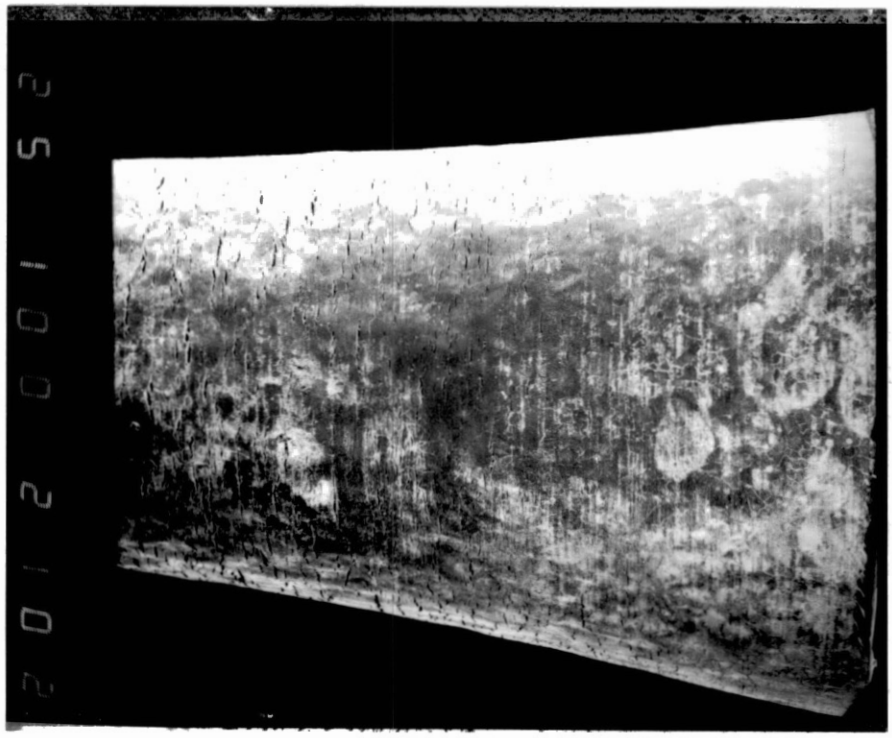

Figure 37. Coarse grain test side view continuation to near the shoulder. Cracking is discernable throughout the length of this view; X 1Ø.

Figure 38. Coarse grain test details of Figure 36, near the fracture. The cracks are gaping under extensive plastic deformation; X 200.

Figure 39. Coarse grain test details of Figure 38. The slip bands, pitting, and diverse nature of TG cracking within gaping cracks are illustrated; X 1000.

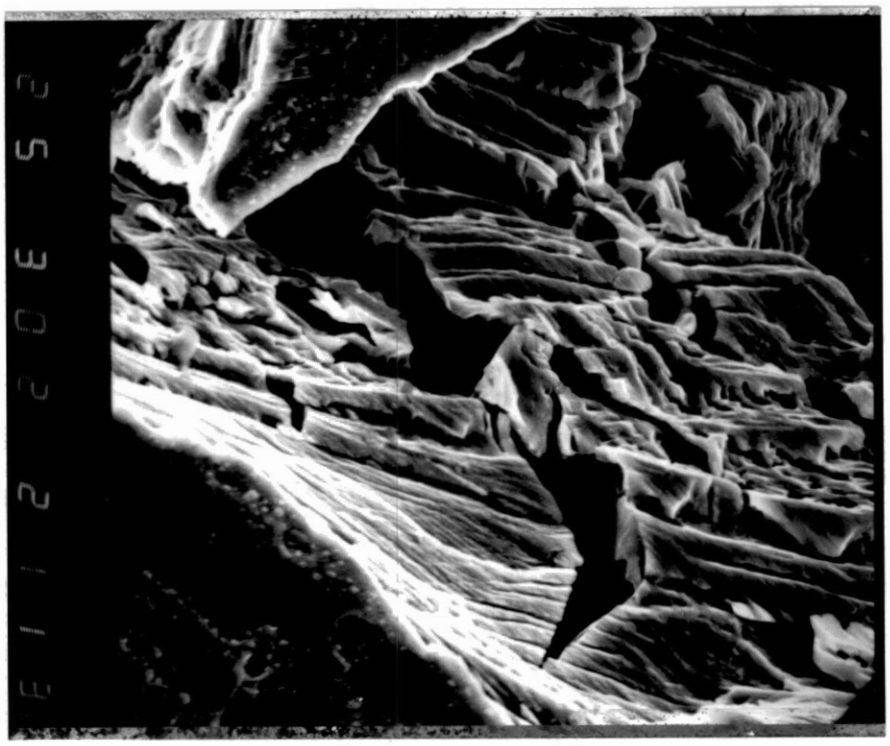

Figure 40. Coarse grain test details of Figure 39, showing the stepped nature of an inner crack surface; X 3000.

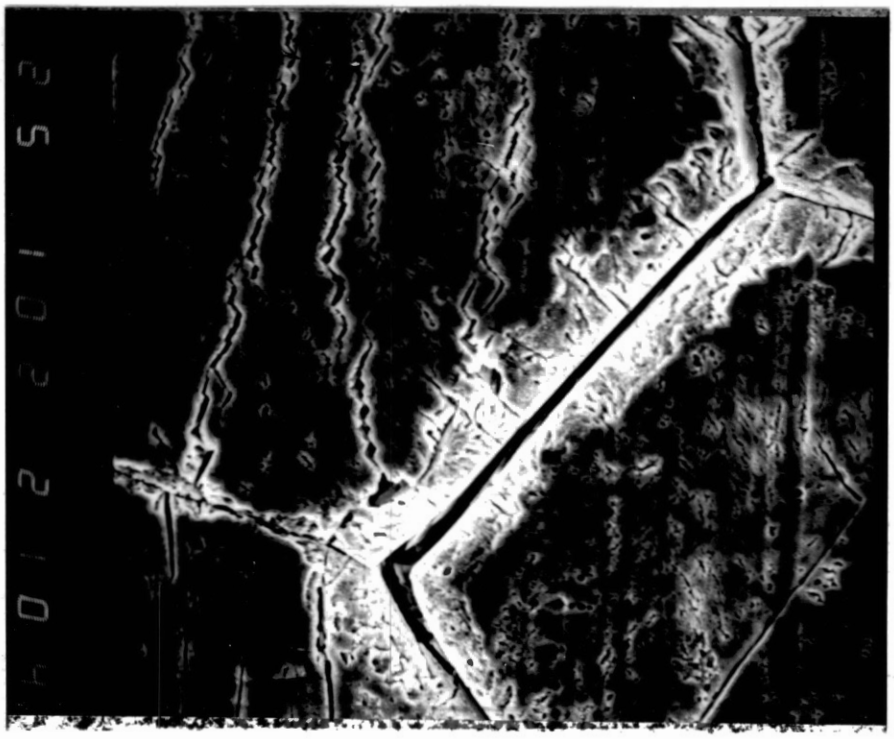

Figure 41. Coarse grain test details of Figure 37, showing IG cracking near the shoulder. Pitting and additional corrosion are noted adjacent to grain boundaries. The TG cracking shows a zigzag nature; x 1000.

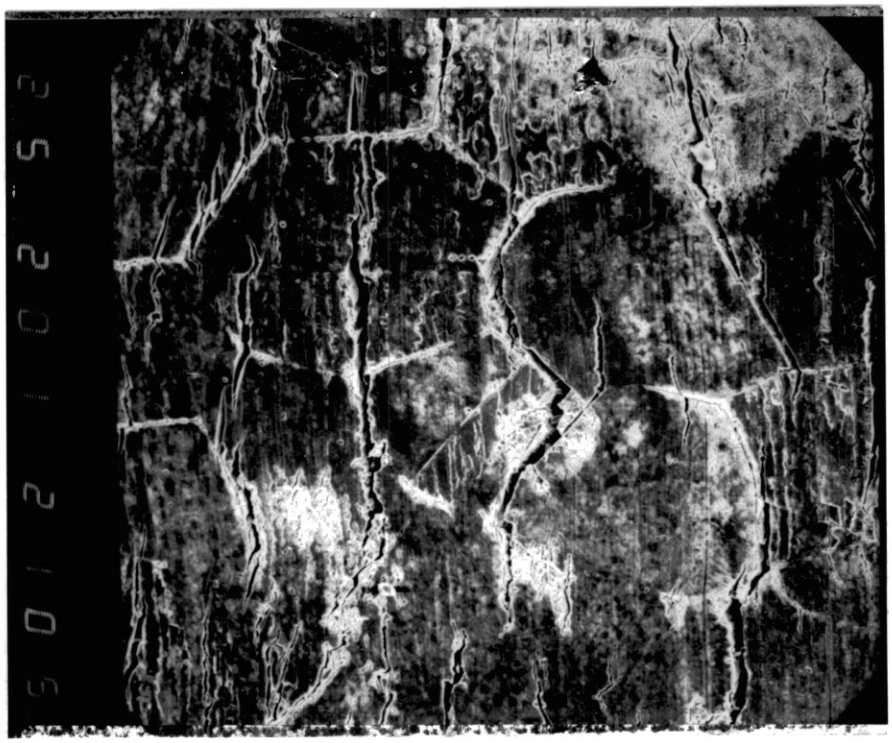

Figure 42. Coarse grain test details of an intermediate location on Figure 37. The IG cracking disappears as the TG cracking becomes more conspicuous; X 200.

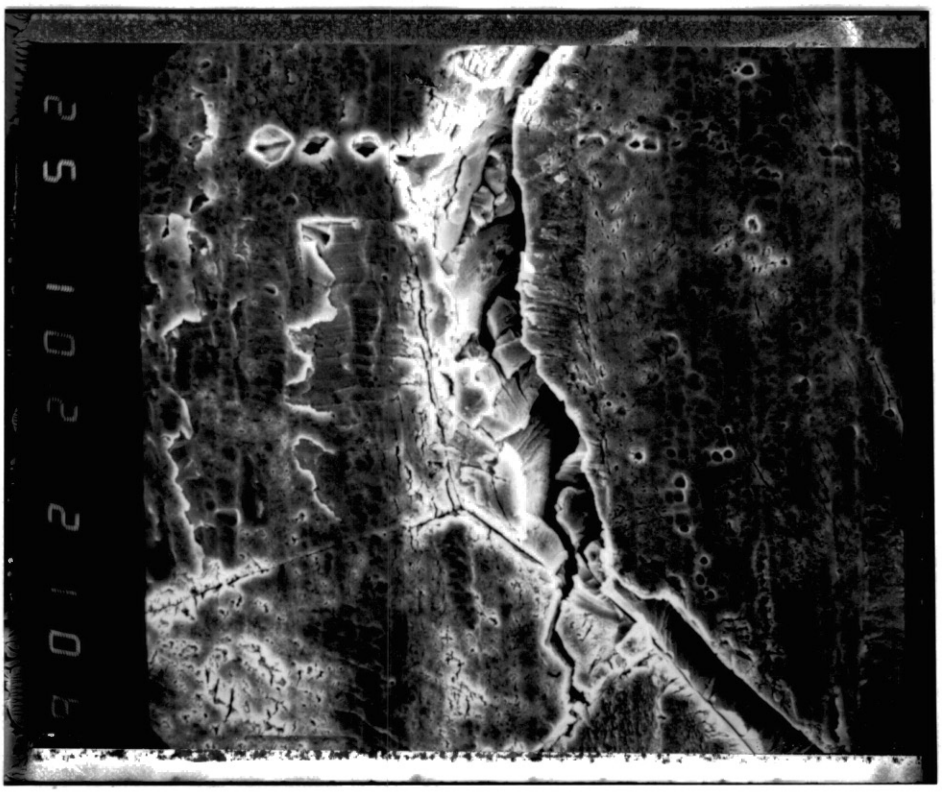

Figure 43. Coarse grain test details of Figure 42. Pitting, slip bands, and small cracks can be seen. Although the crack appeared IG in Figure 42, this magnification reveals TG cracking adjacent to a mildly cracked grain boundary; x 1000.

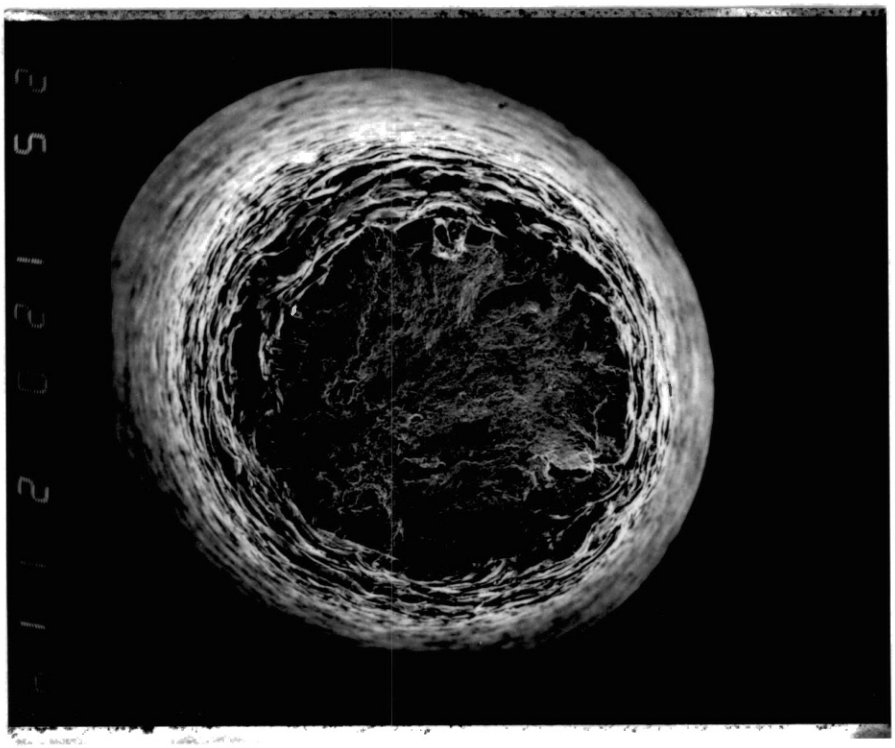

Figure 44. Coarse grain test fracture surface. A distinct rim of TG cracking and extensive side cracks are shown; X 12.

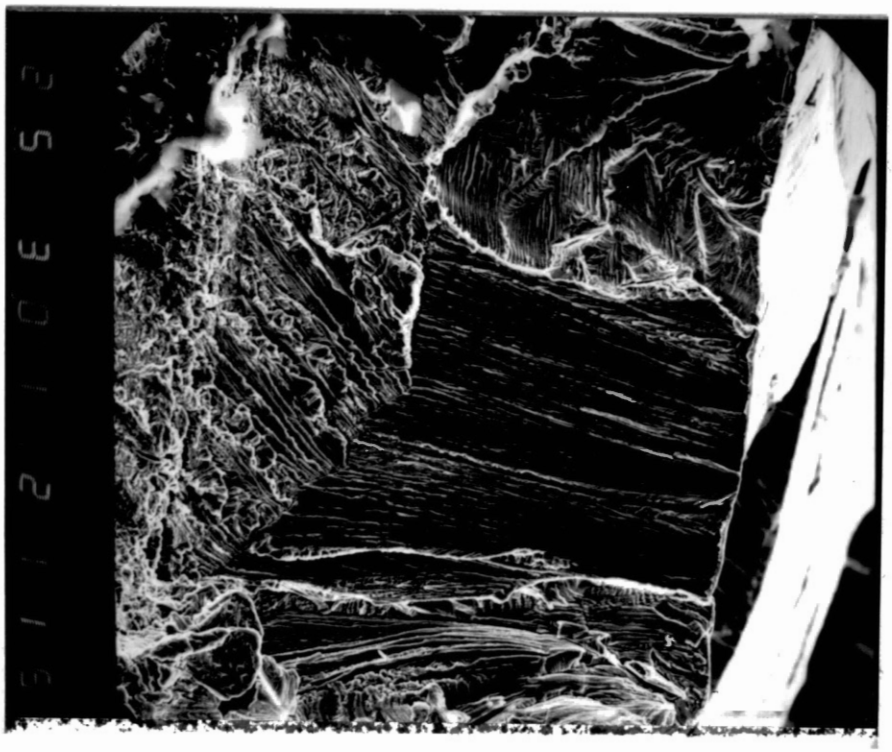

Figure 45. Coarse grain test details of the TG fracture zone. The grain boundaries are clearly discernable. The cracking details vary between grains. The TG zone gradually ends about two grains deep; X 300.

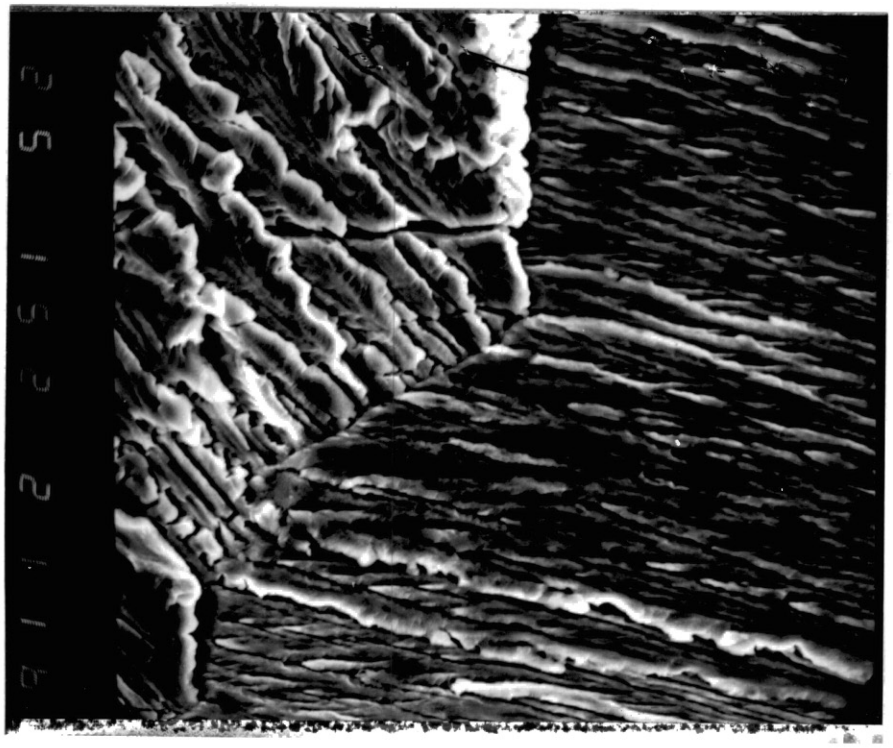

Figure 46. Coarse grain test details of Figure 45 showing the variable surface details across a grain boundary; X 1500.

CHAPTER VI

DISCUSSION AND ANALYSIS

The preceding study has combined literature and experimental research to determine the possibility of stress corrosion cracking of Monels at room temperature. The objectives of the study have been achieved. As anticipated, the most damaging environments generally occur with only slight corrosion, and, preferably, localized attack. Environments displaying such a characteristic can induce stress corrosion cracking in Monel at room temperature.

Due to the results of this study, it has become obvious that the damaging environments can be very diverse. Experiments were conducted with vastly different solutions, and only the sodium hydroxide tests failed to display any propensity towards embrittlement. Therefore, it is anticipated that numerous other environments can be found to cause the stress corrosion cracking of this material. It is also unlikely that the concentrations used in the present study would be considered optimum for SCC. For example, the tests conducted with ammonium persulfate resulted in extensive general corrosion damage. It is probable that, if the solution were diluted, less general corrosion would occur and the embrittlement would increase.

Chapter 2 revealed that Monel is widely used in situations involving hydrofluoric acid. Therefore, it is not surprising that this study showed

that Monel is not attacked by deaerated, pure HF. It has been demonstrated, though, that the presence of an oxidizer, like CuF_2, $CuCl_2$, or aeration, leads to SCC. This indicates that HE is not involved in the SCC of Monel. A similar inference comes from the attack by ammonia salts. It was previously established that ammonia causes SCC in copper base alloys, and that HE is not involved in the attack. Monel is one third copper, so it is implied that the attack on Monel by ammonia does not occur by HE.

During this study, the failure characteristics observed were consistent with the reported cases of Monel failure in HF, as discussed in chapter 2. The most distinct tendencies noticed are the side cracking and the prevalence for transgranular cracking. The surface fractography displayed the expected distinctions. Also, the cold worked and annealed materials demonstrated varying amounts of cracking. Furthermore, the experimental works of Good and King indicated the characteristic occurrence of longitudinal splitting of Monel when subjected to environmental embrittlement. The longitudinal cracks were also noticed in the SCC of Monel, but to a lesser degree.

The effects of changing the grain size, prior cold work, and increasing the yield strength of the material tested through age hardening have been discussed. It was found that, in each instance, TG cracking was facilitated by the lower yield strength. This is consistent with the behavior reported in liquid mercury tests. Appropriately, Fredell's study[29] on HE of Monel revealed an opposite effect. For example, the finer grain sizes suffered more embrittlement by hydrogen. This is appropriate since the finer grains allow an increased diffusion of hydrogen into the material.

The presence of both copper and copper oxide was noted in several tests completed for this study. The deposits were often seen in relation to the liquid / vapor interface. Such occurrence was also noted by Copson and Cheng[15]. Additionally, the tests conducted with 0.38M HF + 0.063 M CuF_2 left a copper flash in the vapor zone, and copper oxide in the immersed zone, when the sample was held under load. This characteristic is completely consistent with the observations made by Graf and Wittich[35].

It is understood that the grain boundaries of a material are at a higher energy state than the grain matrix. As the material suffers plastic deformation, though, the energy state of the matrix is altered, becoming greater than that of the grain boundary. As corrosion attempts to reduce an energy state to its lowest level, it would naturally result in a preferential attack on the grain boundaries until plastic deformation causes the attack to occur within the grain. Therefore, it was speculated at the beginning of the investigation that if SCC does occur, a cracking mode transition should develop, going from IG to TG to MVC, as the stress is increased. In several of the test specimens, IG cracking was a common occurrence in the shoulder regions, corresponding to the area where the stresses and strains would be relatively low. This is consistent with the prior LME and HE studies.

The increased energy states, discussed above, are intensely associated with slip bands. Dislocation systems within a grain are typical material characteristics and represent alterations in the stress states of the grain's matrix. This would then imply that TG cracking would be preferentially associated with the slip bands. However, this study has not determined whether the association is merely preferential or a completely necessary behavior. The photographs of the test samples do show slip band

cracking in several cases. Unfortunately, the slip bands were not always evident. Thus the issue is yet unresolved.

While this study has been able to induce SCC in Monel, the embrittlement did not occur throughout the cross section of the test samples. The cracks appearing relatively far from the fracture surface remained sharp, while those appearing close to the fracture have blunted. Conversely, the cracks away from the fracture were consistently shallow, while those near the fracture often proceeded several grains deep. This would be expected since the shallow cracks were only subjected to low levels of stress. Additionally, the blunting of the deeper cracks is presumed to be due to the domination of the stresses in that area. Thus, at the strain rates investigated, the strain component took precedence over the corrosion component. Accordingly, it would prove beneficial to investigate the SCC at lower strain rates. Lower strain rates should enhance the propagation of the TG cracks.

Another related matter involves corrosion fatigue. Corrosion fatigue induces many of the same characteristics seen in stress corrosion cracking. Price and Good[69], found that some alloys, such as Incoloy 800, are resistant to LME in the slow strain rate tests. However, subsequent tests, under fatigue loading, displayed a large degree of embrittlement by liquid metal. They also determined that alloys susceptible to LME in the slow strain rate tests, such as Monel, have a negligible resistance when subjected to the same environments under fatigue loading. This would seem to imply that an environment that causes stress corrosion cracking in Monel, or other nickel base alloys, could be more detrimental under fatigue loading. This is certainly reasonable, since fatigue can often ensure that cracks will be initiated. Yet, the concept is not universally

accepted, as some alloy systems can demonstrate more resistance under fatigue. A follow-up study on the relationship of stress corrosion cracking and corrosion fatigue in Monel would be beneficial.

Nickel base alloys are commonly used in severe environments. However, there exists only limited reports of room temperature SCC failures. The high corrosion resistance of the alloy system ensures few failures. However, it also increases the likelihood that the failures that do occur will be due to SCC. Additionally, there exists an SCC environment window for every material system. Since the susceptibility to SCC is dependent upon numerous parameters, it is likely industrial use has not yet combined the particular parameters that would open the window on the nickel base alloys.

However, an issue set forth in the introduction of this thesis merits reiteration. The incidences of stress corrosion cracking failure are on the rise. There are several, interconnected reasons for the increase. As technological capabilities are improved, the severity of the environment for particular processes increases. As this occurs, the materials used in the processes are pushed to the extreme limits of their capabilities. Once these limits are exceeded, alloys displaying improved resistance must be used. Yet, in time, these alloys are also pushed to their limit. With the improved resistance to general corrosion attack, the result is often localized failure. This investigation illustrates that numerous typical environments can induce such failure in Monel.

Furthermore, the results from previous studies of HE and LME have shown severe embrittlement of Monel at room temperature. Numerous other nickel base alloys were also subject to the embrittlement by hydrogen and mercury, but to a lesser extent than that suffered by Monel. By analogy,

other nickel base alloys would be expected to suffer SCC at room temperature. Thus, a warning is to be put forth in anticipation that additional incidences of SCC in nickel base alloys will be identified in the near future.

CHAPTER VII

CONCLUSIONS

1. Stress corrosion cracking can be induced in Monel at room temperature in numerous environments.
2. A cracking sequence of intergranular (IG) to transgranular (TG) to microvoid coalescence (MVC) occurred with increasing strain, as in the prior experiments involving hydrogen embrittlement (HE) and liquid metal embrittlement (LME) of Monel.
3. The cracking in hydrofluoric environments requires the presence of an oxidizer. Different reactions and products are formed.
4. The cracking patterns and fractography resemble those occurring in hydrogen embrittlement and liquid metal embrittlement; there were no unique features.
5. The study was not devised to assess stress corrosion cracking mechanisms. However, the widely differing appearance of the intergranular cracking and the variable degree of pitting are suggestive that more than one mechanism is operative.
6. It is anticipated that all of the nickel base alloys are susceptible to room temperature stress corrosion cracking.
7. It is reasoned that corrosion fatigue will enhance SCC embrittlement such that problematic environments may become extremely harsh to nickel alloys when subjected to fatigue.

BIBLIOGRAPHY

1. Asphahani, A. I., "Slow Strain-Rate Technique and Its Applications to the Environmental Stress Cracking of Nickel-Base and Cobalt-Base Alloys," Stress Corrosion Cracking -The Slow Strain-Rate Technique, ASTM Special Technical Publication (STP) 665, G. M. Ugiansky and J. H. Payer, Editors, ASTM, Philadelphia, Pa., c. 1979, pp. 279-293.

2. ASTM G15-86, "Standard Definitions of Terms Relating to Corrosion and Corrosion Testing", Annual Book of ASTM Standards, ASTM, Pa, pp. 104-107, 1988.

3. Atkinson, J. T. N., and H. VanDroffelaar, Corrosion and Its Control: An Introduction to the Subject, National Association of Corrosion Engineers, c. 1982.

4. Baker, Richard G., "The Real World of Corrosion: Stress Corrosion Cracking," Plating and Surface Finishing, p. 18.

5. Barteri, M., et al., "Microstructural Study and Corrosion Performance of Duplex and Superaustenitic Steels in Sour Well Environments", Corrosion - NACE, Vol. 43, Sept. 1987, pp. 518-524

6. Bernhardsson, B., et al., "Selection of Stainless Steels for Refineries and the Petrochemical Industry," Anti-Corrosion, Jan. 86, pp. 14-17

7. Bianchi, G. L., and J. R. Galvele, "Short Communication; Embrittlement of Copper By The Surface Mobility Mechanism," Corrosion Science, Vol. 27, No. 6, pp. 631-635, 1987.

8. Blain, J., J. Masounave, and J. I. Dickson, "A Comparison of SCC Velocity Measurements Under Conditions of Constant Load and Constant Displacement," Corrosion Science, Vol. 24, No. 1, pp. 1-12, 1984.

9. Budinski, K., Engineering Materials; Properties and Selection, 2nd Edition, Reston Publishing Company, Inc., Virginia, c. 1983.

10. Cavanaugh, M. A., J. A. Kargol, J. Nickerson, and N. F. Fiore, "The Anodic Dissolution of a Ni-Base Superalloy," Corrosion -NACE, Vol. 39, No. 4, April 1983, pp. 144-150.

11. Clark, W. G., Jr., "Effects of Prestressing on Stress-Corrosion Crack Initiation in High-Strength Type 4340 Steel," Fracture Mechanics: Twelfth Conference, ASTM STP 700, American Society for Testing and Materials, Philadelphia, Pa, 1980, pp. 97-111.

12. Cole, H. G., "Stress Corrosion Cracking of High-Tensile Steels," Corrosion, Vol. 1, Corrosion of Metals and Alloys, L. L. Shreir, Editor, John Wiley & Sons, Inc., NY, c. 1963, pp. 8.46-8.54.

13. Comley, M. A., and T. E. Evans, "Nickel and Nickel Alloys," Corrosion, Vol. 1, Corrosion of Metals and Alloys, L. L. Shreir, Editor, John Wiley & Sons, Inc., NY, c. 1963, pp. 4.103-4.125.

14. Copson, H. R., "Laboratory Techniques for the Investigation of Stress Corrosion Cracking," Stress Corrosion Cracking And Embrittlement, W. D. Robertson, Editor, John Wiley & Sons, Inc. NY, c. 1956, pp. 187-200.

15. Copson, H. R., and C. F. Cheng, "Stress Corrosion Cracking Of Monel in Hydrofluoric Acid," Corrosion - NACE, Vol. 12, December 1956, pp. 71-77.

16. Corrosion Fatigue: Mechanics, Metallurgy, Electrochemistry, and Engineering, ASTM Special Technical Publication (STP) 801, Crooker, T. W., and B. N. Leis, Editors, ASTM, Philadelphia, Pa., c. 1983.

17. "Corrosion of Copper and Copper Alloy," Metals Handbook, 9th Edition, Vol. 13, Corrosion, ASM International, Metals Park, Ohio, c. 1987, pp. 614-640.

18. Craig, B., "Environmentally Induced Cracking," Metals Handbook, 9th Edition, Vol. 13, Corrosion, ASM International, Metals Park, Ohio, c. 1987, pp. 145-189.

19. Dean, S. W., "General Methods of Corrosion Evaluation," ASTM Standardization News, March 1986, pp. 40-44.

20. Degnan, T. F., "Corrosion by Hydrogen Fluoride and Hydrofluoric Acid," ASM Metals Handbook, 9th Ed., Vol. 13, Corrosion, ASM International Metals Park, Ohio, c. 1987, pp. 1166-1184.

21. Delamare, F., and G. E. Rhead, "Increase in the Surface Self-Diffusion of Copper Due to the Chemisorption of Halogens", Suracef Science, Vol. 28, pp. 267-284, 1971.

22. Devereux, O., A. J. McEvily, and R. W. Staehle, Editors, Corrosion Fatigue: Chemistry, Mechanics, and Microstructure, National Association of Corrosion Engineers, Conference held at University of Connecticut, June 14- 18, 1971, c. 1972.

23. Edeleanu, C., "The Phenomena of Stress Corrosion Cracking in Austenitic Stainless Steels," Stress Corrosion Cracking And Embrittlement, W.D. Robertson, Editor, John Wiley & Sons, Inc. NY, c. 1956, pp. 126-139.

24. Edeleanu, C., and A. J. Forty, "Some Observations on the Stress-Corrosion Cracking of d-Brass and Similar Alloys," Philosophical Magazine, Vol. 5, pp. 1029-1040, 1960.

25. Efird, K. D., "Failure of Monel Ni-Cu-Al Alloy K-500 Bolts in Seawater," Materials Performance, April 1985, pp. 37-40.

26. Erlings, J. G., H. W. deGroot, and J. F. M. van Roy, "Stress Corrosion Cracking and Hydrogen Embrittlement of High-Strength non-magnetic alloys in brines," Materials Preformance, October 1986, pp. 28-34.

27. Fatigue and Microstructure, 1978 ASM Materials Science Seminar: St. Louis, American Society for Metals, Metals Park, Oh, c. 1979

28. Feliu, V., and S. Feliu, "A Noniterative Method for Determining Corrosion Parameters From a Sequence of Polarization Data," Corrosion - NACE, Vol. 42, No. 3, March 1986, pp. 151-156.

29. Fredell, R. F., "A Detailed Comparison of Hydrogen and Mercury Embrittlement in Monel 400," (Unpub. M.S. Thesis, Oklahoma State University, 1983).

30. Fontana, M. G., Corrosion Engineering, 3rd Edition, McGraw-Hill Book Company, NY, c. 1986.

31. Friend, W. Z., Corrosion of Nickel And Nickel-Base Alloys, John Wiley & Sons, Inc., NY, c. 1980.

32. Galvele, J. R., "Enhanced Surface Mobility as the Cause of Stress Corrosion Cracking," Journal of Electrochemical Society, Vol. 133, p. 953, 1986.

33. Galvele, Jose' R., "A Stress Corrosion Cracking Mechanism Based on Surface Mobility," Corrosion Science, Vol. 27, No. 1, pp. 1-33, 1987.

34. Graf, L., "Stress Corrosion Cracking in Homogeneous Alloys," Stress Corrosion Cracking And Embrittlement, W.D. Robertson, Editor, John Wiley & Sons, Inc. NY, c. 1956, pp. 48-60.

35. Graf, L., and W. Wittich, "Untersuchung von Sonderfallen der Spannungskorrosion bie homogenen, nicht ubersattigten Mischkristallen und der hierbei auftretenden elektrochemischen Prozesse," Werkstoffe und Korrosion, Jahrgang 1966, Heft 5, pp. 385-405.

36. Green, J. A. S., and H. W. Hayden, "Influence of Two Modes of Loading on the Stress Corrosion Susceptibility of Ti-8Al-1Mo-1V Alloys in Various Chloride-Containing Environments," Hydrogen in Metals, I. M. Bernstein and A. W. Thompson, editors, American Society for Metals, Metals Park, OH, 1974, p. 235.

37. Harwood, J. J., "The Phenomena and Mechanism of Stress Corrosion Cracking," Stress Corrosion Cracking And Embrittlement, W. D. Robertson, Editor, John Wiley & Sons, Inc. NY, c. 1956, pp. 1-20.

38. Hertzberg, R. W., Deformation and Fracture Mechanics of Engineering Materials, 2nd. Edition, John Wiley & Sons, NY, NY, 1983.

39. Hines, J. G., "Theories of Stress Corrosion," Corrosion, Vol. 1, Corrosion of Metals and Alloys, L.L. Shreir, Editor, John Wiley & Sons, Inc., NY, c. 1963, pp. 8.3-8.20.

40. Hines, J. G., "Stress Corrosion Cracking of Stainless Steels," Corrosion, Vol. 1, Corrosion of Metals and Alloys, L. L. Shreir, Editor, John Wiley & Sons, Inc., NY, c. 1963, pp. 8.21-8.33.

41. Hoar, T. P., and J. M. West, "Mechano-Chemical Anodic Dissolution," Nature, Vol. 181, No. 4612, March 22, 1958, p. 835.

42. Hoyt, S. L., Metal Data, Battelle Memorial Institute, Reinhold Publishing Corporation, NY, c. 1952.

43. Jones, R. H., "Crack Growth Resistance," Journal of Metals, December 1987, pp. 32-39.

44. Kamdar, M. H., Editor, "Embrittlement by Liquid and Solid Metals," Fall Meeting of the Metallurgical Society in St. Louis, Mo., The Metallurgical Society of AIME, Warrendale, Pennsylvania, c. 1984.

45. King, R. K., "Environmentally Induced Fracture of Nickel Alloys: A Comparison of Hydrogen and Mercury Embrittlement with Respect to Temperature," (Unpub. Ph.D. Thesis, Oklahoma State University, 1985.)

46. Latanision, R. M., and M. Kurkela, "Hydrogen Permeability and Diffusion in Nickel and Ni-Base Alloys," Corrosion - NACE, Vol. 39, No. 5, May 1983, pp. 174-178.

47. Latanision, R. M., O. H.Gastine, and C. R. Compeau, "Stress Corrosion Cracking And Hydrogen Embrittlement: Differences And Similarities," Environment-Sensitive Fractures of Engineering Materials, 1977 Symposium Proceedings of AIME, Z. A. Foroulis, Editor, Pa, 1979, pp. 48-70.

48. Latanision, R. M., "Physical Metallurgy of Nickel-Base Alloys as It Relates to Corrosion," Journal of Materials Engineering, Vol. 10, No. 2, 1988, pp. 143-162.

49. Lynch, S. P., "Hydrogen Embrittlement and Liquid-Metal Embrittlement in Nickel Single Crystals," Scripta Metallurgia, Vol. 13, pp. 1051-1056, 1979.

50. Lynch, S. P., "A Comparative Study of Stress-Corrosion Cracking, Hydrogen-Assisted Cracking, and Liquid-Metal Embrittlement In Al, Ni, Ti, and Fe-Based Alloys," Hydrogen Effects in Metals, I. M. Bernstein and A. W. Thompson, editors, American Society for Metals, Metals Park, OH, 1981, pp. 863-871.

51. Lynch, S. P., and P. Trevena, "Stress Corrosion Cracking and Liquid Metal Embrittlement in Pure Magnesium," Corrosion -NACE, Vol. 44, No. 2, February 1988, pp. 113-124.

52. McGuire, R. E., "Knowledge Is Key to Stress - Corrosion Battle," Oil & Gas Journal, June 9, 1986, pp. 48-52.

53. Menzies, I. A., "The Fundamental Principles of Corrosion," Corrosion and Protection of Metals, published for The Institution of Metallurgists by Iliffe Books, Inc., London, 1965, pp. 3-36.

54. Meletis, E. I., and R. F. Hochman, "Techniques for Determination of the Crystallographic Characteristics of Environmentally Induced Brittle Fractures," Journal of Testing and Evaluation, ASTM, pp. 142-148, 1984.

55. Meletis, E. I., and R. F. Hochman, "The Crystallography of Stress Corrosion Cracking in Face Centered Cubic Single Crystals," Corrosion Science, Vol. 24, No. 10, pp. 843-862, 1984.

56. Meletis, E. I., and R. F. Hochman, "A Review of the Crystallography of Stress Corrosion Cracking," Corrosion Science, Vol. 26, No. 1, pp. 63-90, 1986.

57. NACE, "Corrosion Basics: Intergranular Corrosion," Materials Performance, December 1986, p. 61.

58. NACE, "NACE Glossary of Corrosion Related Terms," Materials Performance, January 1986, pp. 59-65.

59. Namboodhiri, T. K. G., and R. S. Tripathi, "The Stress-Assisted Dezincification Of 70/30 Brass In Ammonia," Corrosion Science, Vol. 26, No. 10, pp. 745-756, 1986.

60. Newman, R. C., R. Roberge, and R. Bandy, "Environmental Variables in the Low Temperature Stress Corrosion Cracking of Inconel 600," Corrosion - NACE, Vol. 39, No. 10, October 1983, pp. 386-390.

61. Nichols, F. A., "Loading Mode and Stress Corrosion Cracking Mechanisms," Corrosion - NACE, Vol. 39, No. 11, November 1983, pp. 449-451.

62. Nickel And Nickel Alloys, The International Nickel Company, NY, Caxton Press, c. 1947.

63. Oriani, R. A., Stress Corrosion Cracking and Hydrogen Embrittlement of Iron Based Alloys, R. W. Staehle, J. Hochmann, R. D. McCright, and J. E. Slater editors, NACE, Houston, 1977, pp. 351-358.

64. Owens, C. M., "Stress Corrosion Cracking Performance of Mill-Annealed, Inconel 600 Tubing in Steam Generators," Materials Performance, January, 1986, pp. 49-54.

65. Parkins, R. N., "Stress-Corrosion Cracking of Steels," Corrosion, Vol. 1, Corrosion of Metals and Alloys, L. L. Shreir, Editor, John Wiley & Sons, Inc., NY, c. 1963, pp. 8.34-8.45.

66. Parkins, R. N., "The Interactions of Stress and Corrosion In the Stress Corrosion Cracking of Iron Base Alloys," Mechanics And Mechanisms Of Crack Growth, Proceedings of a Conference Organised by the Physical Metallurgy Centre of the British Steel Corporation, Cambridge, April 4-6, 1973, pp. 84-107.

67. Parkins, R. N., "Development of Strain-Rate Testing and Its Implications," Stress Corrosion Cracking - The Slow Strain-Rate Technique, ASTM Special Technical Publication (STP) 665, G. M. Ugiansky and J. H. Payer, Editors, ASTM, Philadelphia, Pa., c. 1979, pp. 5-25.

68. Price, C. E., and R. S. Fredell, "A Comparative Study of the Embrittlement of Monel 400 at Room Temperature by Hydrogen and by Mercury," Metallurgical Transactions A, Vol. 17A, May 1986, pp. 889-898.

69. Price, C. E., and J. K. Good, "The Fatigue Behavior of Nickel, Monel, and Selected Superalloys, Tested in Liquid Mercury and Air; A Comparison," Journal of Engineering Materials and Technology, ASTM, April 1984, Vol. 106, pp. 178-183.

70. Price, C. E., and J. K. Good, "The Fractography of Hydrogen and Mercury Embrittlement in Inconel 600," Journal of Materials Engineering, Vol. 9, No. 3, 1987, pp. 283-291.

71. Price, C. E., and J. K. Good, "The Tensile Fracture Characteristics of Nickel, Monel, and Selected Superalloys Broken in Liquid Mercury," The Journal of Engineering Materials and Technology, Vol. 106, April 1984, pp. 184-190.

72. Price, C. E., and R. K. King, "The Embrittlement Of Monel 400 By Hydrogen And Mercury, As A Function Of Temperature," Corrosion Cracking, V. S. Goel, Editor, Conference Proceeding for Decem-

ber 1985, ASM, 1986, pp. 81-88.

73. Price, C. E., and J. A. Morris, "The Comparative Embrittlement of Example Nickel Alloys by Hydrogen and Mercury," Journal of Materials for Energy Systems, ASM, Vol. 7, No. 3, December 1985, pp. 246-255.

74. Price, C. E., and R. G. Norman, "A Comparison Of Hydrogen And Mercury Embrittlement In AISI 4142 Steel," Acta Metall., Vol. 35, No. 7, pp. 1639-1648, 1987.

75. Price, C. E., G. R. Peevy, and J. K. Willoughby, "The Effect Of Prestress On The Embrittlement Of Monel 400 By Mercury," Scripta Metallurgica, Vol. 20, pp. 1297-1298, 1986.

76. Price, C. E., and L. B. Traylor, "A Comparison Of Microvoid Sizes In Nickel Base Alloys Tested In Air And In The Presence Of Hydrogen," Scripta Metallugica, Vol. 17, pp. 901-904, 1983.

77. Price, C. E., and L. B. Traylor, "Fractography of Hydrogen and Mercury Embrittlement in Nickel 200," Corrosion, Vol. 43, No. 4, April 1987, pp. 229-238.

78. Priest, D. K., "The Mechanism of Stress Cracking Observed in a Magnesium Alloy," Stress Corrosion Cracking And Embrittlement, W. D. Robertson, Editor, John Wiley & Sons, Inc. NY, c. 1956, pp. 81-91.

79. Pugh, E. N., "Progress Toward Understanding the Stress Corrosion Problem," Corrosion - NACE, Vol. 41, No. 9, September 1985, pp. 517-526.

80. Robertson, W. D., "Metallurgical Mechanism for Mercury Stress Cracking Of Copper Alloys," Journal of Metals, December 1951, pp. 1190-1191.

81. Robertson, W. D., "Structural Factors Associated with Stress Corrosion Cracking of Homogeneous Alloys," Stress Corrosion Cracking And Embrittlement, W. D. Robertson, Editor, John Wiley & Sons, Inc. NY, c. 1956, pp. 32-47.

82. Shahinian, P., and M. R. Achter, "Influence of Environment on Crack Propagation at High Temperatures," Proceedings of The Crack Propagation Symposium, Vol. 1, Cranfield, 1961, pp. 29-75.

83. Shaw, B. J., "Design and Use of a Load Monitoring Environmental Test Chamber for Stress Corrosion Testing," Journal of Testing and Evaluation, ASTM, Vol. 13, No. 6, November 1985, pp. 416-423.

84. Sih, G. C., Editor, Mechanics of Fracture 1, Methods of Analysis and Solutions of Crack Problems, Noordhoff International Publishing, Leyden, The Netherlands, c. 1973.

85. "Stress Corrosion - Discussion," Mechanics and Mechanisms of Crack Growth, Proceedings of a Conference Organised by the Physical Metallurgy Centre of the British Steel Corporation, Cambridge, April 4-6, 1973.

86. Suery, P., "Detection of Heat Treatment Effects on Environmentally Induced Degradation of a Martensitic Stainless Steel and a Nickel-Base Alloy by the Slow Strain-Rate Method," Stress Corrosion Cracking - The Slow Strain-Rate Technique, ASTM Special Technical Publication (STP) 665, G. M. Ugiansky and J. H. Payer, Editors, ASTM, Philadelphia, Pa., c. 1979, pp. 320-332.

87. Swanson, S. R., Editor, Handbook of Fatigue Testing, ASTM Special Technical Publication (STP) 566, ASTM, Philadelphia, Pa., c. 1974.

88. Tegart, The Electrolytic and Chemical Polishing of Metals, Pergamon Press, London, c. 1959.

89. Theus, G. J., and J. R. Cels, "Slow Strain-Rate Technique: Applications to Caustic Stress Corrosion Cracking Studies," Stress Corrosion Cracking - The Slow Strain-Rate Technique, ASTM Special Technical Publication (STP) 665, G. M. Ugiansky and J. H. Payer, Editors, ASTM, Philadelphia, Pa., c. 1979, pp. 81-96.

90. Torchio, S., and F. Mazza, "The Influence of Chloride Ions on the Stress Corrosiuon Cracking of Al-Brass in LAcidic Sulphate Solutions," Corrosion Science, Vol. 26, No. 10, pp. 813-826, 1986.

91. Traylor, L. B., and C. E. Price, "A Comparison of Hydrogen and Mercury Embrittlement in Monel at Room Temperature," Journal of Engineering Materials and Technology, Vol. 108, January 1986, pp. 31-36.

92. Ugiansky, G. M., and Payer, J. H., Editors, "Significance of Non-propagating Stress Corrosion Cracks and Concept of Threshold Strain Rates," Stress Corrosion Cracking -The Slow Strain-Rate Technique, ASTM Special Technical Publication (STP) 665, ASTM, Philadelphia, Pa., c. 1979, pp. 15-21.

93. Ugiansky, G. M., and C. E. Johnson, "Slow Strain-Rate Stress Corrosion Testing of Metals in Gaseous Atmospheres at Elevated Temperatures," Stress Corrosion Cracking -The Slow Strain-Rate Technique, ASTM Special Technical Publication (STP) 665, G. M. Ugiansky and J. H. Payer, Editors, ASTM, Philadelphia, Pa., c. 1979, pp. 113-131.

94. Yu, J., and R. N. Parkins, "Stress Corrosion Crack Propagation in alpha-Brass and Copper Exposed To Sodium Nitrat Solutions," Corrosion Science, Vol. 27, No. 2, pp. 159-182, 1987.

95. Yu, J., R. N. Parkins, Y. Xu, G. Thompson, and G.C. Wood, "Stress Corrosion Crack Initiation in alpha-Brass Exposed To Sodium Nitrat Solutions," Corrosion Science, Vol. 27, No. 2, pp. 141-157, 1987.

APPENDIX A

SELECTED SYSTEMS OF STRESS CORROSION CRACKING

Structure/Alloy	SCC Environment	Ref.
1. FCC		
Aluminum Alloys		
AlZnMg	Sodium Chloride	79
Al-Cu	$NaCl + H_2O_2$ solution	56
	$NcCl + HNO_3$ solution	56
Al-Zn-Mg	NaCl solution	56,47
Al-7Mg	NaCl	43
Copper Alloys		
α-brass (>15% Zn)	Aqueous Ammonia	18,55,43 56,54,59 79,90
Cu	NH_3 vapors and solutions	43,17,56 55
	$NaNO_2$ solutions	55,56,54 94,43,95
A-Cu-Zn	NH_3 vapors and solutions	43,56,59
	$Cu(NO_3)_2 + CuSO_4$ solutions	17,56
	$Na_2SO_4(H_2SO_4)$ solutions	17,56
Cu-Zn	Amines	56
	$BaCl_2$ solutions	56

	Butane + SO_2	56
	Hydrogen Chloride	56
	HF	56
	HNO_3	56
	NH_4-Monoethanolamine	56
	NaOH	85
	Mercurous nitrate	56
A-Cu-Zn (Al,Mn, Ag,Sn,P,Si,Te,Ti)	NH_3 vapors and solutions	56
	Formate	17
A-Cu-Zn-Al	Cl	9Ø
	NH_3 vapors and solutions	56
	Sulphate solutions	9Ø
A-Cu-Al	NH_3 vapors and solutions	56
Cu-Be	NH_3 vapors and solutions	56
A-Cu-Ni-Si	NH_3 vapors and solutions	56
Cu-Zn-Si	NH_3 vapors and solutions	56
A-Cu-Zn-Sn	$CUSO_4$. NH_3 solutions	56
	$NaNO_2$,$NaNO_3$,$NaClØ_3$,	
	$Na_2SO_4$56	56
	NaMoO,NaCl solutions	56
Cu-Au	NH_4NO_3 solutions	56
	$FeCl_3$ solutions	56
	Aqua regia	56
Cu-23Zn-12Ni	$NaNO_3$ + $Zn(NO_3)_2$ or +	17
	$Ca(NOZ_3)_2$ or +$Cu(NO_3)_2$ 17	
	or + NH_4	17

Cu	Acetate ($Cu(C_2H_3O_2)_2$) solutions	17
Admiralty Brass	Nitrate ($NaNO_2$)	17
	Stagnant H_2O + NH_3 or Nitrate	17
	Freshwater	17
Cu-Be	NH_3 vapors and solutions	56
Iron Alloys		
γ-Stainless Steel	Aqueous Chlorides	40,79
	Hot Conc. Chlorides	18,40
	Chloride Contaminated Steam	18,40
	$MgCl_2$	43,6
300 Series Stainless (fe-Cr-Ni-C)	$BaCl_2$, $CrCl_3$, HgCl, $CaCl_2$	56
	$ZnCl_2$,LiCl,$MgCl_2$, $CoCl_2$	56
	NH_4Cl,$MnCl_2$ solutions	56
	NaCl + $K_2Cr_2O_7$ solutions	56
	NaCl + (NH_4NO_2 of $NaNO_2$)	56
	H_2SO_4 + NaCl solutions	56
	H_2SO_4 at 289C	56
	HCl, HF, HNO_3	52,56,20
	NaOH, KOH solution at 300C	56
	Vinyl chloride, CH_3CH_2Cl + Water	56
	Aluminum, Sodium and Uranyl Sulfate solutions	56
	Caustic (OH^-)	52

	$H_2S_4O_6$	56
	Polythionic acids	56
	Dichlorophenol	56
	Epichlorohydrin	56
	Ethyl benzene	56
	Sodium Aluminate solution	56
	High temperature water	40,13
310 & 310S	H_2SO_4	47
	Oxidizing or sulfidizing	93
	Gas at 450C and 600C	93
304 & 316	HF(70°C)	20
	$MgCl_2$	55,54
Hi-Ni Alloys	High-purity steam	18
Nickel Alloys		
Inconel 600	High-purity steam	48,64
	Aerated boric acid + Na_2S_2O(22-95°C)	60
	High temperature (300C)	48
	Oxygen & thiosulfate (40C)	60
	Caustic soda	48
	Polythionic acid	60
	Low-temperature sulphur envi	48
	Sodium tetrathionate	60
	NaOH at 288C	89
	HF vapors	31
	Polythionic acids or sodium tetrathionate	60
	H_3BO_3 + sodium thiosulfate	60

	Hot conc. caustic soda + oxid	60,31
	H_2SO_4 + $NaAsO_2$	86
Inconel 671	Helium	93
	Coal gasification gases	93
	Oxidizing or sulfidizing	93
	Gas at 450C and 600C	93
Incoloy 800	NaOH at 288C	89
	Coal gasification gases	93
Incoloy 825	NaOH at 190C	1
	$MgCl_2$ at 147C	1
Haynes Stellite 6B	NaOH at 147C	1
Hastelloy C276	400F Sodium Chloride	48
	400F Acetic Acid + H_2S	48
	Low-temp HE (25C)	48
	NaOH at 147C	1
Hastelloy B	NaOH at 147C	1
Inconel X750	400F Sodium Chloride	48
	400F Acetic Acid + H_2S	48
	HF vapors low-temp HE (25C)	48,31
Monel	Hydrofluosilicic acid (140F)	15
	Air+CO_2+H_2O+F at 140F	15
	HF vapors	52,20,25 31
	NaOH, KOH (570F)	13
	Fused caustic soda	13
	HF + $CuCl_1$	20
	HF + CuF_2	35,15,20

Duranickel 301	HF vapors	31
Ni-200	HF vapors	31
	HF + CuF_2 impurities	20
Monel Ni-Cu	HF vapors	56
	H_2SiF_6	56
Monel Ni-Cu-Al	HF vapors	56
Ni-Cu-Fe	H_2SiF_6	56
Ni-Cr-Fe	Distilled water contaminated	56
	With lead salts at 316C	56
	NaCl(HCl) solution at 300C	56
Ni-Fe-Cr	NaCl(HCl) solution at 300C	56
	$MgCl_2$ solution, boiling	56
	NaOH solution at 288C	56
Ni-Cr-Mo	NaOH solution at 147C	56
Ni-Co-Cr-Mo	NaOH solution at 147C	56
Other Alloys		
Ag-1Au	Aquo regia	56
	$FeCl_3$ solution	56
Au-Cu	$FeCl_3$, Acid Sulphate	43
2. BCC		
Copper Alloys		
B-Brass	Water	79
B-Cu-Zn-Al	NH_3 vapors and solutions	56
Iron Alloys		
Ni, Low C Steel	$MgCl_2$ solutions	56
α-Stainless Steel	Aqueous Chlorides	79
	Phosphate	43

	Anhydrous Ammonia	43
	$MgCl_2$,$CO/CO_2/H_2O$	43
	CS_2/H_2O	43
	Hot nitrate	43
	Caustic soda	43
	Carbonate	43
	High temperature water	43
Carbon Steel	Hot nitrate	18,65
	NO_3-, OH-	52,43
	$CO_3/HCO_3/$, $COcO_2/H_2O$	43
	Hydroxide	18,65
	Carbonate/bicarbonate	18
Hi-Strength Steel	Aqueous electrolytes + H_2S	18
Mild, Low C Steels	Sodium aluminate	56
	Monoethanolamine	52,56
	NaH_2PO_4 + H_3PO_4 solutions	56
	$FeCl_3$, $AlCl_3$, $MnCl_2$ solution	56
	H_2O-CO-CO_2	56
	NaOH + Na_2SiO_3	56
	$Ca(NO_3)_2$ + NH_4NO_3 solutions	56
	HCN solution, HCl	56
	Anhydrous liquid NH_3	52,56
	Coal gas liquors	65
	Cyanides and sulphates	65
	Nitrates of Al,An,Mg,NH_3	65

	Na, Mn, or Ca, K, Li, Ni	65
	Pb, Cd	65
	Caustics if contaminated with oxidizing salts	56
Low Alloy Steel	H_2S, H_2S + Acetic Acid Solution	56
	H_2O-CO-CO_2	56
	HCN solutions	56
	NaCl solutions	56
Titanium Alloys		
Ti-Mn	KCl solution	
Ti-16V	Methanolic solution	
Ti-20Mo	Methanolic solution	
Ti-Mo-Zr-Zn	Methanolic solution	
Ti-V-Cr-Al	NaCl solution	47
	Methanol/HCl	
3. HCP		
Magnesium Alloys		
MgAl	Aqueous Chlorides	79
	Aqueous Cl	18
Mg	KHF_2 solution	56
	NaCl + K_2 CrO_4 solution	51,56
Mg-Al	NaCl + K_2CrO_4 solution	12,56
	Distilled Water	12,56
	$MgCo_3$	12,56
	KF solution	12,56
	KHF_2 solution	12,56
	HF	12,56

	K_2CrO_4 solution	12,56
	Air	12
Mg-2Mn	KHF_2 solution	56
Mg-2Mn-Ø.5Ce	Distilled Water	56
	KHF_2 solution	56
Mg-Al-Zn	KHF_2 solution	12,56
	Distilled Water	12,56
	HF	12,56
	NaCl + K_2CrO_4 solution	12,56
	Sea Water	56
Titanium Alloys		
Ti	Nitric acid; ammonia	52
	Methanol/HCl	43,56
Ti-Al	Methanol + I_2 solution	56
	Aqueous Cq-, Br-, I-	18
	Organic liquids	18
	N_2O_2	18
	N_2O_4	56
	Halide (Cl,Br,I) solution	56
	Salt water, alcohol, liquid or gaseous alkanes, CCl	56 56
Ti-Al-Sn	NaCl solution	56
	Methanol/HCl	56
	$MgCl_2$	56
	HCl solution	56
	N_2O_4	56
	Salt water, alcohol, liquid or gaseous alkanes, CCl4	56 56

Zirconium Alloys	Aqueous Cq-	18
	Organic liquids	18
	I_2 at 350C	18
Zr	Methanol/HCl	56
	Hot chloride salts	56
	Nitrate-iodine salt	56
	HNO_3	56
ZR-Sn	Methanol/HCl	56
	Hot chloride salts	56
	Nitrate-iodine salt	56
	HNO_3	56
Other Alloys		
Be	Synthetic sea water	56

4. Other

Aluminum Alloys		
Al	Aqueous Cq-, Br-, I-	47
7075-T651	Aqueous Cl- I-	47
2024-T351	Aqueous Cl-	8
Copper Alloys		
A/B-Cu-Zn	Sea water	56
Cu-Pt,-Pd,Ga	NH_3 vapors and solutions	56
A-Cu-Al-Fe	NH_3 vapors and solutions	56
Cu-Zn-Si	NH_3 vapors and solutions	56
Cu-Sb	NH_3 vapors and solutions	56
Cu-Zn-Mn	Nh_3 vapors and solutions	56
Cu-Ge	Ny_3 vapors and solutions	56
C26000	Acetate solutions	17

	Amines (methyl, ethyl, butyl) if Cu in solution	17
	Chlorides	17
	Nitrite ($NaNO_2$)	17
	$Na_2SO_4 + H_2SO_4$ (Sulfate)	17
C68700	Amines (methyl, ethyl, butyl) if Cu in solution	17
C72000	Citrate containing dissolved Cu	17
C70600	Nitrate ($NaNo_2$)	17
C44300 Cu-Zn-Antimony	Chlorides	17
	$NaNO_3 + Zn(NO_3)_2$ or +	17
	$Ca(NO_3)_2$ or + $Cu(NO_3)_2$	17
	or + NH_4	17
	Tungstate (Na_2WO_4)	17
	Chlorates	17
Iron Alloys		
200 Series Stainless	$MgCl_2$ solutions	56
(Fe-Cr-Mn-C)	Chloride solutions	56
400 Series Stainless	$MgCl_2$, NH_4Cl solutions	56
(Fe-Cr-C)	H_2S solutions	56
	Sulphide environments	56
Dalmine D 22-75	NaCl	5
Titanium Alloys		
Ti8AllMolV	NaCl	47
	Aqueous Chlorides	79
Ti-Al-V	N_2O_4	56

	Methanol	56
	NaCl solution	56,5Ø
Ti-Ø.35Ø	Salt water, alcohol, liquid	56
	or gaseous alkanes, CCl	56
Ti-Al-Mo-V	NaCl solution	56,79
	Molten salts	56
	Halide (Cl, Br, I) solution	56
	Distilled water	56
	Salt water, alcohol, liquid	56
	or gaseous alkanes, CCl	56
Ti-7Al-2Nb-1Ta	Distilled water	56
Other Alloys		
Ag-Cd	$FeCl_3$ solution	56

APPENDIX B

DEVELOPMENTS TOWARD UNDERSTANDING STRESS

CORROSION CRACKING MECHANISMS

1940	Dix demonstrated that an SCC path in a material occurred perpendicular to the activating stress and that grain boundary precipitation caused preferential reaction
1947	Keating, and Evans in independent work illustrated that SCC cracks occurred in alternating mechanical/electrochemical steps; localized corrosion produced notches where the material would fail due to mechanical weakening
1950	Gilbert & Hadden demonstrated that cracking proceeded in a jerky pattern with jumps in the potential
1952	Logan demonstrated the effects of localized yielding at the crack tips; set forth the theory that the film ruptures at the crack tip while the sides remain protected
1954	Robertson & Bakish illustrated that differential oxidation potential of material elements lead to local inhomogeneity which introduced a short-

circuited galvanic cell and producing equilibrium grooves in a grain

1954 Harwood

utilizing a cleavage model, illustrated that SCC susceptibility was inversely proportional to the square root of the grain size, thereby requiring an increased stress for cleavage to occur in fine grains

1954 Copson

suggested that pitting or trenching by corrosion causes a stress concentration which induces plastic deformation in the metal ahead of the corrosion which causes a crack to grow

also speculated that microscopic body stresses caused the variations in specimen SCC susceptibility

1954 Priest

stated that the plastic deformation of the SCC material is not the cause of a crack, but rather is the result of propagation

1956 Graf

demonstrated that the susceptibility to SCC of an alloy was associated with the more noble elements acting as cathodes within a grain cell thereby accelerating nearby attack; further supports the increasing incidence of SCC when noble elements redeposits

1956 Evans

formulated a theory that hydrogen caused SCC embrittlement by diffusing ahead of the crack front thereby limiting the propagation to a brittle fracture mode

1956 Gilman

suggested the existence of three possible cracking modes: secondary cleavage, plastic shearing, and plastic necking with the later being the most likely

1956 Hoar & Hines

further demonstrated the effects of localized yielding which directly assisted in removing cations from the metallic lattice at the crack tip

1958 Hoar & West, and Scully

in separate work demonstrated that the localized yielding greatly decreased the activation polarization at the crack tips that allowed anodic dissolution to occur in alloys susceptible to SCC; also demonstrated that resistant alloys did not display such an effect

1959 Edeleanu

speculated that electrochemistry can explain many of the SCC specialized features and that the energy differences induced by such factors as cold working, yielding, elastic strain energy, etc. could be maintained at the crack tip

1959 Parkins, and Engell & Baumel

demonstrated that grain boundaries suffered from preferential attack in mild stressed steel, the presence of the cementite boundaries in the material resulted in a jerky cracking pattern with jumps in the potential

1959 Forty

illustrated the step like crack propagation and theorized that preferential dissolution of one phase of an alloy caused a

porous region in which dislocations merged; caused a brittle fracture when the increased energy induced the occurrence of a burst of slip

1960 Edeleanu

attempted to relate cracking pattern with microstructure, in 18-8 stainless steel, martensite formed plates ahead of the cracks lending preferred path

1960 Nutting & Swann

speculated that crack formation was assisted by the formation of corrosion slots where stresses were concentrated due to the pinning of stacking faults

1960 Robertson & Tetelmen

explained IGSCC via preferential dissolution of a disordered grain boundary which lead to a weak, spongy barrier which, when stressed, opened up as the dislocations piled into the area; demonstrating the beneficial effect of a material capable of high cross-slip

explained TGSCC via preferential dissolution on the slip planes at a Lomer-Cottrell barrier causing cracks to be initiated as the dislocations accumulated at the corrosion pores

1960 Edeleneau & Forty

first proposed the film induced cleavage model where the crack is propagated through the brittle film, well into the ductile material, by cleavage before blunting can occur

1963 Pickering & Swann

suggested that, due to a selective dissolution process, corrosion tunnel formation allowed mechanical tearing of the material

between weakened slots inducing crack formation

1965 Menzies

developed a differential aeration principle based on the previous work of Evans and Pourbaix whereby different oxygen concentrations, as related to the stacking faults within a material, induce localized cathodic/anodic areas for initiation of SCC

1971 Delamare & Rhead

found that the surface mobility of a material played an important role in the susceptibility to SCC

1972 Wilde & Kim

showed that some cases of SCC cracking occur at cathodic potentials which prevent the occurrence of hydrogen adsorption

1973 Parkins

speculated that a passivating film played a major role in SCC and demonstrated that an entire spectrum of mechanisms must be operative in SCC due to the specificity of cracking environments

1974 Green & Hayden

illustrated different cracking models involved with different loading modes; hydrogen diffusion employed in mode I loading but not in mode III loading

1979 Parkins

combined anodic dissolution and mechanical crack tip film disruption mechanisms through experimental evidence that showed the tip environment was effectively buffered to resemble the bulk fluid environment; illustrated that in a non-passivating system, the bare surface current density supplied the driving force for crack propagation; and in a passivating system, cracks were

extended by slip step emergence for TC modes or by increased crack tip stress/strain for IG modes

1979 Pednekar, Agrawal, Chaung, & Staehle
first utilized slow strain rate tests to illustrate cleavage-like fracture surfaces in TGSCC of copper samples

1979 Silcock & Swann
developed the corrosion tunneling model where the slots, formed by corrosive action, form cracks by being interconnected by shear fractures

1981 Lynch
proposed that chemisorption at crack tips weakened the shear strength of interatomic bonds leading to localized plastic deformation which induced the nucleation of a dislocation at the crack tip

1983 Nichols
postulated that hydrogen diffusion effected SCC susceptibility in mode II loading, since mode II would be essentially impossible to maintain, and that hydrostatic stress concentration is necessary for cracking to occur

1983 Bursle & Pugh
decided that TGSCC resulted from a discontinuous cleavage of the crack tip film by a hydrogen embrittlement-induced decohesion mechanism

1983 Paskin, Sieradski, Som, & Dienes
utilized computer simulations to illustrate a dynamic embrittlement model where a cleavage crack, initiated in the film and propagated through ductile material, caused blunting when the

dislocation stresses were trapped behind the crack tip

1984 Alvarez

illustrated that anodic dissolution is the SCC rate controlling step which occurs as a continuous process

1984 Beggs

confirmed that the cracks advanced by a sudden appearance of a fine crack that would begin to open as a result of creep at the crack tip

1984 Meletis & Hochman

theorized that crack growth was due to a surface energy reduction mechanism followed by a mechanical fracture along the path of lowest surface energy, thereby illustrating the cleavage involvement

1985 Sieradzki & Newman

utilized the evidence of fractography and the spasmodic acoustic emissions of SCC cracking to indicate a short-range, discontinuous cleavage as the rate controlling step;

indicated that a crack jumps well beyond the film boundary before it is arrested

1985 Lynch

proposed that surface adsorption enhances plasticity; that shear fracture connects the corrosion tunnels and that crack extension occurs by the microvoid formation ahead of the crack tip working in conjunction with alternating slip

1985 Pugh

concluded that resistance to TGSCC would be illustrated in materials that demonstrate ready cross-slip due to the absence of

effective ordering or the presence of high stacking fault energy

1986 Namboodhiri & Tripathi

reaffirmed preferential dissolution model with a theory of stress-enhanced dealloying process which would be caused by deformation-induced polarization differences within a cell

1986 Galvele

explains the proportionality between current densities and crack velocities and proposed that SCC could be explained by a surface mobility characterization which would lead to a method of predicting susceptible material / environment combinations

1987 Galvele

produced a model based on the surface mobility of a material where a crack would grow when vacancies arrived at, or adatoms were discharged from, the crack tip; this theory relates the characteristics of SCC and LME, and proposes a method for determining critical environments for non-hydride forming metals

1988 Lynch & Trevena

concluded that the localized microvoid coalescence causes SCC and LME by adsorption of hydrogen into the metal lattice to weaken the interatomic bonding

VITA[2]

Leah Gail Everhart

Candidate for the Degree of

Master of Science

Thesis: STRESS CORROSION CRACKING IN MONEL 400

Major Field: Mechanical Engineering

Biographical:

Personal Data: Born in Clovis, New Mexico, September 16, 1958, the daughter of Mr. and Mrs. Winfred F. Henley. Mother of Carissa Gail Everhart.

Education: Graduated from Benton High School, Benton, Arkansas, in May, 1976; received Associate of Arts in Engineering from Westark Community College, Fort Smith, Arkansas, in December, 1981; received Bachelor of Science Degree in Mechanical Engineering from Oklahoma State University in May, 1987; completed the requirements for Master of Science Degree in Mechanical Engineering at Oklahoma State University in May, 1989.

Professional Experience: Science Lab Technician, Westark Community College, Fort Smith, Arkansas, July 1983 to August 1984; Communications Technician, Oklahoma State University Computer and Information Science Departments August 1984 to May 1985; Summer Engineering Intern, General Motors Tooling and Process Engineering Department, Oklahoma City, summer 1986; Engineer Intern, April 1987; graduate and undergraduate teaching assistant, Oklahoma State University, August 1986 to December 1988.

Professional Organizations: Pi Tau Sigma; Phi Kappa Phi; American Society of Mechanical Engineers; National Society of Professional Engineers; Oklahoma Society of Professional Engineers; Society of Women Engineers; Mortar Board; Golden Key; Phi Theta Kappa WCC.